МІНІСТЕРСТВО ОСВІТИ І НАУКИ УКРАЇНИ
Національний університет кораблебудування
імені адмірала Макарова

СИСТЕМИ КЕРУВАННЯ ЕЛЕКТРОПРИВОДІВ

ELECTRIC DRIVES CONTROL SYSTEMS

Навчальний посібник

Рекомендовано Вченою радою НУК

ВИДАВНИЦТВО
НАЦІОНАЛЬНОГО УНІВЕРСИТЕТУ
КОРАБЛЕБУДУВАННЯ
ІМ. АДМІРАЛА МАКАРОВА
2023

УДК 681.51(076)
С40

Автори:
І. С. Білюк, канд. техн. наук, доцент;
С. О. Гаврилов, канд. техн. наук, доцент;
О. В. Савченко, викладач, зав. лаб. кафедри автоматики;
А. М. Фоменко, доцент НУК;
Д. Ю. Шарейко, канд. техн. наук, доцент

Рецензенти:
Ю. П. Кондратенко, доктор технічних наук, професор, завідувач кафедри інтелектуальних інформаційних систем, Чорноморський національний університет імені Петра Могили;
О. О. Ушкаренко, доктор технічних наук, професор, професор кафедри програмованої електроніки, електротехніки і телекомунікацій, Національний університет кораблебудування імені адмірала Макарова;
В. І. Костюченко, кандидат технічних наук, доцент, доцент кафедри суднових електроенергетичних систем, Національний університет кораблебудування імені адмірала Макарова

Рекомендовано Вченою радою НУК ім. адмірала Макарова
як навчальний посібник
(*протокол № 06 від 01.07.2022 р.*)

С40 **Системи** керування електроприводів. Electric Drives Control Systems : навчальний посібник / І. С. Білюк, С. О. Гаврилов, О. В. Савченко, А. М. Фоменко, Д. Ю. Шарейко. – Миколаїв : НУК, 2023. – 172 с.

ISBN 978-966-321-453-5

Розглянуто основні принципи побудови та роботи, властивості та характеристики сучасних систем керування електродвигунами постійного і змінного струмів.

Призначено для студентів спеціальності 141 «Електроенергетика, електротехніка та електромеханіка» при вивченні дисциплін «Системи керування електроприводів» та «Електропривод робототехнічних систем» (Electric Drive of Robotic Systems).

УДК 681.51(076)

ISBN 978-966-321-453-5

CONTENTS

PREFACE

Electrical drives act as the electromechanical energy converter in a wide range of applications. It is critically important that the correct drive is matched to the application with due regard to its requirements. With the recent developments in power semiconductors and microprocessors with signal processing capabilities, the technology of the modern drive system has changed dramatically in recent years. However, the selection of a drive system relies on a systems approach – without which, it is highly probable that either the mechanical, electrical electronic or computational will not perform to the required standard or fail if not fully considered.

The structure of the book is as follows. Chapter 1 gives a fundamentals of electric motors, introduces the fundamental operating principle needed to understand electric motors and describes clear differences among the motors by comparing their operating principles.

Chapter 2 concentrate on the problem of control of direct current motors, describes DC motors, which used to be the typical motor for speed control and torque control, and the concept of torque control for DC motors, which will be helpful for understanding the vector control for torque control of AC motors. Furthermore, this chapter goes into detail about the design of the current and speed controllers of DC motors, which is readily applicable to the current and speed controllers of AC motors.

Chapter 3 considers the alternating current motors: synchronous motor and induction motor, discusses the basic characteristics of AC motors, including synchronous and induction motors, which are widely used for industrial motors. These characteristics can provide a basis for studying high-performance motor control.

Chapter 4 concentrate on the modeling of alternating current motors and reference frame theory – the modeling of AC motors and d-q reference frame theory for control of AC motors.

Chapter 5 considers the vector control of alternating current motors – the concept of the vector control and its implementation for AC motors.

1 FUNDAMENTALS OF ELECTRIC MOTORS

The electric motors have recently become one of the most important prime movers and their use is increasing rapidly. Nearly 70 % of all the electricity used in the current industry is used to produce electric power in the motor-driven system.

Electric motors can be classified into two different kinds according to the type of the power source used as shown in Fig. 1.1: direct current (DC) motor and alternatig current (AC) motor.

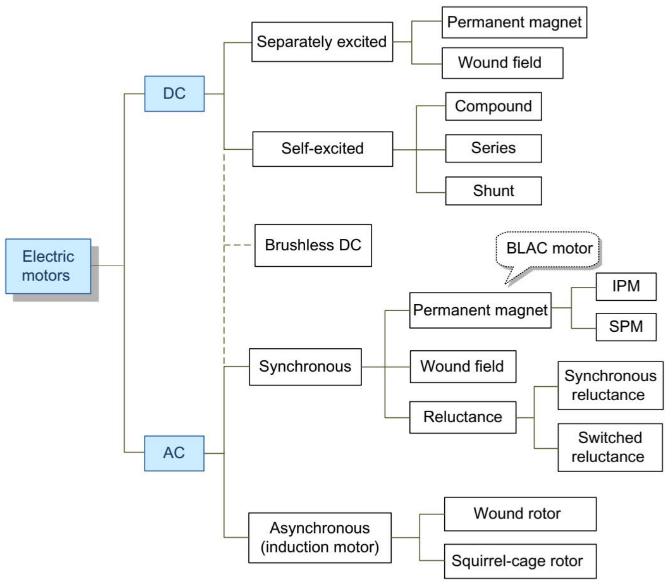

Fig. 1.1

1.1 Configuration of Electric Motors

An electric motor is composed of two main parts: a stationary part called the stator and a moving part called the rotor as shown in fig. 1.2. The air gap between the stator and the rotor is needed to allow the rotor to spin, and the length of the air gap can vary depending on the kind of motors.

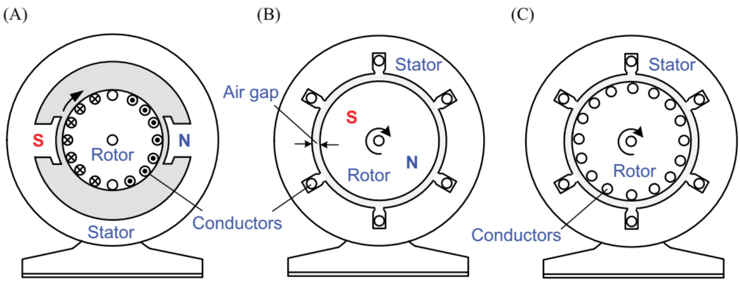

Fig. 1.2

In a synchronous motor as depicted in fig. 1.2b, the magnetic field on the rotor is generated either by a permanent magnet or by a field winding powered by a DC power supply separated from the stator AC power source. In this motor, the rotor magnetic field is stationary relative to the rotor. Hence, to produce a torque, the rotor should rotate at the same speed as the stator rotating magnetic field. This speed is called the synchronous speed. This is why this motor is referred to as the synchronous motor.

In an induction motor as shown in fig. 1.2c, the rotor magnetic field is generated by the AC power. The AC power used in the rotor excitation is transferred from the stator by electromagnetic induction. Because of this crucial feature, this motor is referred to as the induction motor. In an induction motor, the rotor magnetic field rotates relative to the rotor at some speed.

The stator and the rotor part each has both an electric and a magnetic circuit. The stator and the rotor are constructed with an iron core as shown in fig. 1.3. To obtain a greater magnetic flux for a given current in the conductors, the iron core is usually made up of ferromagnetic material with high magnetic permeability, such as silicon steel. In some cases, the stator or the rotor creates a magnetic flux by using a permanent magnet.

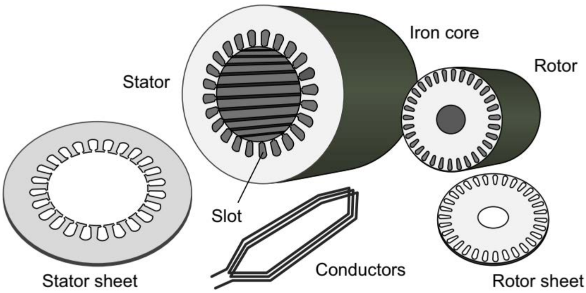

Fig. 1.3

1.2 Basic Operating Principle of Electric Motors

All electric motors are understood to be rotating based on the same operating principle.

The simple concept for the rotation of a DC motor is that the rotor rotates by using the force produced on the current-carrying conductors placed in the magnetic field created by the stator as shown in fig. 1.4a. There are two stationary magnetic fields in a DC motor as shown in fig. 1.4b. One stationary magnetic field is the stator magnetic field produced by magnets or a field winding. The other is the rotor magnetic field produced by the current in the conductors of the rotor. It is important to note that the rotor magnetic field is also stationary despite the rotation of the rotor. This is due to the action of brushes and commutators, by which the current distribution in the rotor conductors is always made the same regardless of the rotor's rotation as shown in fig. 1.4a. Thus the rotor magnetic field will not rotate along with the rotor.

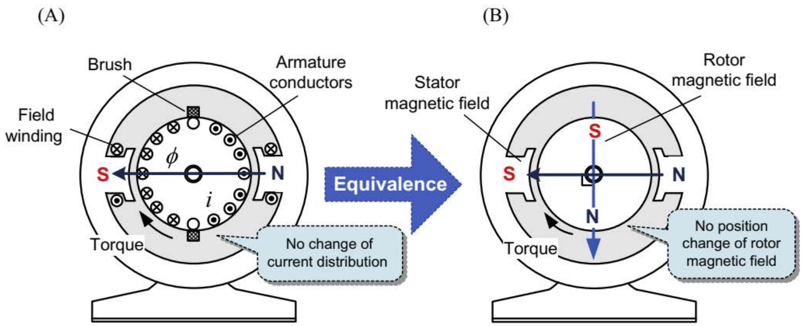

Fig. 1.4

A consistent interaction between these two stationary magnetic fields produces a torque, which causes the rotor to turn continuously.

There are two kinds of AC motors: a synchronous motor and an induction (asynchronous) motor. They generate the rotor magnetic field differently, whereas they generate the stator magnetic field in the same way (fig. 1.2).

AC motors exploit the force between two rotating magnetic fields. In AC motors both the stator magnetic field and the rotor magnetic field rotate, as shown in fig. 1.5.

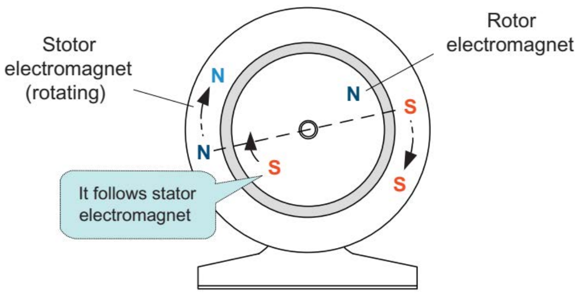

Fig. 1.5

These two magnetic fields always rotate at the same speed and, thus, are at a standstill relative to each other and maintain a specific angle. As a result, a constant force is produced between them, making the AC motor is to run continually.

1.3 Requirements for Continuous Torque Production

The torque produced from the interaction between the magnetic fields generated in the stator and the rotor causes the motor to run. Now, we will take a look at the requirements that ensure continuous torque production by the motor.

An electric motor is a type of electromechanical energy conversion device that converts electric energy into mechanical energy. The principle of torque production in a motor can be understood by analyzing its energy conversion process.

Electromechanical energy conversion devices normally use the magnetic field as an intermediate in their energy conversion processes. Thus an electromechanical energy conversion device is composed of three different parts: the electric system, magnetic system, and mechanical system as shown in fig. 1.6.

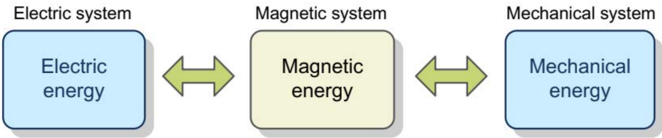

Fig. 1.6

The total amount of energy is constant. fig. 1.7 shows an application of the law of conservation of energy when t he electromechanical energy conversion device is acting as a motor.

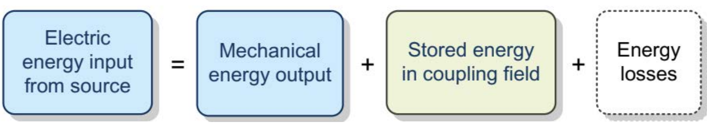

Fig. 1.7

1.4 Mechanical Load System

An electric motor is an electromechanical device that converts electrical energy into mechanical torque. When the torque developed by the motor is transferred to the load connected to it, the load variables such as speed, position, airflow, pressure, and tension will be controlled.

Fig. 1.8 shows a simplified configuration of a motor drive system consisting of a driving motor and a driven mechanical load, in which the torque of the motor is transferred to the load through the shaft and coupling.

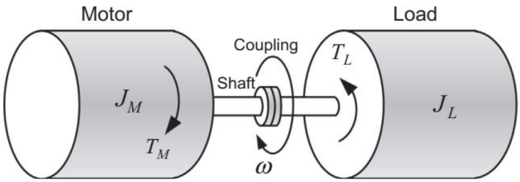

Fig. 1.8

There are several types of loads driven by a motor. In most loads, the required torque is normally a function of speed. There are three typical loads whose speed-torque characteristics are shown in the fig. 1.9.

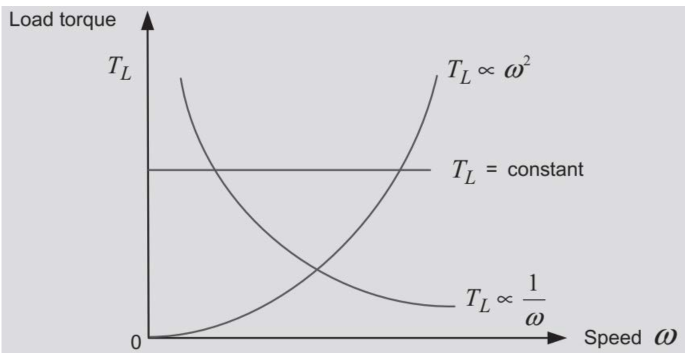

Fig. 1.9

1.4.1 Constant torque load. The torque required by this type of load remains constant regardless of the speed. Loads such as elevators, screw compressors, conveyors, and feeders have this type of characteristic.

1.4.2 Constant power load $\left(T_L \sim 1/\omega\right)$. This load requires a torque, which is inversely proportional to the speed, so this load is considered a constant power load. This type is most often found in machine tool industry and drilling, milling industry.

1.4.3 Load proportional to the square of the speed $\left(T_L \sim \omega^2\right)$. The torque of this load increases in proportion to the square of the speed. This is a typical characteristic of a fan, blower, and pump, which are the most commonly found in industrial drive applications.

1.5 Operating Modes of an Electric Motor

Operation of a motor can be divided into two modes (fig. 1.10) according to the direction of the energy transfer: (A) Motoring mode and (B) generating (braking) mode.

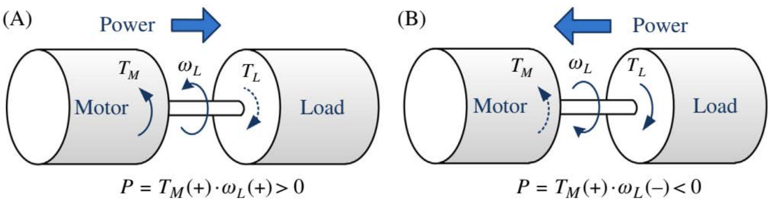

Fig. 1.10

When the motor rotates in the same direction as its developed torque in fig. 1.10a, the motor will supply mechanical energy to the load. In this case, the motor operates as a typical motoring mode.

When the motor is rotating in a direction opposite to its developed torque in fig. 1.10b, the mechanical energy of the load is supplied to the motor. In this case, the motor is acting as a generator. It corresponds to the generating mode, in which the motor absorbs the load energy, providing a braking action.

When braking, the mechanical energy of the load is converted into electrical energy through the motor, and the generated electrical power can be returned to the power source. This method called regenerative braking is the most efficient braking method, but it requires a high-cost power converter. An alternative method for dealing with the generated electrical power is to dissipate it as heat in the resistors. This is called dynamic braking, which is inefficient but inexpensive.

Four-quadrant operation modes are available in variable speed drive systems as shown in fig. 1.11.

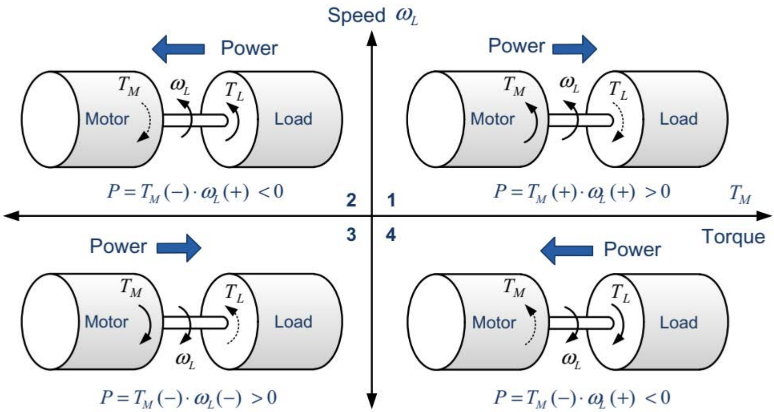

Fig. 1.11

Quadrants 1 and 2 are the motoring and generating operation modes, respectively, in the forward drive, while Quadrants 3 and 4 are the two operation modes in the reverse drive. Braking occurs in Quadrants 2 and 4. To achieve the four-quadrant operation modes in motor drive systems, the torque should be controlled in the positive and negative direction, and the speed should be controlled in the forward and reverse direction.

1.6 Components of an Electric Drive System

A motor drive system consists normally of five parts as shown in fig. 1.12. Within the available power supply, we have to choose these components appropriately to achieve the requirements of the drive performance. We will now briefly take a look at these five parts.

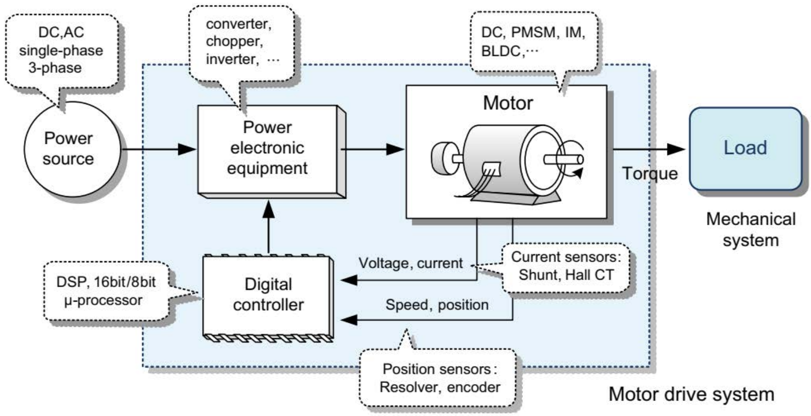

Fig. 1.12

1.5.1 Power Supply. Single-phase or three-phase AC voltage sources are most commonly used as a power supply that provides electric energy for motor drives. The three-phase AC voltage source is generally used for motors of several kilowatts or higher. In many cases, the AC voltage sources are converted into a DC source, which is converted into the form of power needed by a motor through using power electronic converters such as an inverter or a chopper.

1.5.2 Power Electronic Converters. Power electronic converters play the role of taking electrical energy from the power system and turning it into a suitable form needed by a motor. The power electronic converter may be determined according to the given power source and the driving motor.

For DC drives, power electronic converters such as a controlled rectifier or a chopper can be used to adjust the DC power. In AC drives mostly use an inverter to adjust the voltage and frequency in the AC power. In this case, a rectifier is often included to convert the AC power in the mains power system into the DC power. These power electronic converters use power semiconductor devices such as gate turn-off (GTO) thyristor, integrated gate-commutated thyristor (IGCT), insulated gate bipolar transistor (IGBT), power metal oxide semiconductor field effect transistor (MOSFET), and power bipolar junction transistor (BJT).

1.5.3 Electric Motors. For driving motors, we have to choose the one that meets the required speed-torque characteristic of the driven mechanical load. In addition, important performance criteria like efficiency, size, cost, duty cycle, and operating environment need to be considered.

As mentioned earlier, there are two basic types of a driving motor: DC motor and AC motor. Robotic systems use special types such as a BLDC motor or a stepping motor, which cannot be classified into the basic types.

DC motors have an advantage of a simple speed/torque control for their excellent drive performance. However, due to the wear associated with their commutators and brushes, DC motors are less reliable and unsuitable for a maintenance-free operation. On the other hand, AC motors are smaller, lighter, and have more power density than DC motors. AC motors also require virtually no maintenance and thus are better suited for high speeds. However, AC drives with a high performance capability are more complex and expensive than DC drives.

1.5.4 Digital Controllers. The controller in charge of executing algorithms to control the motor is the most important part in the motor drive systems. This controller manipulates the operation of the power electronic converter to adjust the frequency, voltage, or current provided to the motor.

Nowadays, digital controllers are usually used. A digital controller is based on microprocessor, microcontroller, or digital signal processor (DSP), which can be a 16-bit or 32-bit, and also either a fixed-point or floating-point. There is a trade-off between the control performance and the cost. DC motor and BLDC motor drives requiring relatively simple controls may use 16-bit processors, while AC motor drives requiring complex controls such as a vector controlled induction or synchronous motors may need high-performance 32-bit processors or DSP.

1.5.5 Sensors and Other Ancillary Circuits. To achieve a high-performance motor drive, a closed-loop control of position, speed or current is often adopted, and in this case, speed/position or current information is required. Sensors are essential for obtaining this information.

Shunt resistances, Hall effect sensors, or current transformers are mainly used as the current sensor. The shunt resistance is more cost effective, while the Hall effect sensors can usually give a high resolution and isolation between the controller and the system. Encoders and resolvers are widely used as speed/position sensors.

In addition to these components, several circuits for protection, filtering, power factor correction, or harmonics reduction may be necessary to improve the reliability and quality of the drive system.

2 CONTROL OF DIRECT CURRENT MOTOR

2.1 Configuration of Direct Current Motors

Direct current (DC) motors have been widely used in adjustable speed drives or variable torque controls because their torque is easy to control and their range of speed control is wide. However, DC motors have a major drawback in which they need mechanical devices such as commutators and brushes for a continuous rotation. These mechanical parts require regular maintenance and hinder high-speed operations.

A DC motor has two windings as shown in fig. 2.1. One is found in the stator and produces a field flux. This winding is called a field winding. The other one resides in the rotor and is called an armature winding. The armature current interacts with the stator field flux to produce torque on the rotor shaft.

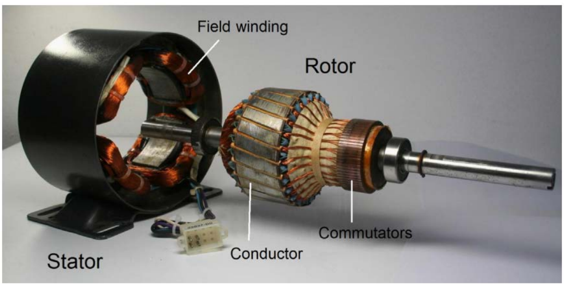

Fig. 2.1

The armature current interacts with the stator field flux to produce torque on the rotor shaft (fig. 2.3). Small DC motors commonly have a permanent magnet instead of a field winding to produce the stator flux. A DC motor also has a mechanical commutation device consisting of brushes and commutators, which converts the DC current given from the DC power supply to AC current in the armature winding.

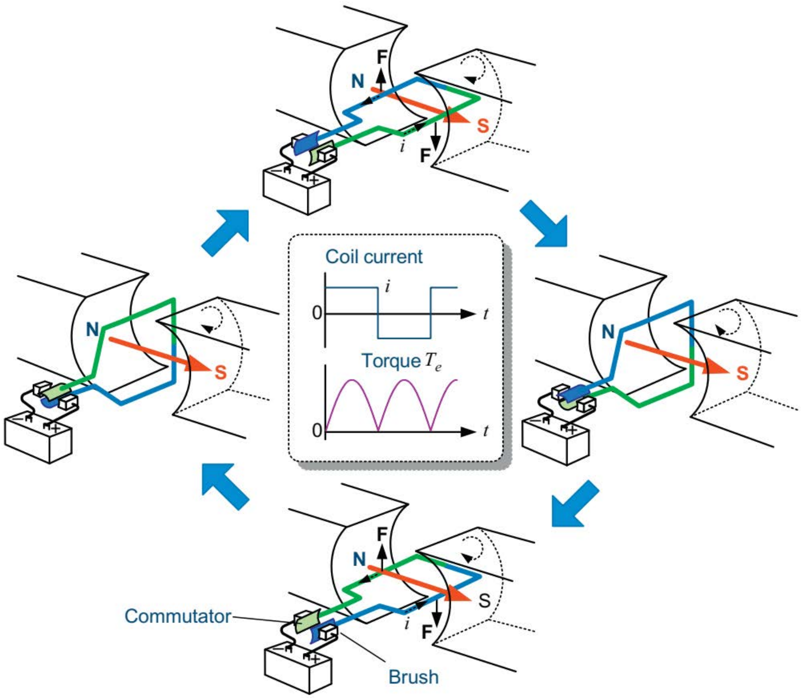

Fig. 2.2

The DC motors can be mainly classified into two different categories: a **separately excited DC motor** and a **self-excited DC motor**. In a separately excited DC motor, the armature winding and field winding each have separate DC power supplies, while in a self-excited DC motor, the two windings share one DC power supply.

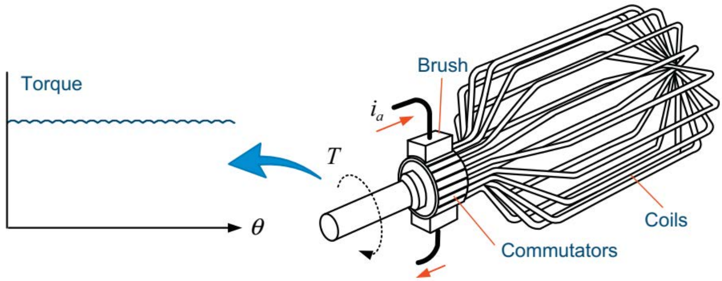

Fig. 2.3

The self-excited DC motors can also be categorized into a **shunt motor**, **series motor**, and **compound motor** depending on the ways in which the two windings are connected to the DC power supply. Nowadays the DC motors mostly use a permanent magnet to produce the field flux and the DC power supply thus applies only to the armature winding.

2.2 Modelling of Direct Current Motors

A complete dynamic model of the DC motor drive system can be expressed as the following four equations: armature circuit, back-electromotive force (back-EMF), torque, and mechanical load system.

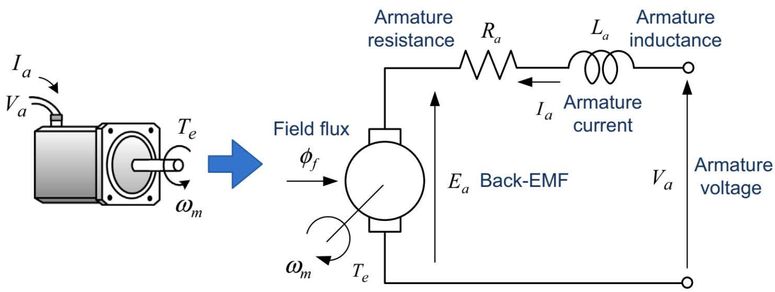

Fig. 2.4

2.2.1 Armature Circuit. The voltage equation for the armature winding of a DC motor

$$V_a = R_a i_a + L_a \frac{di_a}{dt} + e_a ,$$

where $\boldsymbol{i_a}$ is winding current, $\boldsymbol{L_a}$ is winding inductance, $\boldsymbol{R_a}$ is winding resistance, and $\boldsymbol{e_a}$ is back-EMF induced by the rotation of the armature winding in a magnetic field.

2.2.2 Torque. The torque experienced by the conductors of the armature winding carrying a current $\boldsymbol{i_a}$ in the uniform stator magnetic flux $\boldsymbol{\varphi_f}$ is given by

$$T_e = k_T \varphi_f i_a ,$$

where $\boldsymbol{k_T}$ is the torque constant (Nm/Wb/A). The numerical values of $\boldsymbol{k_T}$ and $\boldsymbol{k_e}$ constants are equal in SI units (the International System of Units), i.e., $k_T=k_e$.

2.2.3 Back-electromotive Force. The back-EMF in the armature winding

$$e_a = k_e \varphi_f \omega_m ,$$

where $\boldsymbol{k_e}$ is the back-EMF constant (Vs/rad/Wb), $\boldsymbol{\varphi_f}$ is the uniform stator magnetic flux. Commonly, since the flux remains constant, the back-EMF is proportional to the angular velocity $\boldsymbol{\omega_m}$.

2.2.4 Mechanical Load System. When a DC motor with the output torque is driving a mechanical load system, the rotor speed can be determined from the equation of motion

$$T_e = J \frac{d\omega_m}{dt} + B\omega_m + T_L ,$$

where $\boldsymbol{\omega_m}$ is the angular velocity of the rotor, $\boldsymbol{T_L}$ is the load torque, $\boldsymbol{J}$ is the moment inertia and $\boldsymbol{B}$ is the friction coefficient of the DC motor drive system, respectively.

It is interesting to note that the torque of a DC motor can be expressed as a simple arithmetical product of the stator magnetic flux φ_f and the armature current i_a. This is because the stator magnetic flux φ_f and the conductors carrying current i_a are always perpendicular to each other. Thus the DC motors inherently have a maximum torque per ampere characteristic.

2.3 Steady-state characteristics

From the steady-state equations, the speed-torque relation may be written as

$$\omega_m = \frac{V_a}{k\varphi_f} - \frac{R_a}{\left(k\varphi_f\right)^2} T_L$$

$$\left(k = k_T = k_e\right).$$

Equation implies that the steady-state speed of a DC motor can be adjusted by the armature voltage $\boldsymbol{V_a}$ or the stator field flux $\boldsymbol{\varphi_f}$. Thus there are two speed control methods for the DC motor: **armature voltage control** and **field flux control**. In addition to the two methods, we can see from Equation that the speed can be controlled by varying the armature resistance R_a. However, this inefficient method is no longer in use.

We can see that, from this torque-speed relation, the speed of the DC motor decreases steadily with increasing load torque (or armature current) as shown in fig. 2.5. Here, N is the speed expressed in terms of revolution per minute (r/min) for angular speed ω_m. From the curve, we can find the speed and the current at a certain load.

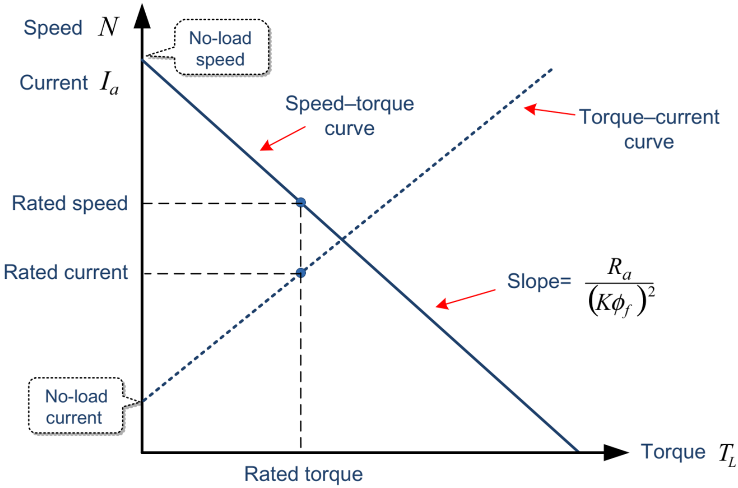

Fig. 2.5

2.3.1 Armature Voltage Control. With a constant stator field flux the torque-speed characteristic can be reduced to

$$\omega_m = \frac{V_a}{k\varphi_f} - \frac{R_a}{\left(k\varphi_f\right)^2} T_L = K_1 V_a - K_2 T_L \,,$$

where $\boldsymbol{K_1 = V_a / k\varphi_f}$ and $\boldsymbol{K_2 = R_a / (k\varphi_f)^2}$.

From this expression, we can see that the speed $\boldsymbol{\omega_m}$ of the DC motor changes linearly with the armature voltage $\boldsymbol{V_a}$. Thus, for a constant torque load such as elevators and cranes, the speed of the load can be controlled linearly by adjusting the armature voltage $\boldsymbol{V_a}$ of the DC motor as shown in fig. 2.6.

To employ the armature voltage control, variable DC power supplies such as phase-controlled rectifiers or choppers are needed. Because a voltage higher than the rated voltage should not be applied to the motor, this armature voltage control method can provide a speed control range only up to the rated speed. To operate in a speed range above the rated speed, the DC motor has to adopt the field flux control, which will be described later. Permanent magnet DC motors, however, cannot use the field flux control method, so they are incapable of an operation above the rated speed.

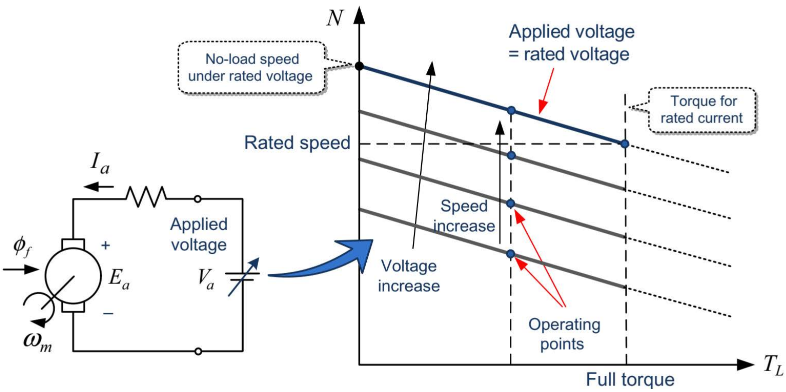

Fig. 2.6

2.3.2 Field Flux Control. Under a constant armature voltage

$$\omega_m = \frac{V_a}{k\varphi_f} - \frac{R_a}{\left(K\varphi_f\right)^2} T_L = \frac{K_1}{\varphi_f} - \frac{K_2}{\varphi_f^2} T_L,$$

where $\boldsymbol{K}_1 = \boldsymbol{V_a} / \boldsymbol{k}$ and $\boldsymbol{K}_2 = \boldsymbol{R_a} / \boldsymbol{k}^2$.

From Equation, we can see that the speed of the DC motor varies inversely with the field flux. fig. 2.7 shows the torque-speed characteristic of the DC motor using the field flux control. When using this field flux control method, the field flux has to be controlled below the rated value to avoid magnetic saturation of iron core because the rated flux is commonly given as a value near the knee of the magnetization curve as shown in the left side of fig. 2.7. If the field flux is reduced below the rated value, then the speed can increase above the rated speed.

When the speed of the DC motor can be controlled above the rated value by adjusting the field flux control, there are potential problems that can arise. When the field flux is reduced to increase the speed, the developed torque will also be reduced for the same armature current. If the armature current is increased to produce the same torque, then the efficiency will be lowered due to the increased copper losses. The armature current also may not be fully increased due to the thermal limit and the capacity of the DC power supply. Moreover the inductance of the field winding is normally designed to be large to produce the flux effectively. Thus the field flux cannot be changed rapidly, and this will result in a slow response of the speed regulation. In addition, in a high-speed range, the speed regulation will be poor for the applied load, and the resultant lower field flux will be easily influenced by the armature reaction. Besides these electrical problems, the DC motors also suffer from speed limitations due to mechanical commutation devices. On this account, the achievable speed range of this field flux control is generally limited up to three times the rated speed.

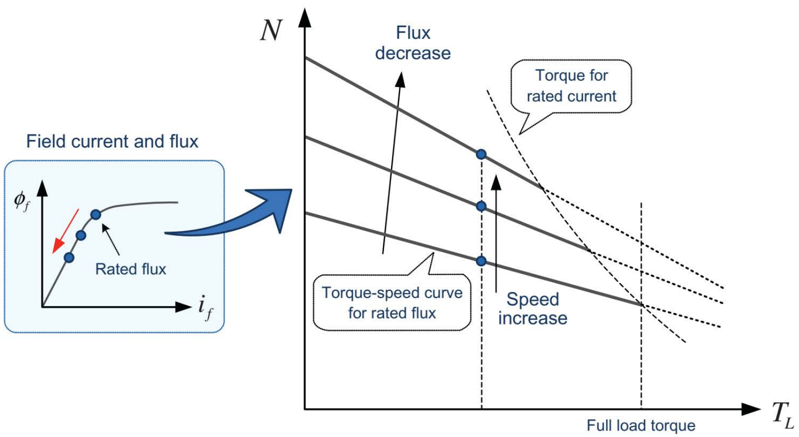

Fig. 2.7

2.4 Operation Regions of Direct Current Motors

The operating speed range of the DC motor is divided into two regions as follows (fig. 2.8): **constant torque region** and **constant power region**. The operation in these two regions can be achieved through the armature voltage control and the field flux control.

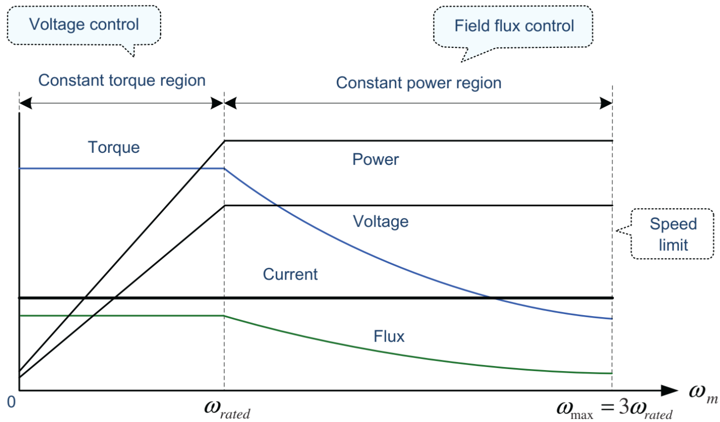

Fig. 2.8

2.4.1 Constant Torque Region (0 < $\boldsymbol{\omega_m}$ < base speed $\boldsymbol{\omega_b}$). In the operating region below the rated speed, the field flux is maintained at a constant and the torque production is controlled only by the armature current $\boldsymbol{I_a}$. This region is called the constant torque region because the same torque can be developed by the same armature current at any speed within this region.

As the operating speed is increased, the back-EMF is increased. Thus the applied motor voltage should also be increased to maintain the same armature current, i.e., the same torque. Like this, in this region, the terminal voltage of the DC motor varies with its speed. Because the voltage applied to the motor should not exceed the rated value, the range of this region is normally limited to the speed at which the terminal voltage of the DC motor reaches the rated value. This speed may be different from the rated speed depending on the operating conditions. Thus it is usually referred to as the base speed ω_b.

2.4.2 Constant Power Region ($\boldsymbol{\omega_m}$ > base speed $\boldsymbol{\omega_b}$**)**: field-weakening region. Once the motor voltage reaches the rated value, the speed can no longer be controlled by the voltage. At speeds higher than the base speed, the applied voltage remains constant. Thus, instead of the voltage control, the speed can be increased by the reduction of the field flux (is called field-weakening operation).

The reduction of the field flux can make the back-EMF constant regardless of the speed increase. This allows the armature current, which produces a torque, to flow. However, even though the same current is flowing, the output torque will be decreased with the operating speed due to the reduced field flux. Because the terminal voltage and the current remain constant in this region, the motor operates in a constant power, $P = V_a \times I_a = T_e \times \omega_m$. Thus this speed region is called the constant power region.

2.5 Transient Response Characteristics

The transient characteristic is very important for high-performance motor drives. This is because the transient response characterizes the dynamics of the drive system.

As an example, transient responses to a step speed command are shown in fig. 2.9. Even though all three responses reach the same final speed, their response times and moving trajectories to reach the final speed are different. Although an oscillatory or slow response can ultimately achieve the speed command, it has no practical use.

An easy way to examine the transient response is to use the transfer function of the system. We can obtain the transfer function for the DC motor drive system by taking the Laplace transform of the differential equations. Here, s denotes the Laplace operator.

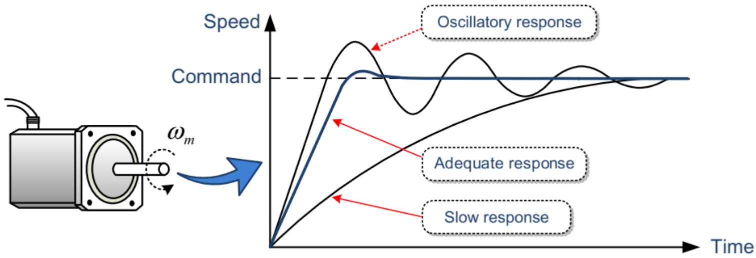

Fig. 2.9

$$v_a = R_a i_a + L_a \frac{di_a}{dt} + e_a \to V_a(s) =$$

$$= (R_a + sL_a) I_a(s) + E_a(s) =$$

$$= (R_a + sL_a) I_a(s) + k_e \varphi_f \omega_m(s),$$

$$T_e = J \frac{d\omega_m}{dt} + B\omega_m + T_L \to T_e(s) =$$

$$= (Js + B)\omega_m(s) + T_L = k_T \varphi_f I_a(s).$$

Equations together can be represented by the closed-loop block diagram as shown in fig. 2.10.

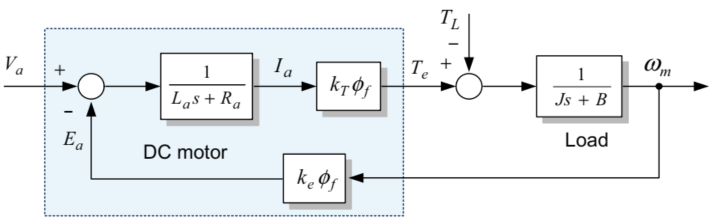

Fig. 2.10

From the block diagram in fig. 2.10, the transfer function from the input armature voltage $\boldsymbol{V_a(s)}$ to the output angular velocity $\boldsymbol{\omega_m(s)}$ is given by

$$\frac{\omega_m(s)}{V_a(s)}=\frac{\dfrac{1}{L_a s+R_a}k_e\varphi_f\dfrac{1}{Js+B}}{1+\left(\dfrac{1}{L_a s+R_a}k_e\varphi_f\dfrac{1}{Js+B}k_T\varphi_f\right)}=$$

$$=\frac{\dfrac{k}{JL_a}}{s^2+\left(\dfrac{R_a}{L_a}+\dfrac{B}{J}\right)s+\left(\dfrac{R_a}{L_a}\dfrac{B}{J}+\dfrac{k^2}{JL_a}\right)}$$

$$\left(k=k_T\varphi_f=k_e\varphi_f\right).$$

This transfer function is a second-order system including two poles, which are important factors in determining the transient response of the system.

If $\boldsymbol{L_a=0}$ (in most motor drive systems), equation can be written as

$$\frac{\omega_m}{V_a}=\frac{k}{R_aJs+K^2}=\frac{1}{k}\frac{\omega_c}{s+\omega_c}\left(\omega_c=\frac{k^2}{R_aJ}\right).$$

This equation implies that, in a DC motor, the relationship between the speed $\boldsymbol{\omega_m}$ and the armature voltage $\boldsymbol{V_a}$ can be considered as a first-order, low-pass filter with a cut-off frequency $\boldsymbol{\omega_c}$.

In most motor drive systems, the time response of an electric system is faster than that of a mechanical system. In that case, we can ignore the transient of the electric circuit so that L_a=0. This means that the speed ω_m is directly proportional to the armature voltage V_a with its changing rate below the ω_c, though there is a time delay between the two. Generally, it can be assumed that the rotational speed of a DC motor is proportional to the voltage applied to it.

Letting the electromechanical time constant $\boldsymbol{T_m = JR_a/k^2}$ and the electrical time constant $\boldsymbol{T_a = L_a/R_a}$, equation can be rewritten as

$$\frac{\omega_m}{V_a} = \frac{\frac{1}{k}\left(\frac{1}{T_m T_a}\right)}{s^2 + \frac{1}{T_a}s + \frac{1}{T_m T_a}}.$$

The poles can be obtained from the roots of the denominator (also called the characteristic equation)

$$s_{1,2} = -\frac{1}{2T_a} \pm \frac{1}{T_a}\sqrt{\frac{1}{4} - \frac{T_a}{T_m}}.$$

We can also find out the response characteristic from the damping ratio for this second-order system

$$G(s) = \frac{\omega_n^2}{s^2 + 2\zeta\omega_n s + \omega_n^2}.$$

The undamped natural frequency $\boldsymbol{\omega_n}$ and the damping ratio ζ for the DC motor drive system are given by

$$\omega_n = \frac{1}{\sqrt{T_a T_m}} = \frac{k}{\sqrt{JL_a}}, \qquad \zeta = \frac{1}{2}\sqrt{\frac{T_m}{T_a}} = \frac{1}{2}\frac{R_a}{k}\sqrt{\frac{J}{L_a}}.$$

If $T_m > 4T_a$, then the characteristic equation has two real roots. A DC motor drive system with a large J or R_a corresponds to this case, and its response is either ① or ② in fig. 2.11. If $T_m < 4T_a$, then the characteristic equation has two complex roots. In this case, the system response is oscillatory such as ③ in fig. 2.11.

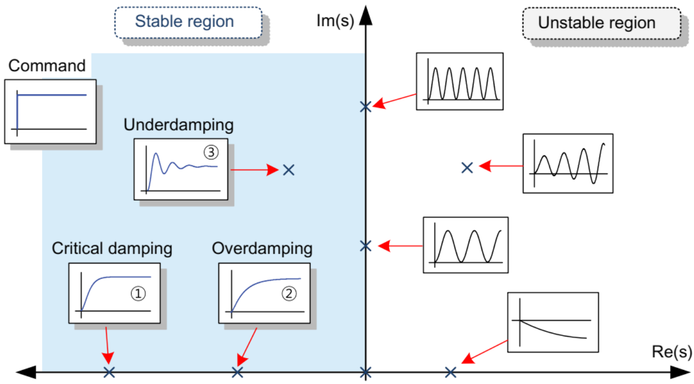

Fig. 2.11

There are three typical responses of the system according to the value of the damping ratio ζ: underdamping (0<ζ<1), critical damping (ζ=1), or overdamping (ζ>1).

In the case of underdamping (0<ζ<1), the system comes rapidly to equilibrium but has a slight oscillatory response. As ζ is increased, the oscillation is reduced. In the case of overdamping (ζ>1), the system is not oscillatory but has a very slow response. A critically damped system response (ζ=1), which comes to equilibrium as fast as possible without oscillating, is the most desirable.

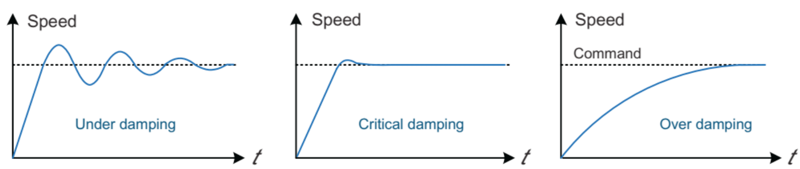

(A) Underdamping (ζ<1) (B) Critical damping (ζ=1) (C) Overdamping (ζ>1)

Fig. 2.12

The damping ratio ζ, which implies the dynamic performance of the speed to the applied armature voltage, depends on the electromechanical time constant value Tm and the electrical time constant value T_a. If $T_m > 4T_a$, then ζ<1 and its speed response will be oscillatory. By contrast, in the case of $T_m < 4T_a$, the system will have a stable speed response without oscillation. Normally, small motors have $T_m > 4T_a$, while servo motors or high power motors have $T_m < 4T_a$, resulting in an oscillatory response. Even though the system response is inherently oscillatory, we can achieve the desired response by adopting an adequate controller, which will be described later.

2.6 Motor Control System

Fig. 2.13 illustrates the typical configuration of controllers in the motor drive systems, in which the controllers required for position, speed and current control are usually connected in a cascade.

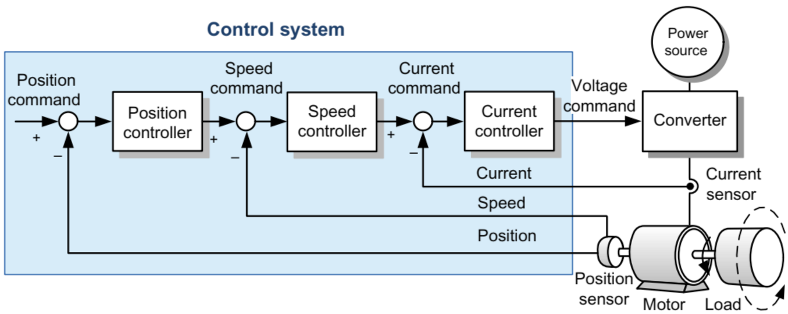

Fig. 2.13

Among these, the current controller must be placed at the most inner loop and has the widest bandwidth. As mentioned above, since the speed and position can be controlled through the current control, the response time for the current control must be the fastest among the three. Likewise, the response for the control of the inner loop should be sufficiently faster than that of the outer loop to improve the response performance and the stability of the outer control loop.

2.6.1 Types of Control. The aim of control is to adjust the control input so that the state or output of the system reaches the required goal. In the motor drive systems, the state or output may be the current, flux, speed, position, or torque, while the control input is only the input voltage. There are two basic types of control: **open-loop control** and **closed-loop control**, also known as **nonfeedback** and **feedback**, respectively.

2.6.1.1 Open-loop control (fig. 2.14). A drawback of the open-loop control is that it requires perfect knowledge of the system. Since the open-loop control does not use the feedback of the system output $Y(s)$, the error between the reference $R(s)$ and the output $Y(s)$ cannot be reflected in determining its control input $U(s)$. Because of its simplicity and low cost, the open-loop control is often used in systems where it has the well-defined relationship between input and output and are not influenced by disturbances.

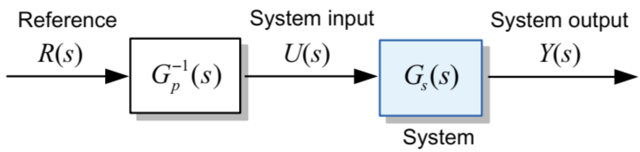

Fig. 2.14

2.6.1.2 The **closed-loop control** (fig. 2.15) is generally used to control the position, speed, current, or flux in the motor drive systems. The controller $G_c(s)$ adjusts its control input $U(s)$ to reduce the error between the output and the desired goal. Thus the role of the controller $G_c(s)$ in the closedloop control is very critical to the system's performance.

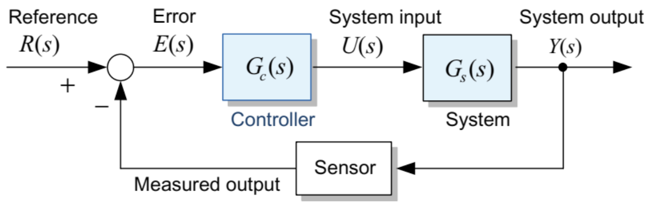

Fig. 2.15

2.7 Types of the Feedback Controller

There are several types of widely used types of the feedback controller in the motor drive systems as follows.

2.7.1 Proportional controller (*P* controller). In this type of controller, which is illustrated in fig. 2.16, the controller output is proportional to the present error $e(t)=r(t)–y(t)$ as given by

$$U(t) = K_p e(t),$$

where $\boldsymbol{K_p}$ represents the proportional gain.

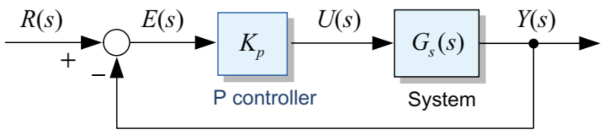

Fig. 2.16

An advantage of the proportional control is its immediate response to errors. The larger the proportional gain is, the faster the response is. Thus it should be noted that the proportional gain determines the control bandwidth. However, there is a limit to increasing the proportional gain because a large gain can lead to system instability or may require unrealizable control input. A drawback of the proportional control is that the error can never be zero. In other words, there exists a steady-state error in the P control.

2.7.2 Integral controller (I controller). In this type of controller, the controller output is the integral of the error as shown in fig. 2.17, so the past errors as well as the present error have an effect on the control input as given by

$$U(t) = K_i \int e(t)\,dt = \frac{K_p}{T_{pi}} \int e(t)\,dt,$$

where $\boldsymbol{K_i}$ represents the integral gain and $\boldsymbol{T_{pi}=K_p/K_i}$ represents the integral time constant.

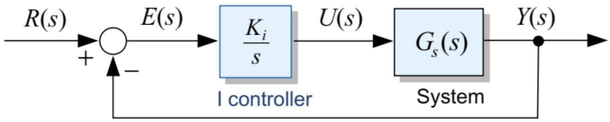

Fig. 2.17

The integral controller can remove the steady-state error completely for the non-time varying reference *R*(*s*). This is because it continuously produces nonzero control input from the accumulated past errors even though the present error is zero. However, due to the accumulated errors in the integral term, it responds slowly to change in errors. For this reason, the integral controller is not normally used alone but is combined with the *P* controller.

2.7.3 Proportional-integral controller (PI controller). A widely used controller in motor drive, which is a combination of a proportional controller and an integral controller to achieve both a fast response and a zero steady-state error. The block diagram of a PI controller is shown in fig. 2.18.

The PI controller has been widely used in motor drive systems as the controller for the current, speed, or flux linkage control because it could give a satisfactory performance. The performance of the PI controller depends heavily on its selected gains. Thus it is very important to select appropriate gains of the

PI controller for obtaining a satisfactory performance in a given system.

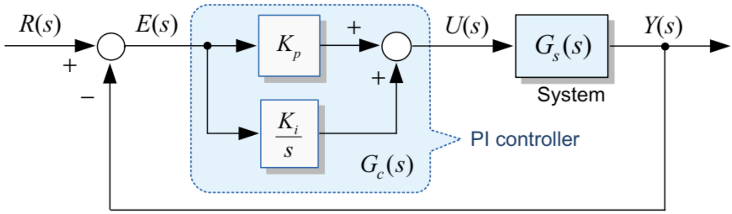

Fig. 2.18

2.8 Current Controller Design

2.8.1 The PI controller consists of a proportional term, which depends on the present error, and an integral term, which depends on the accumulation of past and present errors as follows:

$$G_{pi}(s) = K_p + \frac{K_i}{s},$$

where $\boldsymbol{K_p}$ and $\boldsymbol{K_i}$ are the proportional and integral gain, respectively.

The transfer function can be rewritten as

$$G_{pi}(s) = K_p\left(1 + \frac{1}{T_{pi}s}\right) = K_p\frac{\left(s + \frac{1}{T_{pi}}\right)}{s},$$

where $\boldsymbol{T_{pi}=K_p/K_i}$ is the integral time constant of the PI controller and $\mathbf{1}/\boldsymbol{T_{pi}}$ is called the corner frequency of the PI controller.

The transfer function of a DC motor system that includes a PI current controller as shown in fig. 2.19 is given as

$$I(s) = \frac{K_{pc}s + K_{ic}}{L_a s^2 + (R_a + K_{pc})s + K_{ic}} I^*(s) - \frac{s}{L_a s^2 + (R_a + K_{pc})s + K_{ic}} E(s),$$

where $\boldsymbol{K_{pc}}$ and $\boldsymbol{K_{ic}}$ represent the proportional and integral gains of the current controller, respectively.

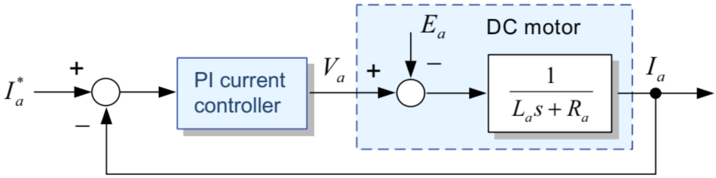

Fig. 2.19

For a large system inertia, the effect of $E(s)$ on the current control can be ignored since the variation of $E(s)$ due to the speed variation is very small. However, for servo motors designed with a small inertia for a fast speed response, the effect of $E(s)$ cannot be ignored.

A current control system containing a PI controller is shown in fig. 2.20. Here, assume that the feedforward control compensates the back-EMF of the DC motor perfectly.

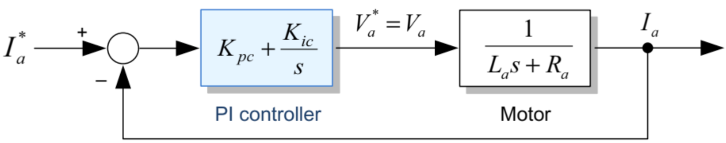

Fig. 2.20

In this PI current controller, the relationship between the current error and its output voltage is given as

$$V_a = K_{pc}\left(1+\frac{1}{T_{pi}s}\right)\left(I_a^*-I_a\right),$$

where $\boldsymbol{T_{pi}=K_{pc}/K_{ic}}$ is the integral time constant of the PI current controller and $\boldsymbol{K_{ic}}$ is the integral gain.

The open-loop transfer function $G_c^o(s)$ of this system is given by

$$G_c^o\left(s\right)=K_{pc}\left(\frac{s+\dfrac{1}{T_{pi}}}{s}\right)\frac{1}{L_a s+R_a}=K_{pc}\frac{\left(s+\dfrac{K_{ic}}{K_{pc}}\right)}{s}\frac{\dfrac{1}{L_a}}{\left(s+\dfrac{R_a}{L_a}\right)}.$$

The value of the proportional gain K_{pc} determines how fast the system responds, whereas the value of the integral gain K_{ic} determines how fast the steady-state error is eliminated. When the value of these gains is larger, the control performance is better. However, large gains may lead to an oscillatory response and result in an unstable system.

2.8.2 Gains selection procedure of the PI current controller

2.8.2.1 Find the switching frequency $\boldsymbol{f_{sw}}$ of the system.

2.8.2.2 Select the control bandwidth $\boldsymbol{\omega_{cc}}$ of the current controller to be within 1/10-1/20 of the switching frequency $\boldsymbol{f_{sw}}$ and below 1/25 of the sampling frequency.

2.8.2.3 Calculate the proportional and integral gains from the selected bandwidth $\boldsymbol{\omega_{cc}}$ as

$$K_{pc}=L_a\omega_{cc}, \qquad K_{ic}=R_a\omega_{cc}.$$

The bandwidth $\boldsymbol{\omega_{cc}}$ of a current controller is limited by the following two factors:

− the switching frequency $\boldsymbol{f_{sw}}$ of the power electronic converter realizing the output of the current controller;

− the sampling period for detecting an actual current for feedback in the digital controller.

Since a motor current cannot change faster than the switching frequency of the power electronic converter, the switching frequency limits the bandwidth of the current control. If the current is sampled twice every switching period, as a rule of thumb, the maximum available bandwidth can be up to 1/10 of the switching frequency. On the other hand, if it is sampled once every switching period, the maximum available bandwidth can be up to 1/20 of the switching frequency. For this case, it is desirable to restrict the bandwidth to 1/25 of the sampling frequency.

2.8.3 Anti-windup Controller. There are several methods to avoid the integrator windup such as **back calculation**, **conditional integration**, and **limited integration**.

The anti-windup scheme of back calculation as shown in fig. 2.21 is widely used because of its satisfactory dynamic characteristic.

In this scheme, when the output is saturated, the difference between the controller output and the actual output is fed back to the input of the integrator with a gain of $\boldsymbol{K_a}$ so that the accumulated value of the integrator can be kept at a proper value. The gain of an anti-windup controller is normally selected as $\boldsymbol{K_a = 1/K_p}$ to eliminate the dynamics of the limited voltage.

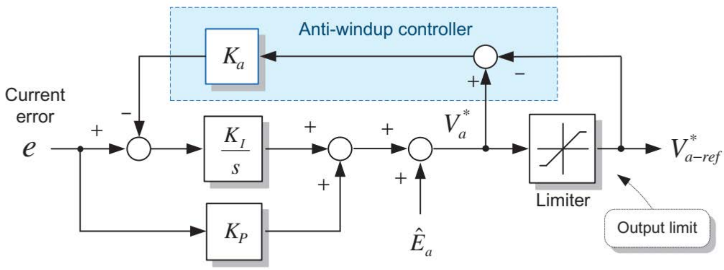

Fig. 2.21

The output of the PI current controller, which indicates the voltage reference applied to a DC motor, should be limited to a feasible value by the following reasons. First, a voltage exceeding its rated value should not be applied to a motor. Furthermore, power electronic converters, which produce the voltage applied to the motor, normally have a restricted output voltage due to the limited availability of the input voltage and the voltage rating of switching devices.

Once the output of the PI controller exceeds its limit due to sustained error signals for a significant period of time, the output will be saturated, but the integrator in the controller may have a large value by its continual integral action. This phenomenon is known as integral windup. When the windup occurs, the controller is unable to immediately respond to the changes in the error due to a large accumulated value inside the integrator.

2.9 Speed Controller Design

2.9.1 When controlling the speed of a motor, the speed controller must be placed in the outer loop of the current controller as shown in fig. 2

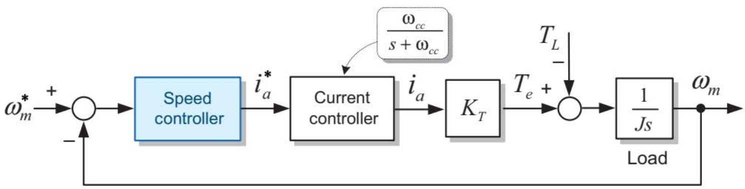

Fig. 2.22

From the block diagram in fig. 2.22, the open-loop transfer function of the speed control system is given by

$$G_s^o(s) = G_{pi}(s)G_c^c(s)\times\frac{K_T}{Js} = \left(K_{ps} + \frac{K_{is}}{s}\right)\times\frac{\omega_{cc}}{s+\omega_{cc}}\times\frac{K_T}{Js}.$$

This open-loop characteristic is the sum of the frequency responses of three parts: a PI speed controller, a PI current controller, and a mechanical system of a motor and a load.

2.9.2 Gains selection procedure of the PI speed controller.

2.9.2.1 Identify the bandwidth of the current controller.

2.9.2.2 Select the bandwidth $\boldsymbol{\omega}_{cs}$ of speed control to be five times less than the bandwidth of current control and ten times less than the sampling frequency of speed.

2.9.2.3 Calculate the proportional and integral gains from the selected bandwidth $\boldsymbol{\omega}_{cs}$ as

$$K_{ps} = \frac{J\omega_{cs}}{K_T}, \quad K_{is} = K_{ps}\omega_{pi} = K_{ps}\frac{\omega_{cs}}{5} = \frac{J\omega_{cs}^2}{5K_T}.$$

In this case, if the bandwidth of current control is chosen to be sufficiently wider than that of speed control, then the current control will not have any influence on the speed control performance, and the stability of the speed control will be improved.

Like the current controller, a PI controller is widely used for speed control. Now, we will explain how the PI speed controller is designed, i.e., how to select the proper gains to achieve the desired speed control performance.

Inaccurate information of the system parameters, J and K_T, may lead to incorrect gains for achieving the required bandwidth, so we may need to adjust additionally the gains by monitoring the transient response as shown in fig. 2.23. If the system has an oscillatory response, we need to decrease the gains. On the other hand, if the system has a very slow response, we need to increase the gains.

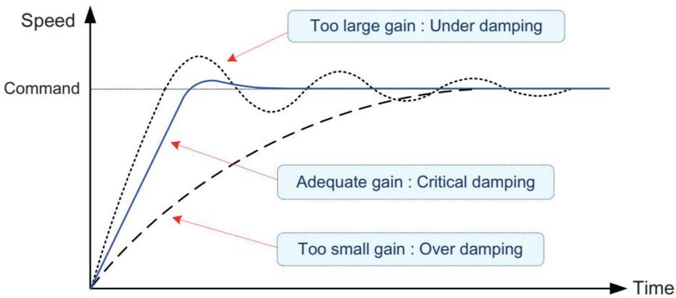

Fig. 2.23

From the open-loop transfer function $G_{os}(s)$, the closed-loop transfer function $G_{cs}(s)$ of the speed control system is given by

$$G_s^c(s) = \frac{G_c^o(s)}{1+G_c^o(s)} = \frac{\left(\frac{K_T K_{ps}}{J}\right)s + \left(\frac{K_T K_{is}}{J}\right)}{s^2 + \left(\frac{K_T K_{ps}}{J}\right)s + \left(\frac{K_T K_{is}}{J}\right)}.$$

We can remove the zero from equation by adjusting the position of the P control part in the PI controller as shown in fig. 2.24. This controller is known as the **IP controller**.

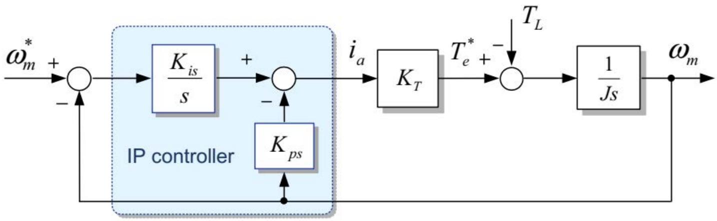

Fig. 2.24

An IP controller is equivalent to a PI controller except for the first-order, low-pass filter with the time constant of $\boldsymbol{K_{ps}/K_{is}}$ on the input side. Therefore, an IP controller exhibits no overshoot due to low-pass filtering of its input command, but its response will be slower than that of a PI controller.

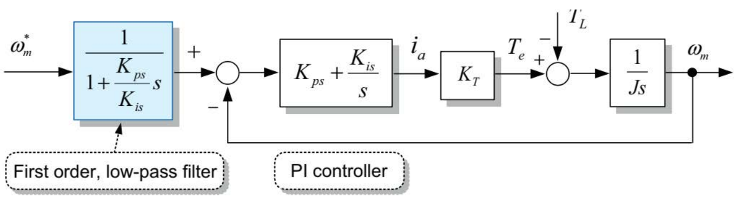

Fig. 2.25

The speed responses of the PI and IP controllers under an equal control bandwidth are shown in fig. 2.26a. It can be seen that the IP controller exhibits no overshoot, but its response is slower than that of the PI controller. On the other hand, the speed responses to a disturbance torque for the two controllers are the same, as we would expect. If the bandwidths are adjusted for the two controllers to have the same overshoot in their response to speed reference, the IP controller can achieve a larger bandwidth than the PI controller. For the same overshoot, the bandwidth of the IP controller can be set as 5.44 times larger than that of the PI controller. In this condition, the IP controller will exhibit an improved speed response to the disturbance torque as shown in fig. 2.26b.

2.10 Power Electronic Converter for Direct Current Motors

The voltage applied to a DC motor can be controlled by using a power electronic converter. Fig. 2.27 shows a simple driving circuit for the forward motoring mode operation. Commonly, in a driving circuit, the switching states of the power devices are determined by the pulse width modulation (PWM) technique to achieve the required voltage command. The voltage command is given by the current controller.

A four-quadrant chopper (or H-bridge circuit) is often used to operate a DC motor in both motoring and braking modes for both forward and reverse directions. The H-bridge circuit is implemented with four power switching devices as shown in fig. 2.28.

This circuit is widely used in DC servo drive systems because it can provide high-performance current control with a bandwidth up to several thousand (rad/s). In this circuit, there are two PWM techniques for adjusting the output voltage: bipolar and unipolar switching schemes.

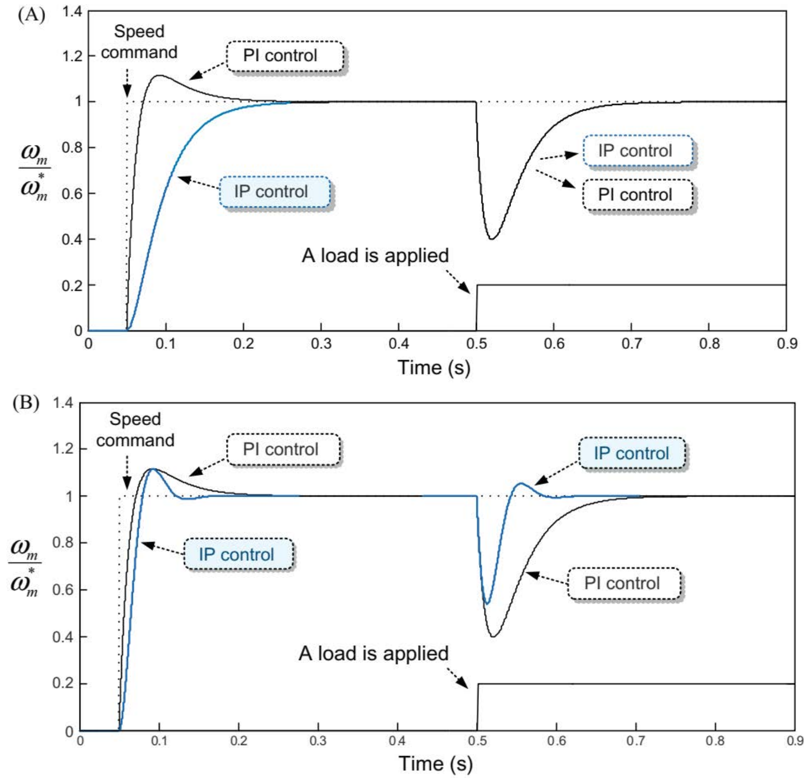

Fig. 2.26

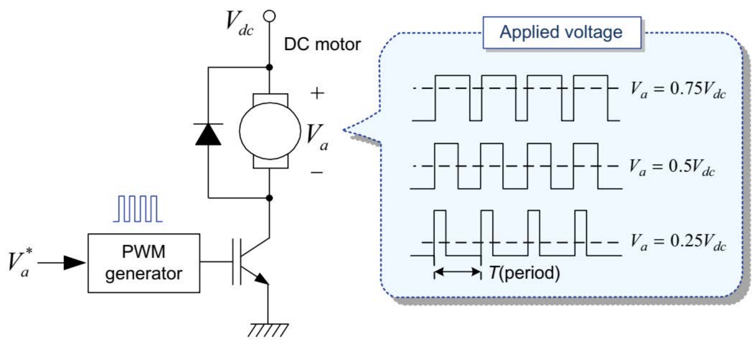

Fig. 2.27

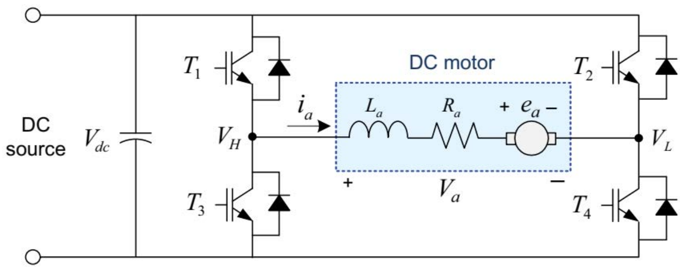

Fig. 2.28

3 ALTERNATING CURRENT MOTORS

3.1 Fundamentals of Induction Motors

3.1.1 Structure of Induction Motors. The structure of a typical induction motor is shown in fig. 3.1. An induction motor has cylindrical stator and rotor configurations, which are separated by a uniform radial air gap. The stator and the rotor are made up of an iron core, which has windings inserted inside. The iron core is not a single solid lump but consists of a stack of insulated laminations of silicon steel, usually with a thickness of about 0.3–0.5 mm to reduce eddy current losses. The iron core is made from a ferromagnetic material such as steel, soft iron, or various nickel alloys to produce magnetic flux efficiently and reduce hysteresis losses.

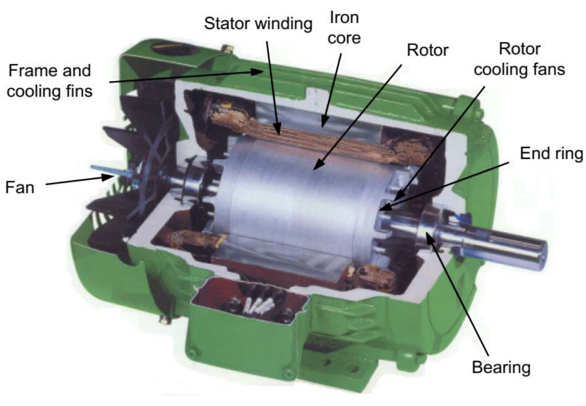

Fig. 3.1

3.1.1.1 In an induction motor, only the stator windings are fed by the three-phase AC power supply. It should be noted that the three-phase stator windings perform the roles of both the armature and field windings of a DC motor. These three-phase windings are placed in the slots that are axially cut along the inner periphery of the iron core as shown in fig. 3.2. They are displaced from each other by 120 electrical degrees along the periphery and are typically connected in delta for low-supply voltage or in wye for high-supply voltage.

The distributed winding configuration of the stator increases the utilization of the iron core and reduces magnetomotive force (mmf) space harmonics, resulting in a lower torque ripple compared to that of the concentrated winding, in which all coils of the phase winding are pla

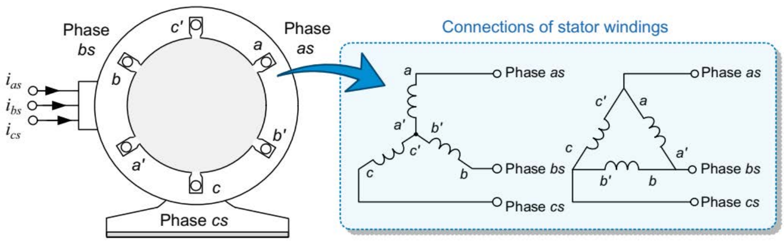

Fig. 3.2

3.1.1.2 There are two types of a rotor used in induction motors: squirrel-cage rotor and wound rotor.

A squirrel-cage rotor has a laminated iron core with slots for placing skewed conductors, which may be a copper, aluminum, or alloy bar. These rotor bars are short-circuited at both ends through end rings as shown in fig. 3.3. The rotor conductors are not placed exactly parallel to the shaft but are skewed by one slot-pitch to reduce cogging torque, and this allows the motor to run quietly. Because of its simple and rugged construction, about 95 % of the induction motors use the squirrel-cage rotor.

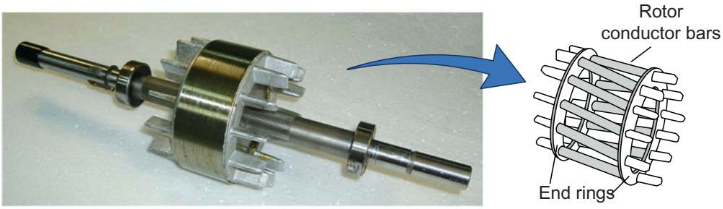

Fig. 3.3

Similar to the windings on a stator, a wound-rotor as shown in fig. 3.4 has a set of three-phase windings, which are usually Y-connected. The rotor windings are tied to the slip rings on the rotor's shaft and thus can be accessible through the brushes.

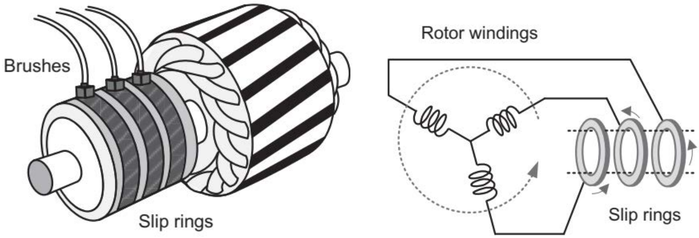

Fig. 3.4

3.1.1.3 Now, we will take a look at the rotating magnetic field, which is the basis for the rotation of AC motors.

The rotating mmf (magnetomotive force) is created by three-phase currents flowing through three-phase stator windings. To begin with, consider an mmf resulting from a current flowing in the winding of phase as as shown in fig. 3.5. We will consider only the centered coil on the magnetic axis of the phase as distributed winding for simplicity. When a current flows in the phase as winding, it will produce a sinusoidally distributed mmf F_{as} centered on its axis. The amplitude of the mmf Fas varies with the instantaneous value of the current as shown in fig. 3.5.

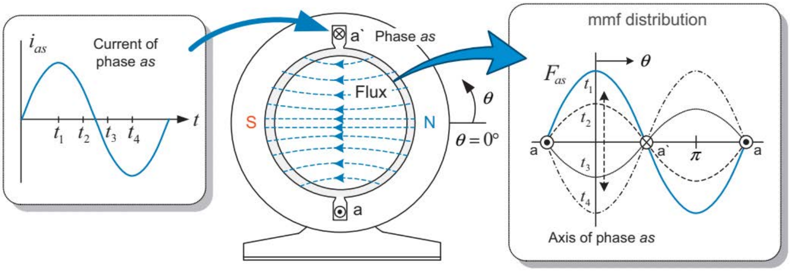

Fig. 3.5

Similarly, the windings of the phase bs and phase cs produce their own mmfs, pulsating along their axes according to their currents as shown in fig. 3.6. If these windings are displaced from each other by 120 electrical degrees in space and are supplied by symmetric three-phase AC sine currents, the vector sum of the three mmfs of these windings becomes a single rotating mmf vector ***F*** in the air gap.

This is called the rotating magnetic field, and its moving speed is directly proportional to the frequency of the currents.

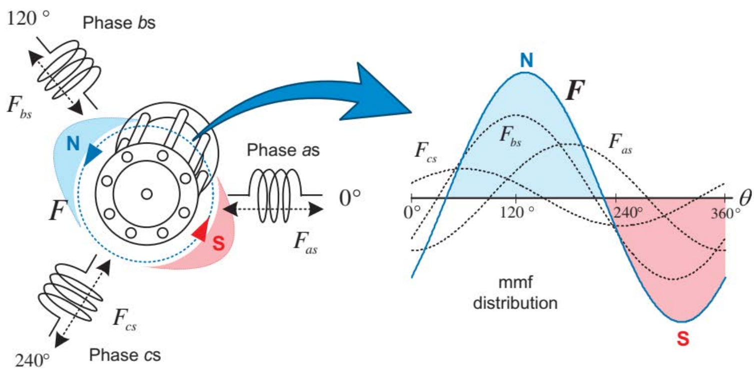

Fig. 3.6

3.1.2 Equivalent Circuit of Induction Motors. To analyze the operating characteristic and performance of an induction motor, we usually use an equivalent circuit based on voltage equations that describe the behavior of the motor.

3.1.2.1 Stator circuit. The voltage equation for the stator windings consists of the voltage drop of the winding resistance $\boldsymbol{R_s}$ and the induced voltage proportional to the rate of change over time of the stator flux linkage $\boldsymbol{\lambda_s}$. Thus the voltage equation for the stator windings is written by

$$v_s = R_s i_s + \frac{d\lambda_s}{dt},$$

where $\boldsymbol{R_s}$ is the resistance of the stator winding and $\boldsymbol{\lambda_s}$ is the flux linkage of the stator winding.

When the stator voltage vs is applied to the stator winding with the effective number of turns N_s, a stator current is flows in the winding. The current is produces a stator mmf N_{sis} and in turn produces a stator flux φ_s in the air gap. Most of the stator flux φ_s crosses the air gap and links to the rotor winding. This air-gap flux is termed mutual flux, which is often called magnetizing flux. Only the mutual flux is contributed to energy conversion, i.e., torque production. However, a small portion of the stator flux cannot cross the air gap but links to only the stator winding itself. This is termed leakage flux.

Thus the stator flux linkage λ_s will be expressed as

$$\lambda_s = N_s\left(\varphi_{ls} + \varphi\right) = N_s\left(\varphi_{ls} + \varphi\right),$$

where $\boldsymbol{\varphi}$ is the magnetizing flux and $\boldsymbol{\varphi_{ls}}$ is the leakage flux.

Here, the flux linkage may be written as

$$\lambda_s = L_{ls} i_s + L_m i_m,$$

where $\boldsymbol{L_{ls}}$ is leakage inductance, $\boldsymbol{L_m}$ is magnetizing inductance, and $\boldsymbol{i_m}$ is magnetizing current.

The voltage equation for the stator windings is written by

$$v_s = R_s i_s + L_{ls}\frac{di_s}{dt} + L_m\frac{di_m}{dt} = R_s i_s + L_{ls}\frac{di_s}{dt} + e_s.$$

Here, $e_s = L_m(di_m/dt)$ is the induced voltage (called back-EMF) in the stator winding.

Based on the resulting voltage equation, the equivalent circuit of the stator winding can be represented as shown in fig. 3.7.

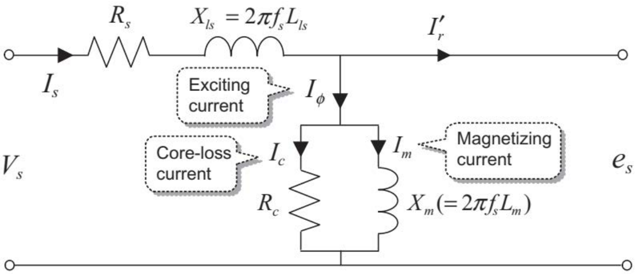

Fig. 3.7

Here, f_s is the frequency of the stator voltage.

To take into account the core loss such as eddy current loss and hysteresis loss, this circuit includes the equivalent resistance R_c representing the core loss. This resistance is connected in parallel with the magnetizing inductance. Accordingly, the exciting current i_φ to produce the flux is comprised of a magnetizing current i_m and a core loss current i_c.

We need to know the induced voltage es to complete the voltage equation. The induced voltage is proportional to the rate of change over time of the stator flux linkage. To obtain the induced voltage, we need to find out the stator flux, which also requires finding of the flux density (fig. 3.8).

The flux density distribution in the air gap can be expressed as

$$B(\theta) = B_{\max}\cos\theta.$$

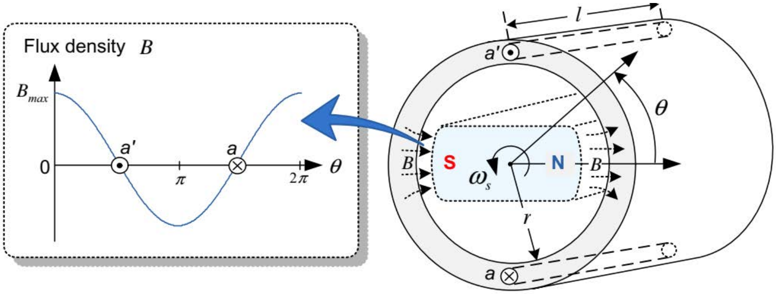

Fig. 3.8

The air-gap flux per pole in the air gap is

$$\varphi = \int_{-\pi/2}^{\pi/2} B(\theta) lrd\theta = 2B_{max} lr,$$

where ***l*** is the axial length of the stator and ***r*** is the radius to the mean of the air gap.

The flux linkage $\boldsymbol{\lambda_a}$ for $\boldsymbol{N_s}$-turn coils of phase as will be the maximum $\boldsymbol{N_{s\varphi}}$ at **θ=0** and zero at **θ=90**. Thus $\boldsymbol{\lambda_a}$ will vary as the cosine of the position angle $\boldsymbol{\theta=\omega_{st}}$ as

$$\lambda_a = N_s \varphi \cos \omega_s t.$$

The voltage induced in the phase as

$$e_a = -\frac{d\lambda_a}{dt} = \omega_s N_s \varphi \sin \omega_s t = E_{\max} \sin \omega_s t.$$

Similarly the voltages induced in the other windings are given by

$$e_b = E_{\max} \sin(\omega_s t - 120°), \quad e_c = E_{\max} \sin(\omega_s t + 120°).$$

The root mean square (rms) value of the induced voltage is

$$E_{rms} = \frac{E_{\max}}{\sqrt{2}} = \frac{\omega_s N_s \varphi}{\sqrt{2}} = 4,44 f_s N_s \varphi,$$

where N_s is the total number of the series turns per phase forming a concentrated full-pitch winding.

A full-pitch winding means that the coil-pitch (i.e., the distance between two sides of a coil) is equal to the pole-pitch (i.e., the distance between two adjacent poles). If the coil-pitch is less than the pole-pitch, then it is called fractional-pitch or short-pitch winding.

3.1.2.2 Rotor Circuit. Next, let us acquire the equivalent circuit of the rotor winding. The rotating magnetic field in the air gap induces voltages in the rotor circuit as well as the stator circuit. This induced voltage becomes the source voltage applied to the rotor circuit. The voltage induced in the rotor circuit can be expressed as

$$E_r = 4{,}44 N_r \varphi K_{\omega r} f_r,$$

where N_r is the total number of turns per phase, $K_{\omega r}$ is the winding factor for the rotor windings, and f_r is the frequency of the voltage induced in the rotor winding.

The induced voltage E_r depends on the rotor speed as

$$E_r = 4{,}44 N_r \varphi K_{\omega r} \times f_r = 4{,}44 N_r \varphi K_{\omega r} \times \left(f_s - f \right).$$

At standstill ($f = 0$), the frequency f_r is the same as the stator frequency f_s. Thus the induced voltage in the rotor winding will be the maximum as

$$E_{r0} = 4{,}44 N_r \varphi K_{\omega r} f_s.$$

Since the rotor winding experiences a flux variation due to the difference in speed between the rotating magnetic field and the rotor, the frequency f_r of the induced voltage in the rotor circuit becomes the difference between the frequency fs of the rotating magnetic field and the rotating frequency f of the rotor.

The slip speed expressed as a fraction of the synchronous speed is called the slip s and can be defined as

$$s = \frac{n_s - n}{n_s}.$$

The frequency $\boldsymbol{f_r}$ in the rotor circuit at the slip $\boldsymbol{s}$ is called the slip frequency and is given as

$$f_r = f_s - f = sf_s.$$

The induced voltages in the rotor circuit at the slip **s** becomes

$$E_r = 4,44 N_r \varphi K_{\omega r} \times f_r = 4,44 N_r \varphi K_{\omega r} \times sf_s = sE_{r0}.$$

The rotor speed is always less than the speed of the stator rotating magnetic field (i.e., the synchronous speed). The difference between the synchronous speed ns and the rotor speed n is called the slip speed.

It should be noted that the slip is a very important factor in the induction motor because most of its performance characteristics of an induction motor, such as the developed torque, current, efficiency and power factor, depends on the operating slip.

The complete equivalent circuit per phase of a three-phase induction motor is shown in fig. 3.9.

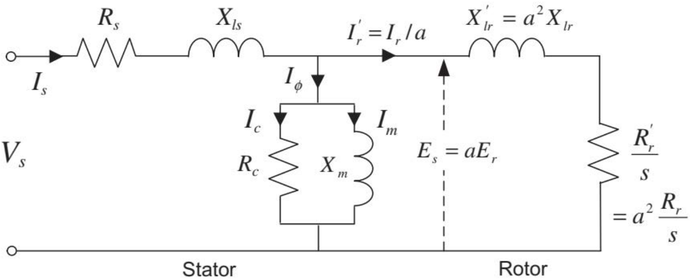

Fig. 3.9

The turns ratio $\boldsymbol{a = N_s / N_r}$ of the stator winding and the rotor winding.

3.1.3 Characteristics of Induction Motors. Now we will discuss the characteristics of an induction motor such as the current, input power factor and output torque.

3.1.3.1 Stator current. The stator current is the input current of an induction motor (fig. 3.9). The input impedance as a function of slip is given as

$$Z_s = R_s + jX_{ls} + \left[X_m / \left(\frac{R_s}{s} + jX_{lr} \right) \right].$$

From the applied stator voltage and the input impedance, the stator current is given as

$$I_s = \frac{V_s}{Z_s} = I_\varphi + I_r.$$

The stator current is the sum of the exciting current $\boldsymbol{I_\varphi}$ and the rotor current $\boldsymbol{I_r}$.

With a constant stator voltage $\boldsymbol{V_s}$, the stator current $\boldsymbol{I_s}$ as a function of speed (i.e., slip $\boldsymbol{s}$) is shown in fig. 3.10 (5-hp, four poles).

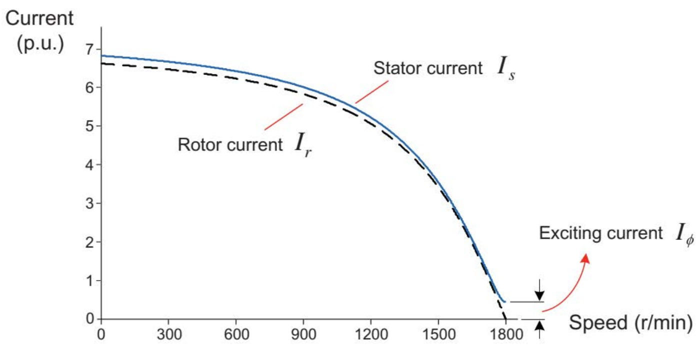

Fig. 3.10

At starting (s=1), since the impedance is minimum, the stator current will be the maximum value, which may be 5–8 times larger than the rated current. As the speed increases, the slip s decreases. As the slip s decreases, the rotor current I_r decreases, and thus the stator current also decreases. At the synchronous speed, i.e., $s = 0$, $R_s = s/N$, so there is no rotor current, i.e., $I_r = 0$. Thus the stator current Is will be equal to the exciting current $I\varphi$.

3.1.3.2 Output Torque. We can derive a general expression for the output torque of an induction motor from the power-flow diagram as shown in fig. 3.11.

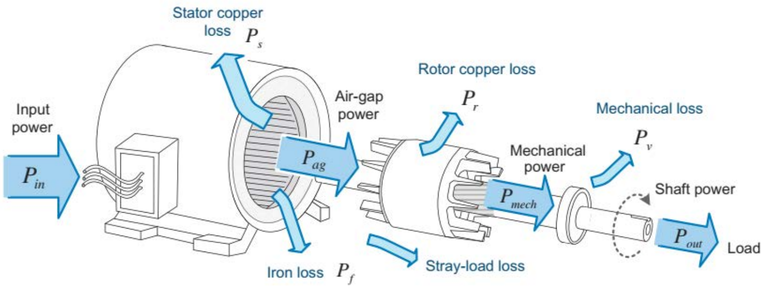

Fig. 3.11

The input power $\boldsymbol{P_{in} = 3V_s I_s \cos\theta_s}$ to an induction motor, excluding the stator losses such as the stator copper loss and the core loss, will be transferred to the rotor across the air gap and then transformed to mechanical power $\boldsymbol{P_{mech}}$.

We can derive the output torque using the mechanical power $\boldsymbol{P_{mech}}$.

The power delivered through the air gap from the stator to the rotor is called the air-gap power $\boldsymbol{P_{ag}}$

$$P_{ag} = I_r^2 \frac{R_r}{s}.$$

It can be divided into two components as

$$P_{ag} = \underbrace{\frac{I_r^2 R_r}{Rotor\,copper\,loss}}_{P_r} + \underbrace{\frac{I_r^2 \frac{R_r}{s}(1-s)}{Mechanical\,output}}_{P_{mech}},$$

$$P_r = I_r R_r = sP_{ag}$$

$$P_{mech} = I_r^2 \frac{R_r}{s}(1-s) = (1-s)P_{ag}.$$

Because the induction motors are operated typically at low slips of 0,01–0,05, the air-gap power is considerably large. This air-gap power P_{ag}, i.e., input power to the rotor, will be dissipated in the resistance R_r of the rotor circuit (i.e., rotor copper loss) and converted into a mechanical output.

The first term on the right-hand side of Equation represents the rotor copper loss P_r. The second term represents the mechanical output power P_{mech} that develops the output toque. We can see that the power distribution depends on the slip s. It is clear that the lower the slip of the motor, the lower the rotor copper loss and the higher the mechanical output power.

The mechanical power is equal to the output torque $\boldsymbol{T_{mech}}$ times the angular frequency $\boldsymbol{\omega_{mech}}$ as

$$P_{mech} = I_r^2 \frac{R_r}{s}(1-s) = T_{mech}\omega_{mech}.$$

Thus the output torque of an induction motor is given by

$$T_{mech} = \frac{P_{mech}}{\omega_{mech}} = \frac{1}{\omega_{mech}} I_r^2 \frac{R_r}{s}(1-s) = \frac{1}{\omega_s} I_r^2 \frac{R_r}{s},$$

where $\boldsymbol{\omega_{mech} = (1-s)\omega_s}$ and $\boldsymbol{\omega_s}$ represents the synchronous angular frequency.

We need to express this torque equation in terms of the input voltage instead of a nonmeasurable rotor current. The rotor current can be easily obtained from the approximate equivalent circuit given in fig. 3.12.

By substituting this rotor current into output torque Equation, the output torque (per phase) is expressed as

$$T_{mech} = \frac{1}{\omega_s} \frac{V_s^2}{\left(R_s + \frac{R_r}{s}\right)^2 + j\left(X_{ls} + X_{lr}\right)^2} \frac{R_r}{s}.$$

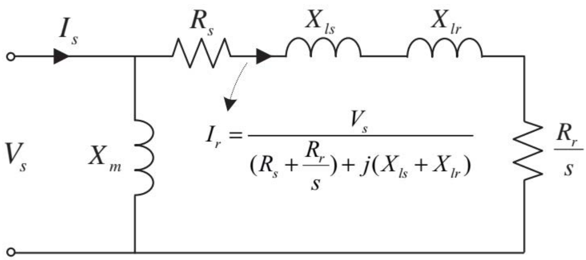

Fig. 3.12

This is the steady-state average torque per phase for a given input voltage V_s, which is a function of the slip. The torque for a given slip is proportional to the square of the stator input voltage.

In the low-slip region, which is the normal operating range of an induction motor, the impedance of equivalent circuit parameters shows the following relations as

$$R_s + \frac{R_r}{s} \gg X_{ls} + X_{lr},$$

$$\frac{R_r}{s} \gg R_s.$$

Thus the equation of torque can be simplified as

$$T_{mech} \approx \frac{1}{\omega_s} \frac{V_s^2}{R_r} s.$$

On the other hand, **in the low-speed range** with larger values of the slip,

$$R_s + \frac{\quad}{\quad} \qquad X_{ls} + X_{lr}$$

Thus the torque varies almost inversely with the slip ***s*** as

$$T_{mech} = \frac{1}{\omega_s} \frac{V_s^2}{\left(X_{ls} + X_{lr}\right)^2} \frac{R_r}{s}.$$

There is a speed at which the maximum torque, often referred to as pull-out torque or **breakdown torque**, is developed. The slip at the maximum torque can be obtained by solving $\boldsymbol{dT_{mech}/ds=0}$ as

$$s_{max} = \frac{R_r}{\sqrt{R_r^2 + \left(X_{ls} + X_{lr}\right)^2}},$$

$$T_{max} = \frac{1}{2\omega_s} \frac{V_s^2}{R_s + \sqrt{R_s^2 + \left(X_{ls} + X_{lr}\right)^2}}.$$

It is important to note that the rotor resistance R_r is an important parameter in determining the slip at which the maximum torque occurs.

The value of the maximum torque is independent of the rotor resistance, which determines the maximum slip value. The speed-torque curve of a typical three-phase induction motor is shown in fig. 3.13. This curve shows the speed versus the output torque when an induction motor is started with full voltage.

The normal operating range of an induction motor is near the synchronous speed, confined to less than 5 % slip. In this low-slip region, the output torque increases linearly with the increasing slip. The slip increases approximately linearly with the increased load, and thus the rotor speed decreases approximately linearly with the load.

As it can be seen from the motion equation

$$T_{motor} - T_{load} = \left(J_{motor} + J_{load}\right) \frac{d\omega}{dt}.$$

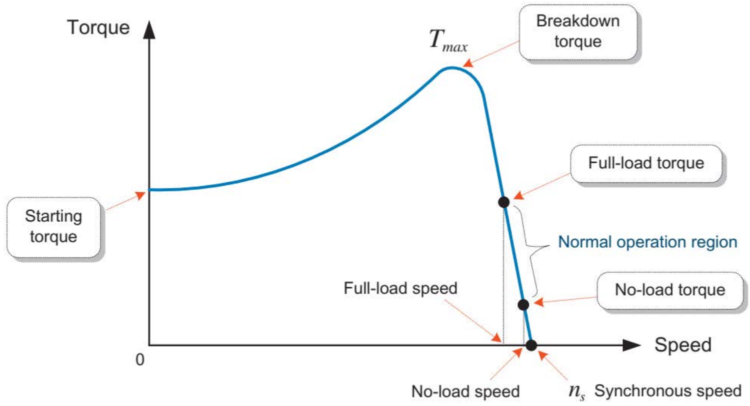

Fig. 3.13

When the motor torque $\boldsymbol{T}_{motor}$ exceeds the load torque $\boldsymbol{T}_{load}$, the motor speed will increase. When the motor torque is less than the load torque, the motor speed will decrease. Thus the equilibrium point will be the speed at which the motor torque equals to the load torque.

Criterion for the stability is given by

$$\frac{d\left(T_{load} - T_{motor}\right)}{d\omega} > 0.$$

When a motor is driving a mechanical load, the motor will operate in a steady state at a speed at which the torque developed by the motor is equal to the torque required by the load.

There are two kinds of an equilibrium operating point: stable point and unstable point. At the stable operating point, the speed will be restored after a small departure from the original equilibrium point due to a disturbance in the input voltage or load. However, at the unstable operating point, the speed will not be restored.

In the induction motor drives, a stable operating point is in the range above the speed at which the maximum torque occurs in the speed-torque curve. As an example, consider fig. 3.14 that shows the speed-torque curve of the induction motor along with two different load curves.

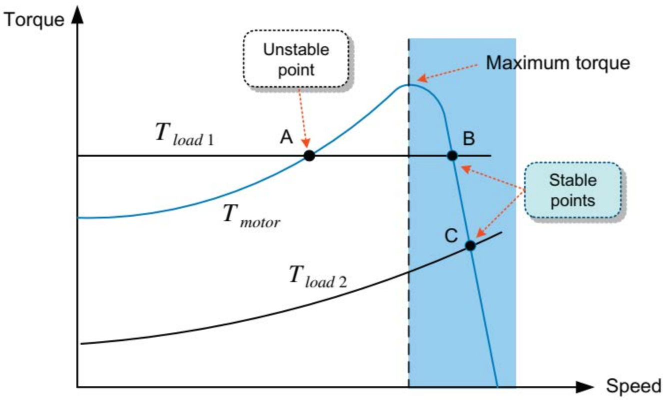

Fig. 3.14

There exist three equilibrium operating points. Among these, point A is an unstable operating point, whereas points B and C are stable operating points. At point A, the system will not be able to maintain its original equilibrium state when there is a disturbance in the drive system. For example, assume that, at point A, there is a reduction in speed caused by a disturbance. In this case, a decrease in the speed causes the motor torque to be less than the load torque. As a result, the system will decelerate and eventually come to a stop. Similarly, an increase in the speed caused by a disturbance will make the motor torque larger than the load torque. Thus the operating point will move from point A to point B. Therefore point A is an unstable operating point. On the contrary, points B and C are stable operating points. At these points, the speed will return to their original points after the deviation in speed by a disturbance

3.1.4 Operating Modes of Induction Motors. An induction motor can be operated in three modes according to its operating speed and rotation direction fig. 3.15 shows the power, operating speed, and torque in the available three operation modes of an induction motor.

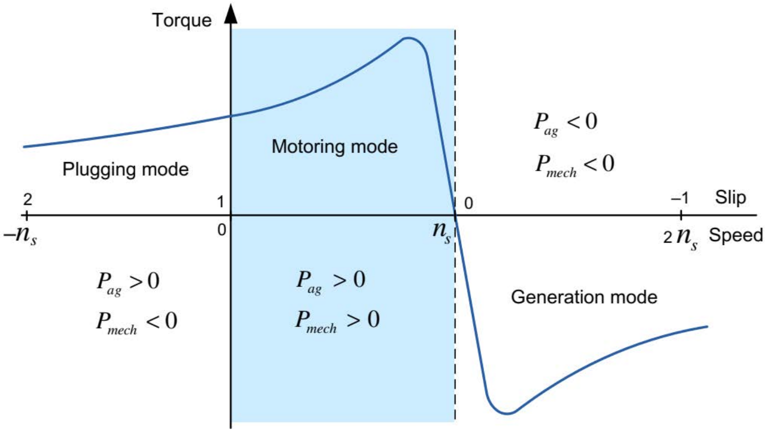

Fig. 3.15

3.1.4.1 Motoring Mode. First, a typical operation of an induction motor is the motoring mode, in which the rotor rotates in the same direction as the stator rotating magnetic field but at a somewhat slower speed. In the motoring mode, the induction motor converts the applied input power into mechanical power through the air gap.

$$P_{ag} = I_r^2 \frac{R_r}{s} > 0, \qquad P_{mech} = (1-s) P_{ag} > 0.$$

3.1.4.2 Generating Mode. In the generating mode the power from the mechanical system flows into the rotor circuit, then across the air gap to the stator circuit and the external electrical system. Thus the induction motor will operate in the generation mode.

This mode may occur when the stator frequency applied to an induction motor is lowered to reduce the speed of the rotor. In this process, the instantaneous speed of the rotor may be higher than the instantaneous synchronous speed because of the inertia of the drive system. This leads to a negative slip, and the direction of the torque developed in the motor will be opposite to the rotation of the rotor. This torque will act as a braking torque that slows down the rotor speed. In this case, the motor operates as a generator, and the generated power is fed back into the power source. This process is called regenerative braking.

$$P_{ag} = I_r \frac{\quad}{\quad} < 0, \qquad P_{mech} = \left(1 - s\right) P_{ag} < 0.$$

3.1.4.3 Plugging Mode. Both powers flow into the rotor and are dissipated in the rotor as heat. Thus the rotor bar may be overheated. This mode can also be used for braking the motor to stop quickly. When an induction motor is running, the direction of the rotation of the stator magnetic field can be reversed by switching any two of the three-phase windings. In this case, the developed torque will be in the direction of the stator magnetic field but opposite to the rotation of the rotor, and the induction motor will operate in the plugging mode.

$$P_{ag} = I_r^2 \frac{R_r}{s} > 0, \qquad P_{mech} = \left(1 - s\right) P_{ag} < 0.$$

3.1.5 Design Types of Induction Motors. The required performance characteristics for a driving motor may be different according to the driven load.

Induction motors can be classified into different designs according to the starting and the normal operating characteristics. For classification of the motor, there are two most widely used standards: National Electrical Manufacture's Association (NEMA) and International Electrotechnical Commission (IEC). The NEMA standards mainly specify four design types: Design A, B, C, and D. Of these, the most widely used are Design B (normal torque) and Design C (high torque). Fig. 3.16 shows the speed-torque curve for the four NEMA designs.

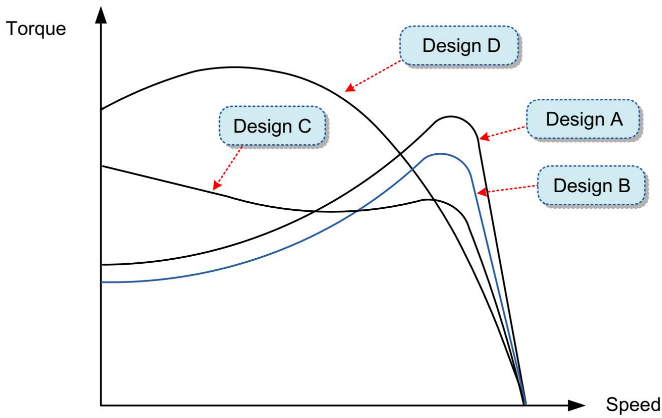

Fig. 3.16

3.1.5.1 Design A. It is characterized by normal starting torque (typically 150–170 % of the rated), high starting current, low operating slip, and high-breakdown torque (the highest of all the NEMA types); common applications include fans, blowers, and pumps.

3.1.5.2 Design B. It is characterized by normal starting torque, low starting current, and low operating slip; common applications being the same as Design A.

Design B is the most commonly used type for general-purpose applications.

3.1.5.3 Design C. It is characterized by high starting torque, low starting current, and higher operating slip than Designs A and B; common applications include compressors and conveyors.

3.1.5.4 Design D. It is characterized by high starting torque (higher than all the NEMA motor types), high starting current, high operating slip (5–13 %), and inefficient operation efficiency for continuous loads; it is commonly used for intermittent loads such as a punch press.

3.2 Speed Control of Induction Motors

The speed control of an induction motor can be classified into two methods as follows:

− Slip control: inefficient, restricted speed control range.

− Synchronous speed control: efficient, wide speed control range.

3.2.1 Slip Control. The torque developed by an induction motor is proportional to the square of the stator voltage as

$$T_{mech} = \frac{1}{\omega_s} \frac{V_s^2}{\left(R_s + \frac{R_r}{s}\right)^2 + j\left(X_{ls} + X_{lr}\right)^2} \frac{R_r}{s} \propto V_s^2 .$$

Traditionally, induction motors have been used as nearly constant speed motors, which are operated by their direct connection to the power grid. However, because of their low cost and ruggedness, the induction motors are also being used for variable speed drives in many applications.

The operating speed of an induction motor depends on the slip or the synchronous speed of the given load.

At a constant stator frequency, the speed of an induction motor can be varied according to the slip. The slip can be changed by varying the stator voltage or the rotor resistance. First, let us take a look at the speed control by changing the stator voltage.

Fig. 3.17 shows the variation of a speed-torque curve with respect to the stator voltage. We can see that the speed control by varying the stator voltage is available only for a limited range. The controllable speed range depends on the value of the slip (i.e., the maximum slip) at which the maximum torque occurs. By comparing fig. 3.17A with B, we can see that the Design C or D motors have a wider speed control range than the Design A or B motors.

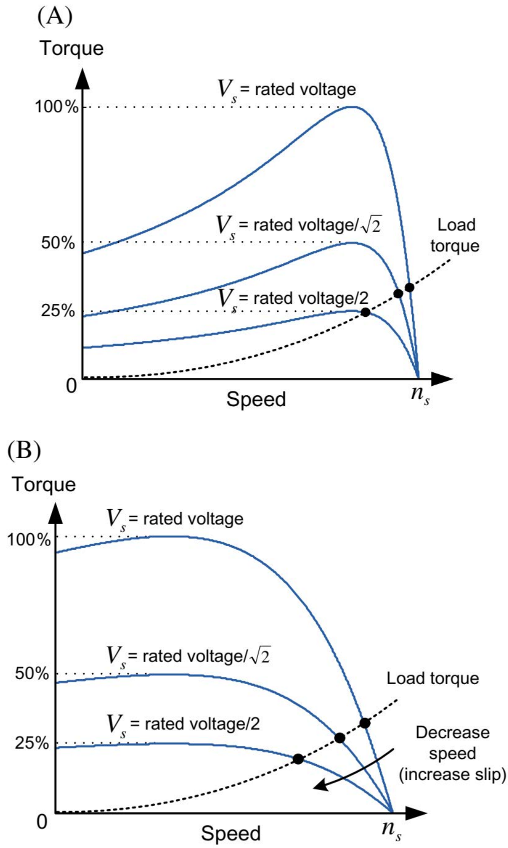

Fig. 3.17

Next, let us examine the speed control by changing the rotor resistance.

To adopt the speed control by changing the rotor resistance, we need to use the wound-rotor type induction motors. The rotor resistance in the wound-rotor type induction motors can be varied by adding an external rheostat or a resistor bank to the rotor windings via the slip rings. Changing the value of the rheostat will change the operating speed of the motor.

The slip at which the maximum torque occurs is proportional to the rotor resistance $\boldsymbol{R_r}$ as

$$s_{max} = \frac{R_r}{\sqrt{R_s^2 + \left(X_{ls} + X_{lr}\right)^2}} \propto R_r.$$

Thus, changing the rotor resistance will alter the shape of the speed-torque curve and in turn, adjust the operating speed of the motor fig. 3.18 shows the speed-torque curves for different rotor resistances.

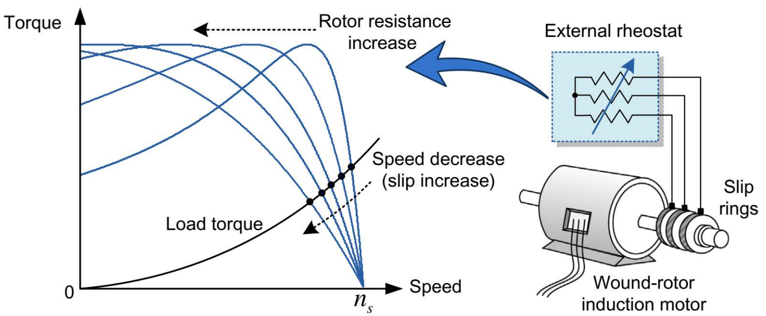

Fig. 3.18

The rotor resistance varying method also gives a limited controllable speed range. Moreover, inserting extra resistances into the rotor circuit seriously reduces the efficiency of the drive.

In the speed control methods of varying the stator voltage or the rotor resistance, the speed is considered to be changed by varying the slip at a constant stator frequency.

The efficiency of induction motors depends on the operating slip, the speed reduction by these methods will lead to a reduction in efficiency. Nevertheless, these speed control methods are applicable to small-sized motors that drive loads requiring a torque proportional to the square of the operating speed such as fans or blowers. For such loads, since the power consumption is reduced significantly according to the reduction in the speed, the reduction in efficiency is relatively small.

3.2.2 Synchronous speed control. The rotor of an induction motor follows the stator magnetic field which rotates at the synchronous speed proportional to the applied stator frequency. Thus, changing the stator frequency is more fundamental to the speed control.

The relationship between the synchronous speed $\boldsymbol{n_s}$ and the stator frequency $\boldsymbol{f_s}$ is

$$n_s = \frac{120 f_s}{P}.$$

The synchronous speed can be altered by changing the number of poles, this requires a complex motor construction. Moreover, it is not possible to provide a continuous change in the synchronous speed. Thus, it is more effective to change the stator frequency. The speed-torque characteristics for a variation in the stator frequency at the rated stator voltage are shown in fig. 3.19.

When changing the stator frequency to adjust the speed, if the stator voltage remains constant, then the stator frequency variations lead to the change of the developed torque as well as the operating speed as shown in fig. 3.19. The explanation is as follows.

At normal operating conditions, since the voltage drop across the stator resistance and leakage reactance are negligible in comparison to the applied voltage, the torque can be simplified as

$$T_{mech} \cong \frac{V_s^2}{\left(\frac{R_r}{s}\right)^2 + \left(\omega_s L_{lr}\right)^2} \frac{R_r}{\omega_s s} = \left(\frac{V_s}{\omega_s}\right)^2 \frac{R_r \omega_{sl}}{R_r^2 + \left(\omega_{sl} L_{lr}\right)^2}.$$

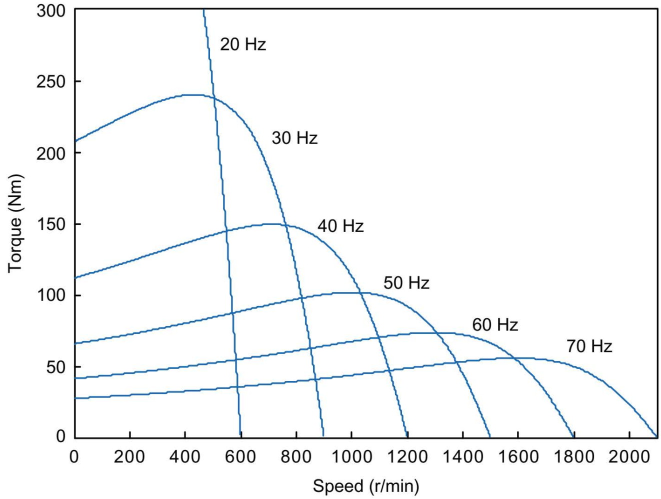

Fig. 3.19

It can be seen that at a fixed stator voltage and slip frequency, the developed torque is inversely proportional to the square of the stator frequency.

The developed torque is proportional to the square of the air-gap flux and thus, is inversely proportional to the square of the stator frequency.

The air-gap flux depends on the ratio of the stator voltage V_s to the stator frequency f_s as

$$\varphi \propto \frac{E_s}{f_s} \approx \frac{V_s}{f_s}.$$

The rotor current is also influenced by the variation of the stator frequency.

Assuming that at normal operating conditions, the stator resistance and leakage reactance are negligible, the rotor current varies inversely with the stator frequency as

$$I_r = \frac{V_s}{\sqrt{\left(\frac{R_r}{s}\right)^2 + \left(X_{lr}\right)^2}} = \left(\frac{V_s}{\omega_s}\right)\frac{\omega_{sl}}{\sqrt{R_r^2 + \left(\omega_{sl} L_{lr}\right)^2}} \propto \frac{1}{f_s}.$$

When adjusting the operating speed by changing the stator frequency, if the stator voltage is varied linearly with the frequency as shown in fig. 3.20, then the air-gap flux **$\varphi \approx V_s/f_s$** will remain constant and thus, the torque and rotor current will remain unchanged.

At low frequencies below a few Hertz, due to the influence from the voltage drop across the stator resistance and leakage reactance, the magnitude of the stator voltage determined by this linear *V*/*f* relationship will be insufficient to keep the magnitude of the air-gap flux constant. This is because the actual air-gap flux φ is not proportional to V_s/f_s, but E_s/f_s. This results in reduction of the air-gap flux and in turn, reduction of the output torque. Thus, for the constant *V*/*f* control at a low operating frequency, we have to boost the stator voltage to compensate for the voltage drop of the stator resistance and leakage reactance as shown in fig. 3.20.

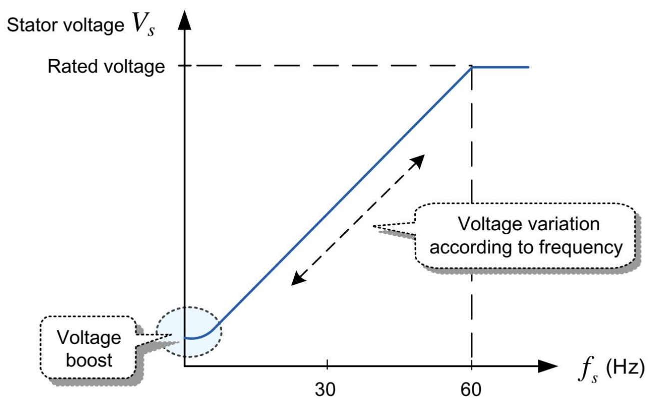

Fig. 3.20

This technique is called **the constant volts per Hertz (*V*/*f*) control**, which has become a popular variable speed drive for induction motors in general-purpose applications today.

The constant *V*/*f* control can be utilized for the speed control below the rated speed. If the stator frequency increases more than the rated frequency, the constant *V*/*f* ratio cannot be maintained due to the limitation of the applied voltage. Thus, for speeds higher than the rated speed, the maximum torque will be reduced due to the reduction in the air-gap flux.

Fig. 3.21 shows the speed-torque characteristics curves for several frequencies under the constant *V*/*f* control. To summarize, under the constant *V*/*f* operation of an induction motor,

– Torque is independent of the stator frequency;

– Rotor current is independent of the stator frequency;

– Synchronous speed is proportional to the stator frequency.

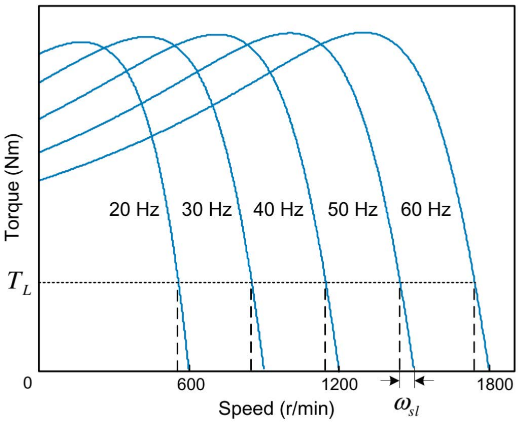

Fig. 3.21

In the induction motor drives with the constant *V*/*f* control, it should be noted that the torque and the rotor current are determined only by the slip angular frequency $\omega_{sl} = s\omega_s$. We can see from fig. 3.21 that the output torque can be produced equally at any speed for the same slip frequency. Thus, even though the speed is reduced by the stator frequency, the operating slip can be kept low so that the efficiency cannot be degraded unlike the slip control. Moreover, at start-up, a high starting torque can be achieved by applying a low stator frequency without requiring a high rotor resistance. After the starting, the stator frequency is increased along with the stator voltage according to the linear *V*/*f* relationship. Up to this point, we have discussed the open-loop speed control by the stator frequency. In the open-loop speed control, however, the steady-state speed can be affected by the load variation because the operating slip frequency depends on the load. In particular, in the low-speed region, the variation of the operating slip frequency may bring about a large error in the steady-state speed. Thus this open-loop speed control needs a proper compensation to offset the speed error according to the load variation. More accurate speed control can be achieved by the closed-loop speed control, which adjusts the slip frequency under the constant *V*/*f* control as the following.

3.2.3 Closed-loop Speed Control by Adjusting the Slip Frequency under Constant *V*/*f* Control. Under the constant *V*/*f* control, the torque of an induction motor can be controlled by adjusting the slip frequency f_r. The torque is rewritten in terms of the slip frequency f_r as

$$T_{mech} = \left(\frac{V_s}{\omega_s}\right)^2 \frac{2\pi f_r R_r}{R_r^2 + \left(2\pi f_r L_{lr}\right)^2}.$$

Since the standard induction motors normally have $\boldsymbol{R_r >> 2\pi f_r L_{lr}}$, if the air-gap flux is constant, then the torque is proportional to the slip frequency $\boldsymbol{f_r}$ as

$$T_{mech} \cong \left(\frac{V_s}{\omega_s}\right)^2 \frac{2\pi}{R_r} f_r.$$

Fig. 3.22 shows the block diagram of the closed-loop speed control system based on torque equation.

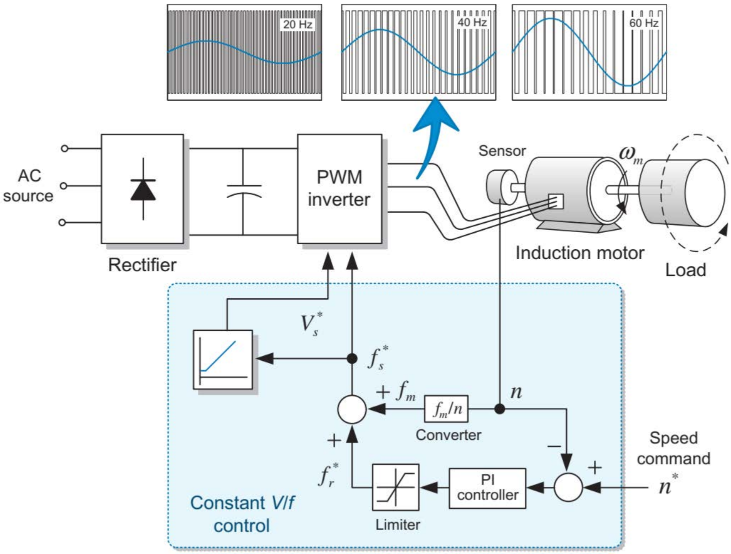

Fig. 3.22

In this speed control system, with the constant *V*/*f* operation, the slip frequency f_r is adjusted so that the actual speed n follows the command speed n^*.

Once the required slip frequency f_r^* is determined in this manner, the stator frequency command can be determined by the sum of the slip frequency and the rotor speed f_m as

$$f_s^* = f_m \pm f_r^*.$$

Since the developed torque of an induction motor can be adjusted by the slip frequency, if the actual speed of the motor is less than its command, then the controller increases the slip frequency to produce a larger torque. On the other hand, if the actual speed is higher than its command, then the controller decreases the slip frequency to reduce the developed torque. In this case, the variation range of the slip frequency should be limited within the maximum slip frequency, at which the breakdown torque occurs.

This speed control scheme for induction motors is widely used in general-purpose drives such as fans, pumps, and conveyors because it can improve the system efficiency and provide a satisfactory starting torque and a satisfactory steady-state performance. This control can give a speed regulation of 1–2 %. However, this control scheme is insufficient to achieve a high dynamic performance.

3.2.4 Operation Regions of Induction Motors. Induction motors have been traditionally used as constant speed motors supplied by the AC power source. However, recently, it has been increasingly used as variable speed motors driven by an inverter. The variable speed induction motor drive can be achieved by controlling the frequency and voltage applied to the motor.

The operation range of an induction motor can be

divided into three regions according to the output torque capability as

− constant torque region: speed range below the base speed;

− constant power region: speed range above the base speed;

− breakdown torque region: speed range above the base speed maintaining the maximum slip frequency.

The speed range above the base speed can be further divided into two subregions: constant power region and breakdown torque region. Because the field flux is reduced for operation in these regions, they are called field-weakening regions. Fig. 3.23 illustrates the output toque characteristic in each region.

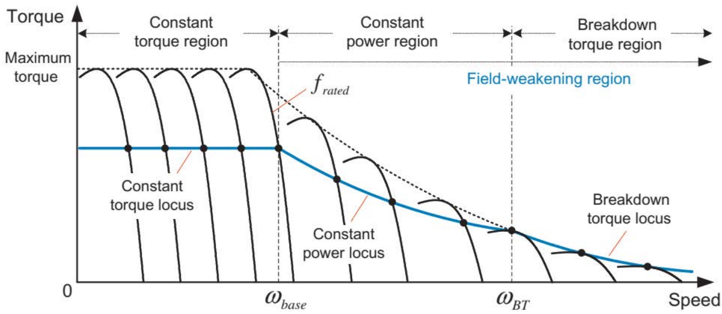

Fig. 3.23

3.2.4.1 Constant torque region. In this region, the motor speed is increased by increasing the stator frequency. To maintain the air-gap flux at a constant value, the applied stator voltage will be increased with the stator frequency according to the linear *V*/*f* relationship. In this control method, since the output torque is proportional to the slip frequency, the output torque can

be produced equally at any speed for the same slip frequency as shown in fig. 3.24.

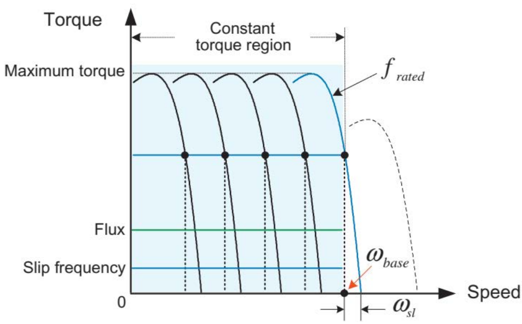

Fig. 3.24

Hence, this speed range is called constant torque region. The maximum torque developed by the induction motor is limited only by the allowable current rating in this region.

3.2.4.2 Constant power region. The induction motor will be operated with a constant voltage in the speed region above the base speed, the air-gap flux as well as the rotor current will decrease as the operating speed increases.

The steady-state equivalent circuit in fig. 3.25 implies that under a constant stator voltage V_s, an increase in the operating frequency causes the reactance to increase, resulting in a decrease of both the exciting current I_φ and rotor current I_r. Therefore the output torque of an induction motor in this region will be different from that in the constant torque region.

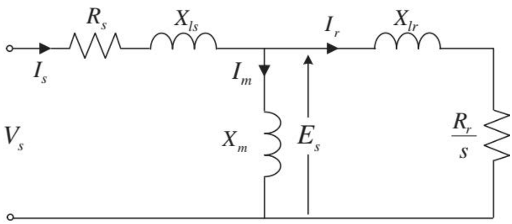

Fig. 3.25

Since the back-electromotive force (back-EMF) of the induction motor increases with the speed, the voltage applied to the motor should also be increased with the speed for the stator current to flow properly. However, since the terminal voltage of the motor should not exceed the rated (or nominal) voltage, the stator voltage cannot be increased above the rated voltage despite the speed increase. The onset speed, at which the terminal voltage of the motor becomes the rated voltage, is called the base speed.

The output torque and the rotor current of an induction motor were given as

$$T_e = 3\frac{1}{\omega_s} I_r^2 \frac{R_r}{s}, \qquad = \frac{E_s}{\left(\frac{}{}\right) \quad jX_{lr}} = \left(\frac{E_s}{}\right) \frac{sl}{\sqrt{R_r + (\omega_{sl} L_{lr})}}$$

The following torque expression as a function of air-gap flux and rotor current can be obtained

$$T_e = 3\left(\frac{E_s}{\omega_s}\right) I_r \frac{R_r}{\sqrt{R_r^2 + \left(\omega_{sl} L_{lr}\right)^2}} \cong K\varphi I_r .$$

Under a constant stator voltage, an increase in the stator frequency leads to a reduction in both the air-gap flux $\varphi \sim E_s/\omega_s$ and the rotor current I_r. Therefore the output torque will decrease in proportion to $1/\omega_s^2$. However, if we make the slip frequency ω_{sl} increase as the stator frequency increases, then the rotor current will remain constant due to the reduced impedance R_r/s by the increase in the slip. In this way, if the rotor current remains constant despite the stator frequency increase, then the developed torque decreases in proportion to $1/\omega_s$, not $1/\omega_s^2$, as shown in fig. 3.26. Thus an enhanced output torque capability can be achieved. Therefore for operation in this region, the slip frequency ω_{sl} should be increased as the stator frequency increases. In this case, since both the voltage and the current remain constant, this region is called the constant power region.

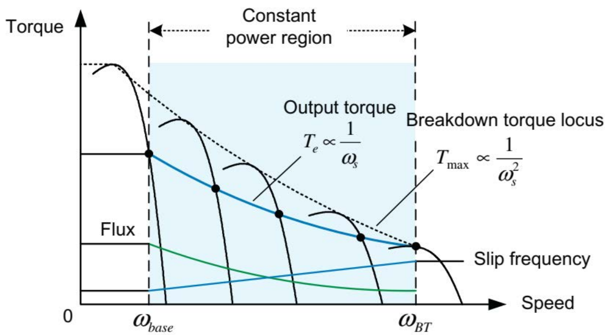

Fig. 3.26

3.2.4.3 Breakdown torque region. In the constant power region, the slip frequency is increased with the speed increase to lower the reduction rate of the output torque. However, there is a limit to increasing the slip frequency because an induction motor has a maximum slip for the stable operation as

$$S_{\max} = \frac{R_r}{\sqrt{R_s^2 + \left(X_{ls} + X_{lr}\right)^2}}.$$

Once the operating slip frequency reaches its maximum value, the rotor current will decrease and, in turn, the output torque will decrease in proportion to $1/\omega_s^2$ as the stator frequency increases. Since the current will be decreased, the input power will not remain constant. In this case, an induction motor will be operated at the maximum slip for producing the breakdown torque. Thus this region is called the breakdown torque region.

Fig. 3.27 depicts characteristics such as voltage, current, developed output torque, flux, and slip frequency over the overall speed range. The curve, which shows the output torque capability versus the speed, is called the capability curve of an induction motor.

The base speed, at which the constant power region starts, does not usually coincide with the rated speed and varies with the available voltage, operating current, flux level, and load condition. The range of the constant power region depends on the maximum value of the slip frequency. As can be seen from equation for Smax, this maximum slip frequency is a function of leakage inductance, and thus, its range depends on the total leakage inductance, $X_{ls}+X_{lr}$. For a standard induction motor, this value is normally 0.2 p.u., producing a constant power range up to two to three times the rated speed. By contrast, induction motors for high-speed drives often have a constant power region range over four times the rated speed.

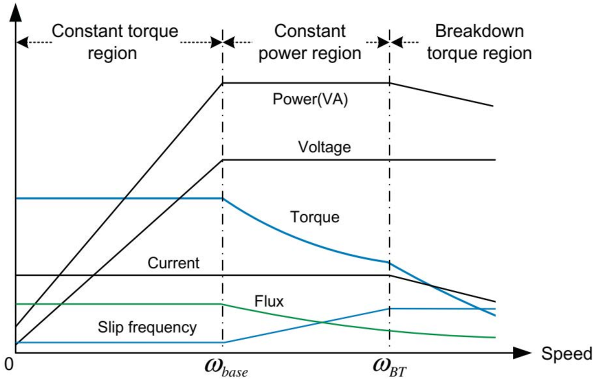

Fig. 3.27

3.3 Synchronous Motors

The name synchronous motors stems from its characteristic to develop the torque only when the rotor operates at the synchronous speed. Traditionally, large-sized synchronous machines have been mainly used as generators. As motors, they have been used to improve the power factor in the power grid by changing the field current, i.e., excitation. In this case, they are called synchronous condensers. In small sizes, they have been often used in applications requiring a constant speed operation.

However, recently, synchronous motors with a permanent magnet rotor are growing rapidly in use for variable speed drives instead of DC motors. This is because permanent magnet synchronous motors (PMSMs) have many advantages over other motors such as high efficiency, high power density, high dynamic response, and high power factor. However, one disadvantage is its higher cost in comparison to an induction motor. In this section, we will study the basic performance characteristics of the synchronous motor under steady-state conditions.

The structure of the stator and rotor of a synchronous motor is shown fig. 3.28 ((A) Cylindrical type, (B) salient pole type, and (C) stator windings).

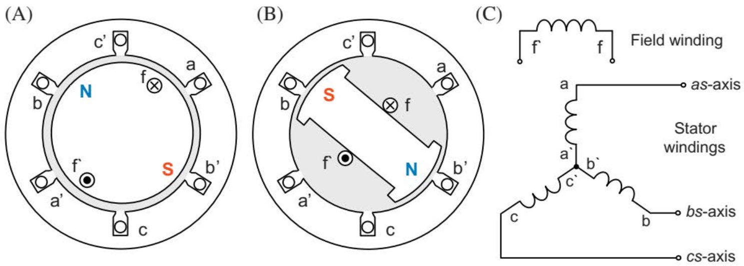

Fig. 3.28

A synchronous motor has the same stator configuration as an induction motor, but a different rotor structure. Unlike an induction motor, a synchronous motor has independent excitations for the stator and rotor windings, i.e., AC excitation to the stator winding and DC excitation to the rotor winding. The function of the stator winding, which is commonly called an armature winding, is to generate a rotating magnet field through its connection to a three-phase AC power source such as an induction motor. The rotor winding, which is called the field winding, generates a field flux with a DC excitation or by a permanent magnet.

There are two types of rotor construction: **cylindrical** (or nonsalient pole) type and **salient pole** type. A salient pole rotor is normally used for low-speed applications such as hydroelectric generators, while a cylindrical rotor is normally used in high-speed applications such as steam or gas turbine generators.

3.3.1 Cylindrical Rotor Synchronous Motors. Since the rotor winding with a DC excitation can be represented as a simple *R*-*L* circuit without back-EMF, we need to discuss an equivalent circuit for only the stator winding.

The stator windings of a synchronous motor are the same as those of an induction motor. Thus, the stator voltage equation of a synchronous motor is given as

$$\upsilon_s = R_s i_s + \frac{d\lambda_s}{dt}.$$

However, since the stator flux linkage of a synchronous motor is different from those of an induction motor, we need to examine the stator flux linkage $\boldsymbol{\lambda}_s$.

A synchronous motor has independent excitations for the stator and rotor windings. In the air gap, these excitations generate two magnetic fields which rotate at the synchronous speed as shown in fig. 3.29. One is generated by the stator winding currents as in an induction motor, and the other is generated by the field winding current. In synchronous motors, the torque is produced by the interaction of these two magnetic fields.

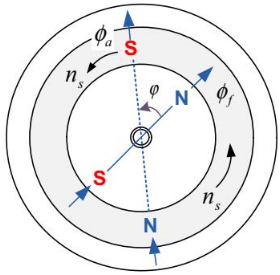

Fig. 3.29

The rotating field flux $\boldsymbol{\varphi}_a$ generated by the three-phase AC currents $\boldsymbol{I}_s$ flowing in the stator winding consists of the armature reaction flux $\boldsymbol{\varphi}_{ar}$ and the leakage flux $\boldsymbol{\varphi}_{al}$ as

$$\varphi_a = \varphi_{ar} + \varphi_{al}.$$

The armature reaction flux $\boldsymbol{\varphi}_{ar}$ corresponds to the magnetizing flux in the induction motor. The field flux $\boldsymbol{\varphi}_f$ generated in the field winding is also a rotating magnetic field rotating at the synchronous speed because the rotor itself rotates at the synchronous speed. In the air gap, there is a resultant of these two field fluxes as

$$\varphi_s = \varphi_f + \varphi_{ar}.$$

Thus the flux linkage $\boldsymbol{\lambda_s}$ of the stator winding with an effective number of turns $\boldsymbol{N_s}$ will be expressed as

$$\lambda_s = N_s\left(\varphi_f + \varphi_{ar}\right).$$

In the stator winding, the voltage is induced by these two fluxes. The voltage $\boldsymbol{E_f}$ induced by the field flux $\boldsymbol{\varphi_f}$ is called the excitation voltage as shown in fig. 3.30. The magnitude of the excitation voltage is proportional to the field current and the rotor speed.

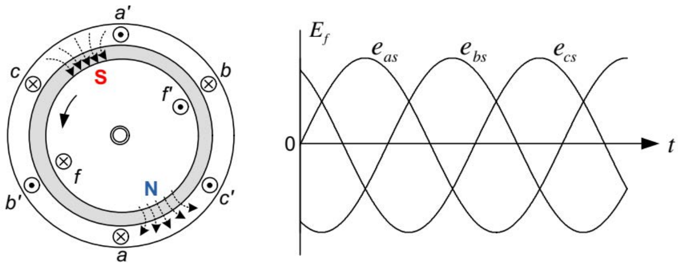

Fig. 3.30

The total induced voltage in the stator winding is the sum of these two induced voltages as

$$E_s = E_f + E_{ar}.$$

The voltage $\boldsymbol{E_{ar}}$ induced by the armature reaction flux $\boldsymbol{\varphi_{ar}}$ is called the armature reaction voltage.

Here, the armature reaction voltage $\boldsymbol{E_{ar}}$ lags the armature reaction flux $\boldsymbol{\varphi_{ar}}$ by 90°, so it can be expressed in terms of the armature reaction reactance $\boldsymbol{X_{ar}}$ as

$$E_{ar} = I_a jX_{ar}.$$

Considering the total induced voltage, the voltage drop of the stator resistance $\boldsymbol{R_s}$, and leakage reactance $\boldsymbol{X_{al}}$, the stator voltage equation

$$V_s = I_s R_s + I_s jX_{al} + E_s = I_s R_s + I_s jX_{al} + I_s jX_{ar} + E_f =$$
$$= I_s R_s + I_s jX_s + E_f = I_s Z_s + E_f,$$

where $\boldsymbol{X_s = X_{ar} + X_{al}}$ is the synchronous reactance and $\boldsymbol{Z_s = R_s + jX_s}$ is the synchronous impedance.

The complete per phase equivalent circuit of a cylindrical rotor synchronous motor under the steady-state condition is shown in fig. 3.31.

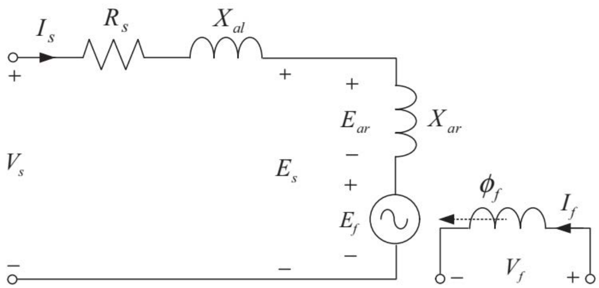

Fig. 3.31

The input power of a synchronous motor is given by

$$P = 3V_s I_s \cos\theta,$$

where $\boldsymbol{\theta}$ is the phase angle between the stator voltage $\boldsymbol{V_s}$ and the stator current $\boldsymbol{I_s}$ (fig. 3.32).

The torque of a cylindrical rotor synchronous motor is obtained by dividing the output power by the synchronous speed ω_s.

The phase angle δ between the stator voltage V_s and the excitation voltage E_f is an important factor of power transfer and stability in synchronous machines and is usually termed the power angle (or load angle). For motoring operation, this angle δ is also called the torque angle, and the stator voltage V_s is ahead of the excitation voltage E_f. The angle δ acts as the slip in an induction motor. The angle δ increases with the increased load.

This angle can also be regarded as the difference angle between the stator and the rotor rotating magnetic fields. In motoring operation, the stator magnetic field is ahead of the rotor magnetic field. The power and torque for synchronous machines are usually expressed as a function of the stator voltage, excitation voltage and their angle δ.

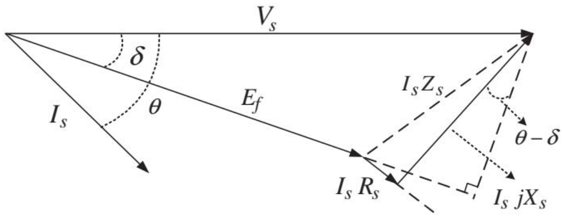

Fig. 3.32

From the phasor diagram shown in fig. 3.32, we have

$$V_s \cos\delta = E_f + I_s X_s \sin(\theta - \delta) + I_s R_s \cos(\theta - \delta),$$

$$V_s \sin\delta = I_s X_s \cos(\theta - \delta) - I_s R_s \sin(\theta - \delta).$$

If the stator winding resistance $\boldsymbol{R_s}$ is neglected, then we can readily obtain

$$I_s \cos\theta = \frac{E_f \sin\delta}{X_s}.$$

The power is expressed by

$$P = 3\frac{V_s E_f}{X_s} \sin\delta = P_{\max} \sin\delta.$$

Thus the developed torque is obtained by dividing the output power by the synchronous speed $\boldsymbol{\omega_s}$ as

$$T = \frac{P}{\omega_s} = 3\frac{V_s E_f}{\omega_s X_s} \sin\delta = T_{\max} \sin\delta.$$

The output power and the torque vary as a sine of the torque angle **δ** as shown in fig. 3.33.

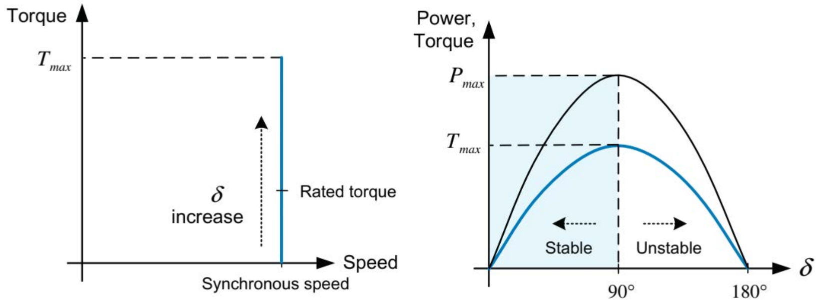

Fig. 3.33

The maximum torque occurs at a torque angle of 90 electrical degrees. This is called the pull-out torque, which indicates the maximum value of torque that a synchronous motor can develop without pulling out of synchronism. In general, its value varies from 1.25 to 3.5 times the full-load torque. In actual practice, however, the motor will never operate at a torque angle close to 90 electrical degrees because the stator current will be many times its rated value at this operation.

3.3.2 Salient Pole Rotor Synchronous Motors. As we can see in fig. 3.34, a salient pole synchronous motor has a nonuniform air gap due to the protruding rotor poles.

In this type of motor, the amount of the flux produced by the stator current varies according to the position of the rotor. A higher flux is generated along the poles in comparison to between the poles because the reluctance of the flux path is low along the poles and high between the poles.

To consider the saliency of the rotor in a synchronous motor model, we need to define the *d* and *q* axes as the following. The d-axis is defined as the axis along the poles, which is also the direction of the rotor flux produced by the field winding. The reluctance of the d-axis path is low due to the small air gap, and thus the inductance L_d of the d-axis is large. On the other hand, the q-axis is defined as the axis between the poles, which is also the direction of the excitation voltage. The reluctance of the q-axis path is large due to the large air gap, and so the inductance L_q of the q-axis is small. Thus, $L_d > L_q$.

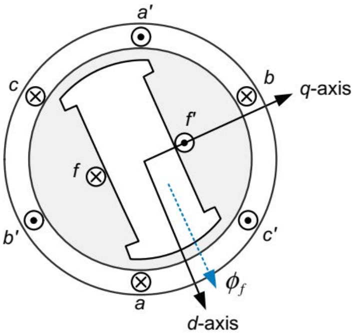

Fig. 3.34

The stator current $\boldsymbol{I_s}$ is expressed as

$$I_s = I_q - jI_d,$$

where $\boldsymbol{I_q = I_s \cos\phi}$, $\boldsymbol{I_d = I_s \sin\phi}$, and ϕ is the phase angle between $\boldsymbol{I_q}$ and $\boldsymbol{I_d}$.

The d and q axes synchronous reactances are given by

$$X_d = X_{ad} + X_{al},$$

$$X_q = X_{aq} + X_{al},$$

where $\boldsymbol{X_{al}}$ is the armature leakage reactance. The salient pole synchronous motor always $\boldsymbol{X_d > X_q}$, normally $\boldsymbol{X_q = (0{,}5\sim0{,}8)X_d}$.

The voltage equation of the salient pole rotor synchronous motor can be expressed by

$$V_s = I_s R_s + I_d jX_d + I_q jX_q + E_f.$$

In order to consider the flux variation with the position of the rotor, it is more effective to analyze the saliency of the rotor by using the divided stator current into two components of the current I_d aligned with the d-axis and the current I_q aligned with the q-axis.

According to the d and q axes currents, the armature reaction flux φ_{ar} is also divided into two components: the d-axis flux φ_d produced by the d-axis current I_d and the q-axis flux φ_q by the q-axis current I_q. The relation between φ_d and I_d is expressed by the d-axis armature reactance X_{ad}, whereas the relation between φ_q and I_q is expressed by the q-axis armature reactance X_{aq}.

The equivalent circuit of the salient pole rotor synchronous motor is shown in fig. 3.35.

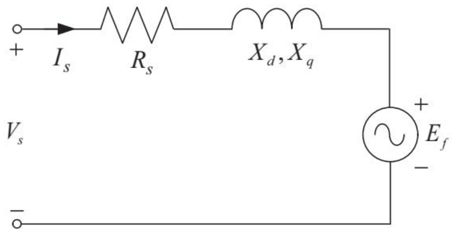

Fig. 3.35

The input power in terms of *d*-*q* axes currents, I_d and I_q, can be expressed as

$$P = 3V_sI_s\cos\theta = 3V_sI_s\cos(\varphi+\delta) = 3V_sI_s(\cos\varphi\cos\delta - \sin\varphi\sin\delta) =$$

$$= 3V_s(I_q\cos\delta - I_d\sin\delta).$$

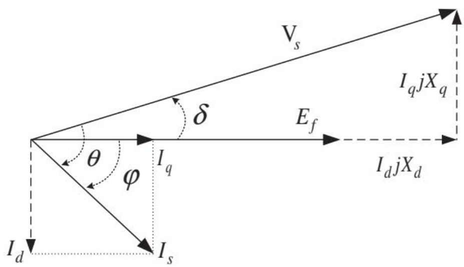

Fig. 3.36

From this phasor diagram, we have

$$V_s\cos\delta = E_f + I_dX_d, \qquad V_s\sin\delta = I_qX_d.$$

The output power and the torque are given by

$$P = 3\frac{V_sE_f}{X_s}\sin\delta + 3\frac{V_s^2(X_d - X_q)}{2X_dX_q}\sin 2\delta.$$

A salient pole synchronous motor has two torque components: electromagnetic torque $\boldsymbol{T_f}$ due to the field flux of the rotor and reluctance torque $\boldsymbol{T_r}$ due to the saliency of the rotor

$$T = \frac{P}{\omega_s} = \frac{3\dfrac{V_s E_f}{\omega_s X_s}\sin\delta + 3\dfrac{V_s^2\left(X_d - X_q\right)}{2\omega_s X_d X_q}\sin 2\delta}{\text{Electromagnetic torque}\,T_f + \text{Reluctance torque}\,T_r}.$$

Fig. 3.37 shows the output torque according to the torque angle δ. Because of this reluctance torque, a synchronous motor with the salient pole rotor can produce more torque than a synchronous motor with the cylindrical rotor. In addition, this motor has the output torque to drive a load even if the field current is zero. Due to the reluctance torque, the torque angle δ at which the pullout torque occurs is less than 90 electrical degrees.

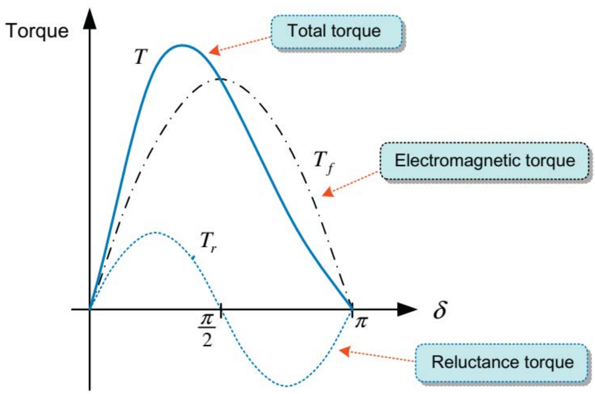

Fig. 3.37

4 MODELING OF ALTERNATING CURRENT MOTORS

For a proper control of a motor, we need to analyze its dynamic performance as well as steady-state performance. This requires a mathematical model, which describes the behavior of a motor. The motor model can be mainly expressed by the voltage and torque equations.

4.1 Modeling of Induction Motor

Consider a three-phase, two-pole induction motor as shown in fig. 4.1.

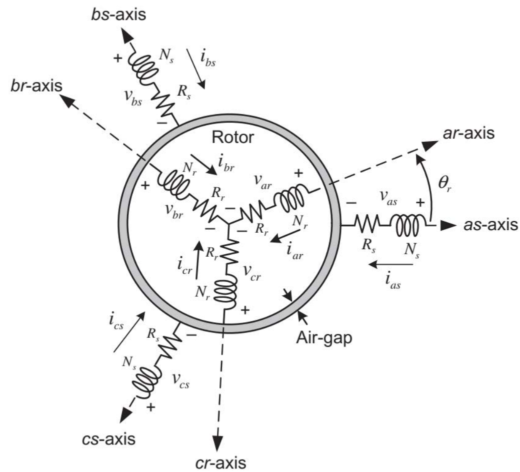

Fig. 4.1

Assume that the stator windings have a number of effective turns N_s, resistance R_s, leakage inductance L_{ls}, and self-inductance L_s. Similarly, the equivalent rotor windings have a number of effective turns N_r, resistance R_r, leakage inductance L_{lr}, and self-inductance L_r. θ_r is the angular displacement between the stator and rotor axes. Here, we will not consider the nonideal characteristics such as the saturation of iron core, slots effect, and cogging torque. Although these are identical sinusoidal distributed windings, each displaced by 120, we will consider only the centered coil of each phase for simplicity.

Since an induction motor has six windings, we can express it by six voltage equations.

$$v_{as} = R_s i_{as} + \frac{d\lambda_{as}}{dt}, \qquad v_{bs} = R_s i_{bs} + \frac{d\lambda_{bs}}{dt},$$

$$v_{cs} = R_s i_{cs} + \frac{d\lambda_{cs}}{dt}, \qquad v'_{ar} = R' i'_{ar} + \frac{d\lambda'_{ar}}{dt},$$

$$v'_{br} = R' i'_{br} + \frac{d\lambda'_{br}}{dt}, \qquad v'_{cr} = R' i'_{cr} + \frac{d\lambda'_{cr}}{dt},$$

where $\boldsymbol{v}_{as}$; $\boldsymbol{v}_{bs}$; $\boldsymbol{v}_{cs}$ are the stator voltages, $\boldsymbol{i}_{as}$; $\boldsymbol{i}_{bs}$; $\boldsymbol{i}_{cs}$ are the stator currents, $\boldsymbol{v'}_{ar}$; $\boldsymbol{v'}_{br}$; $\boldsymbol{v'}_{cr}$ are the rotor voltages, $\boldsymbol{I'}_{ar}$; $\boldsymbol{I'}_{br}$; $\boldsymbol{I'}_{cr}$ are the rotor currents, $\boldsymbol{\lambda}_{as}$; $\boldsymbol{\lambda}_{bs}$; $\boldsymbol{\lambda}_{cs}$ are the stator flux linkages, and $\boldsymbol{\lambda}_{ar}$; $\boldsymbol{\lambda}_{br}$; $\boldsymbol{\lambda}_{cr}$ are the rotor flux linkages. Here, the primed variables denote the rotor variables that are referred to the stator by considering the turns ratio of the two windings. From this point on, we will skip the prime symbol (‘).

To solve the voltage equations, we need to know the flux linkage of each winding. Since there are six windings, one winding will be linked by not only the flux produced by its own winding current but also the flux produced by the current flowing in the other five windings.

For example, the total flux linkage λ_{as} of the phase as winding shown in fig. 4.2.

$$\lambda_{as} = \lambda_{asas} + \lambda_{asbs} + \lambda_{ascs} + \lambda_{asar} + \lambda_{asbr} + \lambda_{ascr} =$$

$$= L_{asas} i_{as} + L_{asbs} i_{bs} + L_{ascs} i_{cs} + L_{asar} i_{ar} + L_{asbr} i_{br} + L_{ascr} i_{cr}$$

where the flux linkage $\boldsymbol{\lambda}_{xsys}$ represents the flux, which is produced by the current $\boldsymbol{i}_{ys}$ flowing in the y_s winding and links the x_s winding.

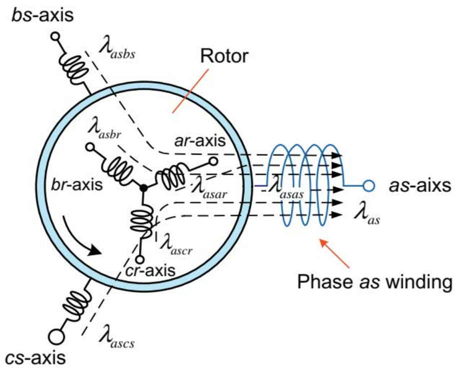

Fig. 4.2

Six flux linkages in the stator and rotor windings can be written by

$$\begin{bmatrix} \lambda_{as} \\ \lambda_{bs} \\ \lambda_{cs} \\ \lambda_{ar} \\ \lambda_{br} \\ \lambda_{cr} \end{bmatrix} = \begin{bmatrix} \lambda_{asas} & \lambda_{asbs} & \lambda_{ascs} & \lambda_{asar} & \lambda_{asr} & \lambda_{ascr} \\ \lambda_{bsas} & \lambda_{bsbs} & \lambda_{bscs} & \lambda_{bsar} & \lambda_{bsbr} & \lambda_{bscr} \\ \lambda_{csas} & \lambda_{csbs} & \lambda_{csbs} & \lambda_{csar} & \lambda_{csbr} & \lambda_{cscr} \\ \lambda_{aras} & \lambda_{arbs} & \lambda_{arcs} & \lambda_{arbr} & \lambda_{arbr} & \lambda_{arcr} \\ \lambda_{bras} & \lambda_{brbs} & \lambda_{brcs} & \lambda_{brar} & \lambda_{brbr} & \lambda_{brcr} \\ \lambda_{cras} & \lambda_{crbs} & \lambda_{crcs} & \lambda_{crar} & \lambda_{crbr} & \lambda_{crbcr} \end{bmatrix} =$$

$$= \begin{bmatrix} L_{asas} & L_{asbs} & L_{ascs} & L_{asar} & L_{asr} & L_{ascr} \\ L_{bsas} & L_{bsbs} & L_{bscs} & L_{bsar} & L_{bsbr} & L_{bscr} \\ L_{csas} & L_{csbs} & L_{csbs} & L_{csar} & L_{csbr} & L_{cscr} \\ L_{aras} & L_{arbs} & L_{arcs} & L_{arbr} & L_{arbr} & L_{arcr} \\ L_{bras} & L_{brbs} & L_{brcs} & L_{brar} & L_{brbr} & L_{brcr} \\ L_{cras} & L_{crbs} & L_{crcs} & L_{crar} & L_{crbr} & L_{crbcr} \end{bmatrix} \begin{bmatrix} i_{as} \\ i_{bs} \\ i_{cs} \\ i_{ar} \\ i_{br} \\ i_{cr} \end{bmatrix}$$

These inductances are largely divided into four groups as

$$\begin{bmatrix} \lambda_{abcs} \\ \lambda_{abcr} \end{bmatrix} = \begin{bmatrix} L_s & L_{sr} \\ (L_{sr})^T & L_r \end{bmatrix} \begin{bmatrix} i_{abcs} \\ i_{abcr} \end{bmatrix},$$

where $\boldsymbol{L_s}$ and $\boldsymbol{L_r}$ represent the inductance matrix of the stator and rotor windings, and $\boldsymbol{L_{sr}}$ represents the mutual-inductance matrix between the stator and rotor windings.

The flux produced by each winding can be separated into two components: the leakage flux which links only its own winding and the magnetizing flux which links both its own winding and the other windings.

4.1.1 Stator Windings. The stator inductance matrix $\boldsymbol{L_s}$ as shown in fig. 4.3 consists of the selfinductances of each stator winding and the mutual-inductance between the stator windings as

$$\boldsymbol{L_s} = \begin{bmatrix} L_{asas} & L_{asbs} & L_{ascs} \\ L_{bsas} & L_{bsbs} & L_{bscs} \\ L_{csas} & L_{csbs} & L_{cscs} \end{bmatrix}$$

Stator self-inductance

Stator mutual-inductance

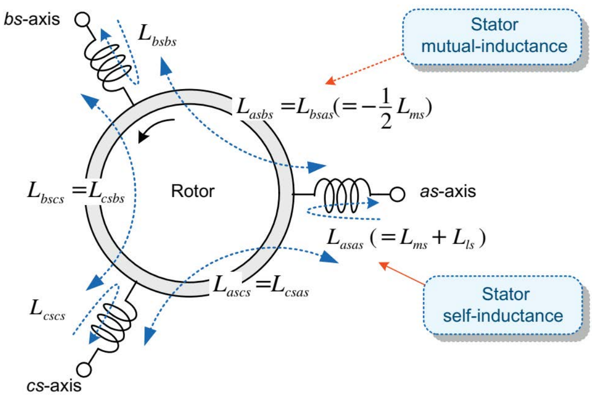

Fig. 4.3

Thus the stator self-inductances $\boldsymbol{L_{asas}}$; $\boldsymbol{L_{bsbs}}$; $\boldsymbol{L_{cscs}}$ consist of the leakage inductance $\boldsymbol{L_{ls}}$ and the magnetizing inductance $\boldsymbol{L_{ms}}$ as

$$L_{asas} = L_{bsbs} = L_{cscs} = L_{ls} + L_{ms},$$

where $L_{ms} = \mu_0 N_s^2 \left(rl/g\right)\left(\pi/4\right)$, $\boldsymbol{\mu_0}$ is the permeability of air, $\boldsymbol{l}$ is the axial length of the air gap, and $\boldsymbol{r}$ is the radius to the mean of the air gap.

$$L_{asbs} = L_{ascs} = L_{bsas} = L_{bscs} = L_{csas} = L_{csbs} = L_{ms}\cos\left(\frac{2\pi}{3}\right) = -\frac{1}{2}L_{ms}.$$

The inductances of the stator windings are given by

$$L_s = \begin{bmatrix} L_{asas} & L_{asbs} & L_{ascs} \\ L_{bsas} & L_{bsbs} & L_{bscs} \\ L_{csas} & L_{csbs} & L_{cscs} \end{bmatrix} = \begin{bmatrix} L_{ls} + L_{ms} & -\dfrac{L_{ms}}{2} & -\dfrac{L_{ms}}{2} \\ -\dfrac{L_{ms}}{2} & L_{ls} + L_{ms} & -\dfrac{L_{ms}}{2} \\ -\dfrac{L_{ms}}{2} & -\dfrac{L_{ms}}{2} & L_{ls} + L_{ms} \end{bmatrix}.$$

4.1.2 Rotor Windings. The rotor inductance matrix L_r as shown in fig. 4.4 consists of the self-inductances of each rotor windings and the mutual-inductance between these windings as

The rotor self-inductances $\boldsymbol{L_{arar}}$; $\boldsymbol{L_{brbr}}$; $\boldsymbol{L_{crcr}}$ consist of the leakage inductance $\boldsymbol{L_{lr}}$ and the magnetizing inductance $\boldsymbol{L_{mr}}$ as

$$L_{arar} = L_{brbr} = L_{crcr} = L_{lr} + L_{mr},$$

where $L_{mr} = \mu_0 N_r^2 \left(rl/g\right)\left(\pi/4\right) = \left(N_r/N_s\right)^2 L_{ms}$.

$$L_{arbr} = L_{arcr} = L_{brar} = L_{brcr} = L_{crar} = L_{crbr} = L_{mr}\cos\left(\frac{2\pi}{3}\right) =$$

$$= -\frac{1}{2}L_{mr} = -\frac{1}{2}\left(\frac{N_r}{N_s}\right)^2 L_{ms},$$

where N_r/N_s is the turns ratio of the stator and rotor windings.

The inductances of the rotor windings are given by

$$L_r = \begin{bmatrix} L_{arar} & L_{arbr} & L_{arcr} \\ L_{brar} & L_{brbr} & L_{brcr} \\ L_{crar} & L_{crbr} & L_{crcr} \end{bmatrix} = \begin{bmatrix} L_{ls} + n^2 L_{ms} & -n^2 \frac{L_{ms}}{2} & -n^2 \frac{L_{ms}}{2} \\ -\frac{L_{ms}}{2} & L_{ls} + n^2 L_{ms} & -n^2 \frac{L_{ms}}{2} \\ -n^2 \frac{L_{ms}}{2} & -n^2 \frac{L_{ms}}{2} & L_{ls} + n^2 L_{ms} \end{bmatrix},$$

$$n = \left(\frac{N_r}{N_s} \right).$$

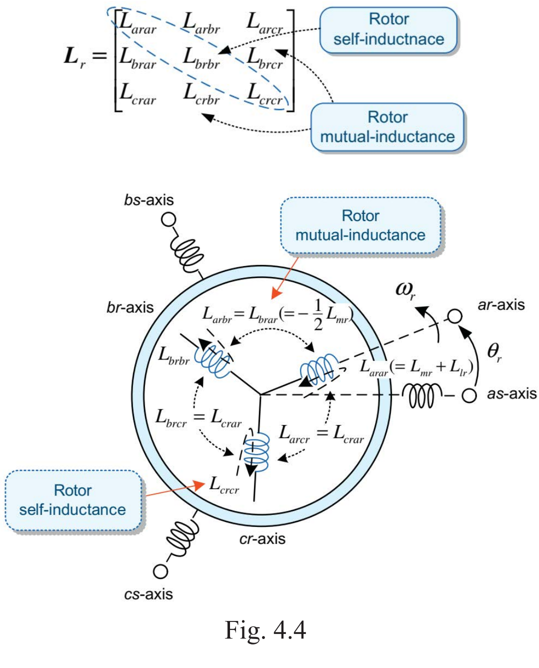

Fig. 4.4

4.1.3 Inductance between the Stator and Rotor Windings. First, we will explore the mutual-inductance matrix Lsr. This is related to the amount of flux, which is produced by the rotor windings and links the stator windings.

The mutual-inductance consists of nine components as

$$L_{sr} = \begin{bmatrix} L_{asar} & L_{asbr} & L_{ascr} \\ L_{bsar} & L_{bsbr} & L_{bscr} \\ L_{csar} & L_{csbr} & L_{cscr} \end{bmatrix}.$$

The mutual-inductance vary sinusoidally with respect to the displacement angle $\boldsymbol{\theta}_r$ of the rotor as shown in fig. 4.5.

$$L_{asar} = L_{mr}\left(\frac{N_s}{N_r}\right)\cos\theta_r = L_{ms}\left(\frac{N_r}{N_s}\right)\cos\theta_r.$$

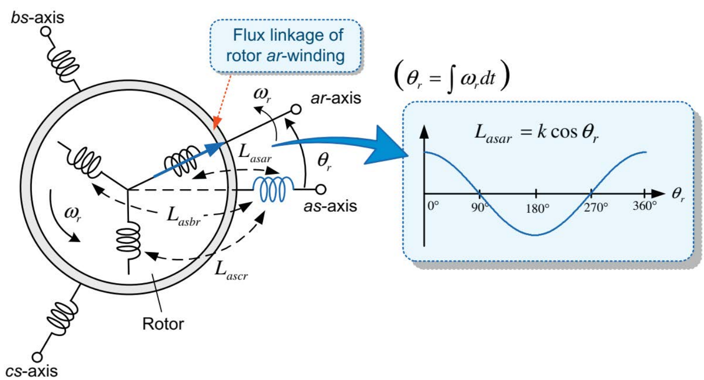

Fig. 4.5

As an example, examine the mutual-inductance L_{asar}, which represents the ratio of the flux linking in the stator *as* winding to the rotor *ar* winding current generating the flux. If the rotor winding is rotating at a speed ω_r, the relative position θ_r between the two windings will vary over time.

The other mutual-inductances are given by

$$L_{asar} = L_{bsbr} = L_{cscr} = \left(\frac{N_r}{N_s}\right)L_{ms}\cos\theta_r,$$

$$L_{asbr} = L_{bscr} = L_{csar} = \left(\frac{N_r}{N_s}\right) L_{ms} \cos\left(\theta_r + \frac{2\pi}{3}\right),$$

$$L_{ascr} = L_{bsar} = L_{csbr} = \left(\frac{N_r}{N_s}\right) L_{ms} \cos\left(\theta_r - \frac{2\pi}{3}\right).$$

With these inductances, the mutual-inductance matrix $\boldsymbol{L}_{sr}$ is given by

$$L_{sr} = \begin{bmatrix} L_{asar} & L_{asbr} & L_{ascr} \\ L_{bsar} & L_{bsbr} & L_{bscr} \\ L_{csar} & L_{csbr} & L_{cscr} \end{bmatrix} =$$

$$= nL_{ms} \begin{bmatrix} \cos\theta_r & \cos\left(\theta_r + \frac{2\pi}{3}\right) & \cos\left(\theta_r - \frac{2\pi}{3}\right) \\ \cos\left(\theta_r - \frac{2\pi}{3}\right) & \cos\theta_r & \cos\left(\theta_r + \frac{2\pi}{3}\right) \\ \cos\left(\theta_r + \frac{2\pi}{3}\right) & \cos\left(\theta_r - \frac{2\pi}{3}\right) & \cos\theta_r \end{bmatrix}.$$

We can readily see that the mutual-inductances are a function of the rotor position and thus vary over time except for at a standstill.

The flux linkage of the stator windings is given by

$$\lambda_{abcs} = L_s i_{abcs} + L_{sr} i_{abcr} =$$

$$= \begin{bmatrix} L_{ls} + L_{ms} & -\frac{L_{ms}}{2} & -\frac{L_{ms}}{2} \\ -\frac{L_{ms}}{2} & L_{ls} + L_{ms} & -\frac{L_{ms}}{2} \\ -\frac{L_{ms}}{2} & -\frac{L_{ms}}{2} & L_{ls} + L_{ms} \end{bmatrix} \begin{bmatrix} i_{as} \\ i_{bs} \\ i_{cs} \end{bmatrix} +$$

$$+nL_{ms}\begin{bmatrix} \cos\theta_r & \cos\left(\theta_r+\frac{2\pi}{3}\right) & \cos\left(\theta_r-\frac{2\pi}{3}\right) \\ \cos\left(\theta_r-\frac{2\pi}{3}\right) & \cos\theta_r & \cos\left(\theta_r+\frac{2\pi}{3}\right) \\ \cos\left(\theta_r+\frac{2\pi}{3}\right) & \cos\left(\theta_r-\frac{2\pi}{3}\right) & \cos\theta_r \end{bmatrix}\begin{bmatrix} i_{ar} \\ i_{br} \\ i_{cr} \end{bmatrix}.$$

Like L_{sr}, the mutual-inductance L_{rs} also becomes time-varying except at a standstill. Therefore the time-varying coefficients will appear in the voltage equations of the rotor windings.

The flux linkage of the rotor windings is given by

$$\lambda_{abcr} = L_r i_{abcr} + L_{rs} i_{abcs} =$$

$$=\begin{bmatrix} L_{ls}+n^2L_{ms} & -n^2\frac{L_{ms}}{2} & -n^2\frac{L_{ms}}{2} \\ -\frac{L_{ms}}{2} & L_{ls}+n^2L_{ms} & -n^2\frac{L_{ms}}{2} \\ -n^2\frac{L_{ms}}{2} & -n^2\frac{L_{ms}}{2} & L_{ls}+n^2L_{ms} \end{bmatrix}\begin{bmatrix} i_{ar} \\ i_{br} \\ i_{cr} \end{bmatrix}+$$

$$+nL_{ms}\begin{bmatrix} \cos\theta_r & \cos\left(\theta_r-\frac{2\pi}{3}\right) & \cos\left(\theta_r+\frac{2\pi}{3}\right) \\ \cos\left(\theta_r+\frac{2\pi}{3}\right) & \cos\theta_r & \cos\left(\theta_r-\frac{2\pi}{3}\right) \\ \cos\left(\theta_r-\frac{2\pi}{3}\right) & \cos\left(\theta_r+\frac{2\pi}{3}\right) & \cos\theta_r \end{bmatrix}\begin{bmatrix} i_{as} \\ i_{bs} \\ i_{cs} \end{bmatrix}.$$

Finally, the total flux linkages of the induction motor are given by

$$\begin{bmatrix}\lambda_{as}\\ \lambda_{bs}\\ \lambda_{cs}\\ \lambda_{ar}\\ \lambda_{br}\\ \lambda_{cr}\end{bmatrix} =$$

$$\begin{bmatrix}
L_{ls}+L_{ms} & -\frac{L_{ms}}{2} & -\frac{L_{ms}}{2} & nL_{ms}\cos\theta_r & nL_{ms}\cos\left(\theta_r+\frac{2\pi}{3}\right) & nL_{ms}\cos\left(\theta_r-\frac{2\pi}{3}\right)\\
-\frac{L_{ms}}{2} & L_{ls}+L_{ms} & -\frac{L_{ms}}{2} & nL_{ms}\cos\left(\theta_r-\frac{2\pi}{3}\right) & nL_{ms}\cos\theta_r & nL_{ms}\cos\left(\theta_r+\frac{2\pi}{3}\right)\\
-\frac{L_{ms}}{2} & -\frac{L_{ms}}{2} & L_{ls}+L_{ms} & nL_{ms}\cos\left(\theta_r+\frac{2\pi}{3}\right) & nL_{ms}\cos\left(\theta_r-\frac{2\pi}{3}\right) & nL_{ms}\cos\theta_r\\
nL_{ms}\cos\theta_r & nL_{ms}\cos\left(\theta_r-\frac{2\pi}{3}\right) & nL_{ms}\cos\left(\theta_r+\frac{2\pi}{3}\right) & L_{ls}+n^2L_{ms} & -\frac{1}{2}n^2L_{ms} & -\frac{1}{2}n^2L_{ms}\\
nL_{ms}\cos\left(\theta_r+\frac{2\pi}{3}\right) & nL_{ms}\cos\theta_r & nL_{ms}\cos\left(\theta_r-\frac{2\pi}{3}\right) & -\frac{1}{2}n^2L_{ms} & L_{ls}+n^2L_{ms} & -\frac{1}{2}n^2L_{ms}\\
nL_{ms}\cos\left(\theta_r-\frac{2\pi}{3}\right) & nL_{ms}\cos\left(\theta_r+\frac{2\pi}{3}\right) & nL_{ms}\cos\theta_r & -\frac{1}{2}n^2L_{ms} & -\frac{1}{2}n^2L_{ms} & L_{ls}+n^2L_{ms}
\end{bmatrix}
\begin{bmatrix}i_{as}\\ i_{bs}\\ i_{cs}\\ i_{ar}\\ i_{br}\\ i_{cr}\end{bmatrix}.$$

4.2 Modeling of Permanent Magnet Synchronous Motor

4.2.1 Structure of Permanent Magnet Synchronous Motors. Synchronous motors can be divided into several categories according to the ratio of electromagnet torque to reluctance torque as shown in fig. 4.6.

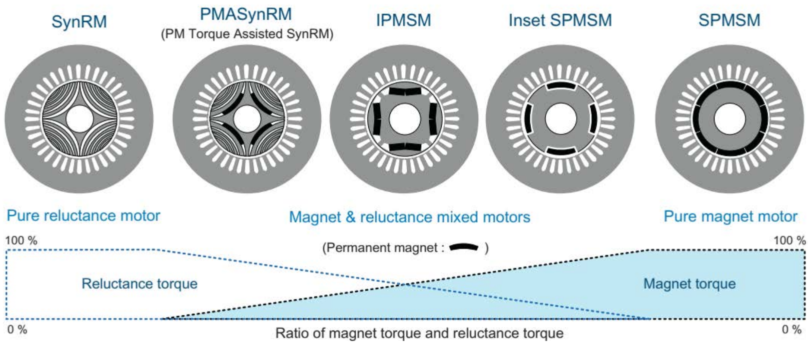

Fig. 4.6

The stator configuration of a synchronous motor is the same as that of an induction motor. The stator windings are connected to a three-phase AC source to generate a rotating magnetic field. However, unlike an induction motor having three-phase windings, the rotor of a synchronous motor has a field winding or a permanent magnet to generate a magnetic field flux on it. In recent years the magnetic field for synchronous motors has been generated mostly by using a permanent magnet rather than a field winding.

In addition to the electromagnetic torque produced by the magnetic fields of the stator and rotor, synchronous motors with a salient rotor can exploit reluctance torque.

PMSMs offer many advantages over other motors. They have a higher efficiency than induction motors because there are no copper losses by the rotor. In addition, they exhibit a high power density, high torque-to-volume ratios, and a fast dynamic response. Besides these advantages, PMSMs with magnetic rotor saliency use reluctance torque as well as magnet torque. Owing to these attractive characteristics, PMSMs are gaining more attention for a wide variety of residential and industrial drive applications, ranging from general-purpose drives to high-performance drives.

A distributed winding has been typically used as a three-phase stator winding configuration to produce a sinusoidal flux in the air gap as shown in fig. 4.7a. However, recently, a concentrated winding has been increasingly used in PMSMs as shown in fig. 4.7b.

Although a concentrated winding gives less sinusoidal magnetomotive force distribution compared to a distributed winding, this type of winding can provide several advantages such as high power density, high efficiency, short end turns, high slot-fill factor, low manufacturing costs by segmented stator structures, low cogging torque, flux-weakening capability, and fault tolerance.

There are two main types of a concentrated winding: single-layer winding configuration, where each slot is occupied by the coil sides of one phase, and double-layer winding configuration, where each slot is occupied equally by the coil sides of two phases.

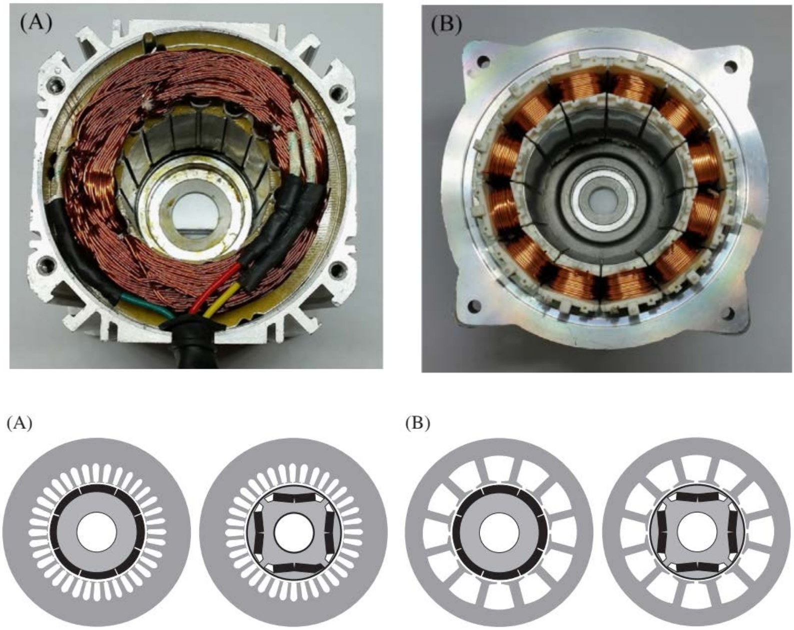

Fig. 4.7

The rotor of PMSMs has a permanent magnet to generate a magnetic field flux on it. The characteristics of PMSMs such as the power density, torque density, weight, and size may vary according to the chosen permanent magnet material. These days, a neodymium magnet (also known as NdFeB) is the most commonly employed for PMSMs due to its excellent magnetic characteristics and low cost. Even though we use the same permanent magnet material, many characteristics of PMSMs are heavily dependent on rotor configurations involving the shape and arrangement of the permanent magnets.

PMSMs can be divided into two types according to the direction of the magnetic flux produced from the permanent magnets as shown in fig. 4.8: **radial-flux type** and **axial-flux type**.

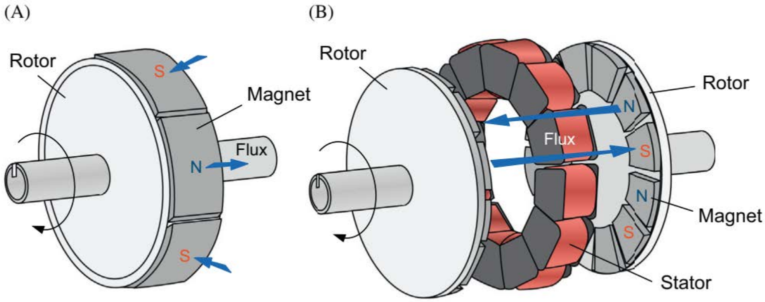

Fig. 4.8

In the radial-flux type, the rotor which is cylindrical in shape rotates inside the stator and the magnetic flux crosses the air gap in a radial direction. On the other hand, in the axial-flux type, the rotor which resembles a pancake rotates beside the stator and the magnetic flux crosses the air gap in an axial direction.

The radial-flux type PMSMs can also be further classified into two categories based on the position of the permanent magnets as shown in fig. 4.9: **surface-mounted permanent magnet synchronous motor** (SPMSM) with magnets mounted on the surface of the rotor (A) and **interior permanent magnet synchronous motor** (IPMSM) with magnets buried inside the rotor iron core (B, C).

As for IPMSM, there are two topologies according to the arrangement of the permanent magnets: parallel topology, in which the magnetic poles are located parallel to the circumference of the rotor as shown in fig. 4.9b and perpendicular topology (also called spoke type), in which the magnetic poles are located perpendicularly to the circumference as shown in fig. 4.9c.

IPMSMs with the parallel topology are more commonly used. The perpendicular topology can concentrate the magnetic flux of the magnets and achieve a high pole number, so that the flux density in the air gap can be higher than the flux density of the magnet itself. Thus although low cost and low flux density magnet material such as ferrite is employed, the motor can exhibit a high torque density. However, due to the flux concentration at the pole edges, there may be a high harmonic distortion in the air-gap flux density near the pole tips and thereby in the back-EMF profile. This also leads to a high ripple in the developed torque. SPMSMs and IPMSMs are different in their characteristics, requiring different control methods.

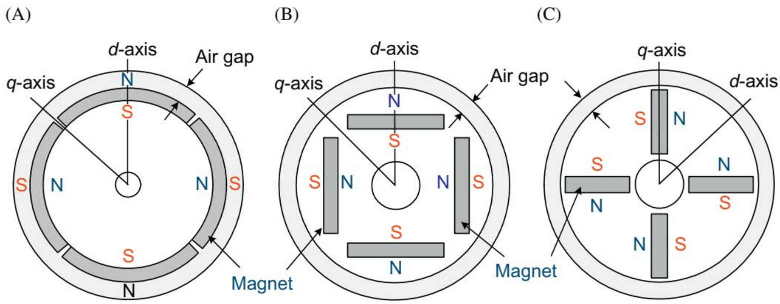

Fig. 4.9

4.2.2 Model of Permanent Magnet Synchronous Motors. For a parallel topology IPMSM, the q-axis inductance is higher than the d-axis inductance because of the magnets placed along with the d-axis. Although the rotor of an IPMSM is cylindrical in shape, we will express it as a magnetic equivalent salient rotor as shown in fig. 4.10 to simplify the analysis of the IPMSM.

As a PMSM has no rotor circuits, we can consider only the voltage equations for the stator windings. The stator windings of a synchronous motor are the same as those of an induction motor. Thus the stator voltage equations will be

$$v_{abcs} = R_s i_{abcs} + \frac{d\lambda_{abcs}}{dt},$$

where $v_{abcs} = [v_{as} v_{bs} v_{cs}]^T$, $i_{abcs} = [i_{as} i_{bs} i_{cs}]^T$, $\lambda_{abcs} = [\lambda_{as}\lambda_{bs}\lambda_{cs}]^T$.

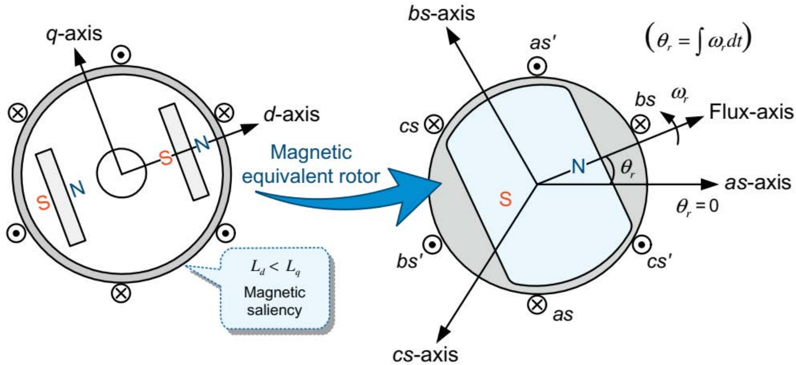

Fig. 4.10

The flux linkage of an IPMSM has the following four components: the flux linkages due to the stator currents and the flux linkage due to the permanent magnet as

$$\lambda_{as} = \lambda_{asas} + \lambda_{asbs} + \lambda_{ascs} + \varphi_{asf},$$

$$\lambda_{bs} = \lambda_{bsas} + \lambda_{bsbs} + \lambda_{bscs} + \varphi_{bsf},$$

$$\lambda_{cs} = \lambda_{csas} + \lambda_{csbs} + \lambda_{cscs} + \varphi_{csf}.$$

These flux linkages can be expressed as the product of the related current and inductance as

$$\lambda_{as} = L_{asas} i_{as} + L_{asbs} i_{bs} + L_{ascs} i_{cs} + L_{asf} I_f,$$

$$\lambda_{bs} = L_{bsas} i_{as} + L_{bsbs} i_{bs} + L_{bscs} i_{cs} + L_{bsf} I_f,$$

$$\lambda_{cs} = L_{csas} i_{as} + L_{csbs} i_{bs} + L_{cscs} i_{cs} + L_{csf} I_f.$$

Since a synchronous motor has a different rotor configuration from that of an induction motor, the components of the flux linkage of the stator windings are different.

The stator inductances of

$$L_s = \begin{bmatrix} L_{asas} & L_{asbs} & L_{ascs} \\ L_{bsas} & L_{bsbs} & L_{bscs} \\ L_{csas} & L_{csbs} & L_{cscs} \end{bmatrix}.$$

The self-inductance of an IPMSM, unlike an induction motor, may be different depending on the angular position of the rotor because the effective air gap may vary with the position of the rotor.

Consider an example of the phase as winding as shown in fig. 4.11.

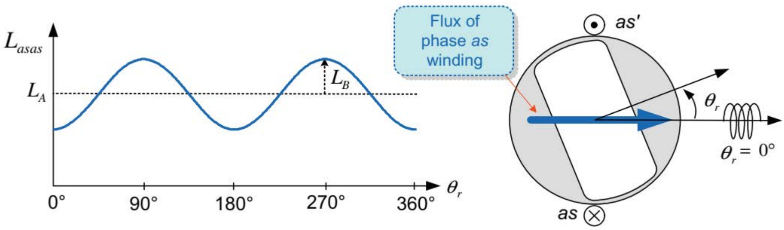

Fig. 4.11

In this case, the self-inductance becomes the maximum value at the rotor positions of both 90 and 270 (the smallest reluctance position), where the flux produced by the phase as current becomes the maximum value. This, in turn, makes the flux linking its own winding to become the maximum value. On the other hand, the self-inductance becomes the minimum value at the rotor positions of both 0 and 180 (the largest reluctance position).

The self-inductances vary sinusoidally with respect to the rotor angle θ_r and can be expressed as

$$L_{asas} = L_{ls} + L_A - L_B \cos 2\theta_r,$$

$$L_{bsbs} = L_{ls} + L_A - L_B \cos 2\left(\theta_r - \frac{2}{3}\pi\right),$$

$$L_{cscs} = L_{ls} + L_A - L_B \cos 2\left(\theta_r + \frac{2}{3}\pi\right).$$

where $\boldsymbol{L_{ls}}$ represents the leakage inductance, $\boldsymbol{L_A}$ represents the average value of the magnetizing inductance, and $\boldsymbol{L_B}$ represents the variation in value of the magnetizing inductance.

Similar to those of an induction motor, the mutual-inductances between the stator windings also vary sinusoidally with respect to the angle θ_r as shown in fig. 4.12.

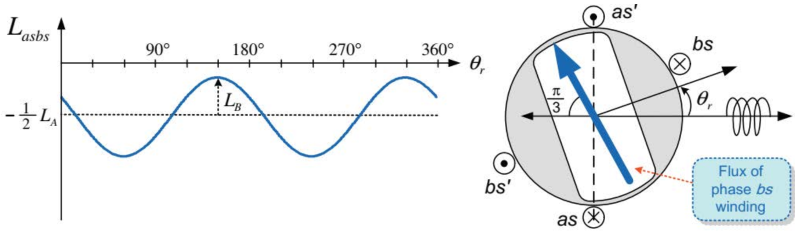

Fig. 4.12

Thus they are given by

$$L_{asbs} = L_{bsas} = -\frac{1}{2}L_A - L_B \cos 2\left(\theta_r - \frac{\pi}{3}\right),$$

$$L_{ascs} = L_{csas} = -\frac{1}{2}L_A - L_B \cos 2\left(\theta_r + \frac{\pi}{3}\right),$$

$$L_{bscs} = L_{csbs} = -\frac{1}{2}L_A - L_B \cos 2\theta_r.$$

With these inductances, the stator inductance is given by

$$L_s =$$
$$= \begin{bmatrix} L_{ls} + L_A - L_B \cos 2\theta_r & -\frac{1}{2}L_A - L_B \cos 2\left(\theta_r - \frac{\pi}{3}\right) & -\frac{1}{2}L_A - L_B \cos 2\left(\theta_r + \frac{\pi}{3}\right) \\ -\frac{1}{2}L_A - L_B \cos 2\left(\theta_r - \frac{\pi}{3}\right) & L_{ls} + L_A - L_B \cos 2\left(\theta_r + \frac{2}{3}\pi\right) & -\frac{1}{2}L_A - L_B \cos 2\theta_r \\ -\frac{1}{2}L_A - L_B \cos 2\left(\theta_r + \frac{\pi}{3}\right) & -\frac{1}{2}L_A - L_B \cos 2\theta_r & L_{ls} + L_A - L_B \cos 2\left(\theta_r - \frac{4}{3}\pi\right) \end{bmatrix}.$$

The mutual-inductances $L_{asf}\ L_{bsf}\ L_{csf}$ relevant to the amount of the permanent magnet flux linking the stator windings. These mutual-inductance are different depending on the position of the rotor because the magnet flux linking to the stator windings varies with the position of the rotor. As an example of the phase as winding, from fig. 4.13, the mutual-inductance becomes a maximum value at the rotor position of 0, while it becomes a minimum value at the rotor position of 180.

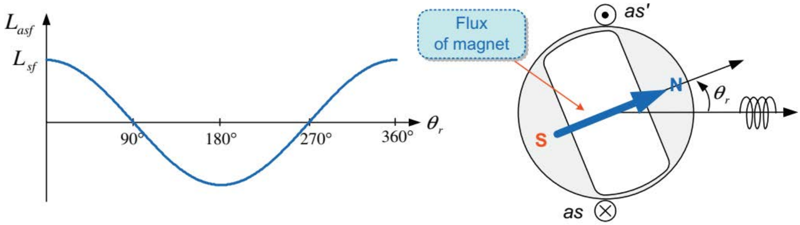

Fig. 4.13

$$\lambda_{abcs} = L_s i_{abcs} + L_f I_f =$$
$$= \begin{bmatrix} L_{ls} + L_A - L_B \cos 2\theta_r & -\frac{1}{2}L_A - L_B \cos 2\left(\theta_r - \frac{\pi}{3}\right) & -\frac{1}{2}L_A - L_B \cos 2\left(\theta_r + \frac{\pi}{3}\right) \\ -\frac{1}{2}L_A - L_B \cos 2\left(\theta_r - \frac{\pi}{3}\right) & L_{ls} + L_A - L_B \cos 2\left(\theta_r - \frac{2}{3}\pi\right) & -\frac{1}{2}L_A - L_B \cos 2\theta_r \\ -\frac{1}{2}L_A - L_B \cos 2\left(\theta_r + \frac{\pi}{3}\right) & -\frac{1}{2}L_A - L_B \cos 2\theta_r & L_{ls} + L_A - L_B \cos 2\left(\theta_r - \frac{4}{3}\pi\right) \end{bmatrix} \begin{bmatrix} i_{as} \\ i_{bs} \\ i_{cs} \end{bmatrix}.$$

Unlike self-inductances, the mutual-inductances vary by $\cos\theta_r$ per one mechanical revolution of the rotor. So we have

$$L_{asf} = L_{sf} \cos\theta_r,$$

$$L_{bsf} = L_{sf}\cos\left(\theta_r - \frac{2}{3}\pi\right), \qquad L_{csf} = L_{sf}\cos\left(\theta_r + \frac{2}{3}\pi\right).$$

All the inductances in the flux linkages of an IPMSM are time varying except for at a standstill of the motor. Therefore the time-varying coefficients will appearing the voltage equations of an IPMSM.

We can see that the voltage equations of an induction motor and a synchronous motor are expressed as the differential equations with time-varying coefficients. Fortunately, by employing the reference frame transformation, these time-varying inductances in the voltage equations can be eliminated. Now, we will study the reference frame transformation and the AC motor models expressed by the *dq* variables.

4.3 Reference Frame Transformation

Reference frame transformation refers to a transformation of the three-phase *abc* variables commonly used in AC systems to *dqn* variables orthogonal to each

other. This transformation is often known as *d*-*q* transformation. fig. 4.14 compares these variables. Here, the direction of the *abc* variables is considered to be the direction of the magnetic axes of their windings.

The direction of d, q, and n axes in orthogonal coordinates will be defined as the following.

– *d*-axis (direct axis);

– *q*-axis (quadrature axis);

– *n*-axis (neutral axis).

***d*-axis** (direct axis). The direction of the *d* variable, which is called the *d*-axis, is normally chosen as the direction of the magnetic flux in the AC motor. In the vector control for AC motors, the *d*-axis is regarded as the reference axis, and the flux-producing component of motor current is aligned along the *d*-axis.

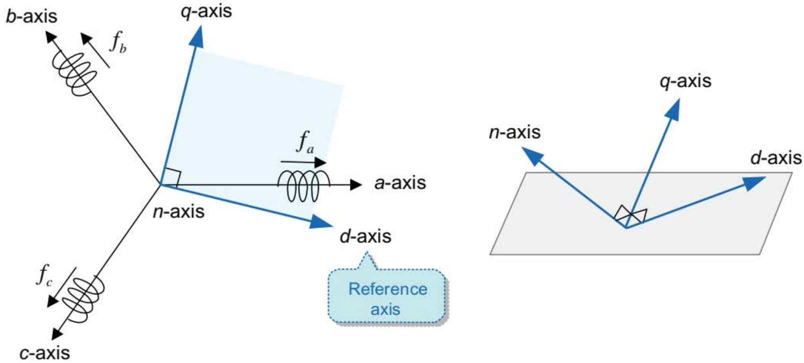

Fig. 4.14

***q*-axis** (quadrature axis). The direction of the *q* variable, which is called the *q*-axis, is defined as the direction 90 ahead of the *d*-axis. In the vector control for AC motors, the torque-producing component of motor current or the back-EMF is aligned along the *q*-axis.

***n*-axis** (neutral axis). The direction of the *n* variable, which is called the *n*-axis, is defined as the direction that is orthogonal to both the *d*- and *q*-axes. The *n*-axis has nothing to do with the mechanical output power of the AC motor but is related to the losses.

4.3.1 Types of the *d*-*q* Reference Frame. The frame of reference, consisting of *d*, *q*, and *n* axes, may rotate at any speed or remain stationary. Therefore, it can be mainly divided into stationary reference frame and rotating reference frame according to whether or not it will rotate as shown in fig. 4.15.

Stationary reference frame This frame of reference remains stationary. In other words, in the stationary reference frame, the *d*-*q* coordinate system does not rotate. This will be denoted by d^s-q^s axes. Normally, in AC motor drives, d^s-axis is chosen as the axis of phase *as*. This reference frame is also called stator reference frame.

Rotating reference frame This frame of reference rotates at an angular speed ω. In other words, in the rotating reference frame, the *d*-*q* coordinate system rotates at a speed ω. The speed of rotation can be chosen arbitrarily. In this book this reference frame will be denoted by $d^ω$-$q^ω$ axes.

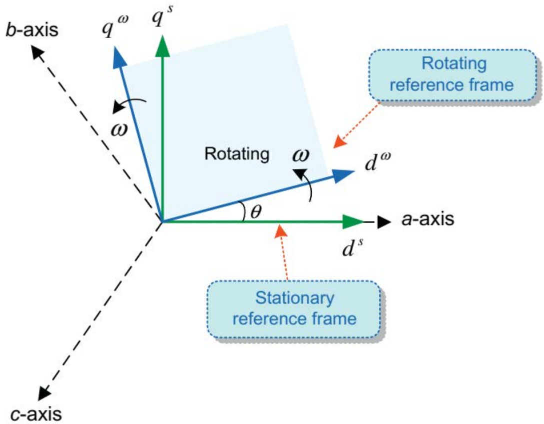

Fig. 4.15

Although the rotation of the *d*-*q* coordinate system can be arbitrarily set to any speed, there are two widely used speeds or reference frames. The first one is a synchronously rotating reference frame or synchronous reference frame, which rotates at the speed of the rotating magnetic field and will be denoted by d^e-q^e axes. The second one is a rotor reference frame, which rotates at the speed of the rotor and will be denoted by d^r-q^r axes.

4.3.2 Reference Frame Transformation by Matrix Equations. The reference frame transformation can be simply considered as the orthogonal projection of the three-phase *abc* variables f_a; f_b; f_c onto the *d*-*q* axis in the stationary reference frame (d^s-q^s axes).

Fig. 4.16 demonstrates the transformation of the three-phase *abc* variables into *dqn* variables in the stationary reference frame.

The *d*- and *q*-axes variables becomes

$$f_d^s = k\left[f_a \cos(0) + f_b \cos\left(-\frac{2}{3}\pi\right) + f_c \cos\left(\frac{2}{3}\pi\right)\right],$$

$$f_d^s = k\left[f_a \sin(0) + f_b \sin\left(-\frac{2}{3}\pi\right) + f_c \sin\left(\frac{2}{3}\pi\right)\right].$$

Here, the coefficient ***k*** can be chosen arbitrarily.

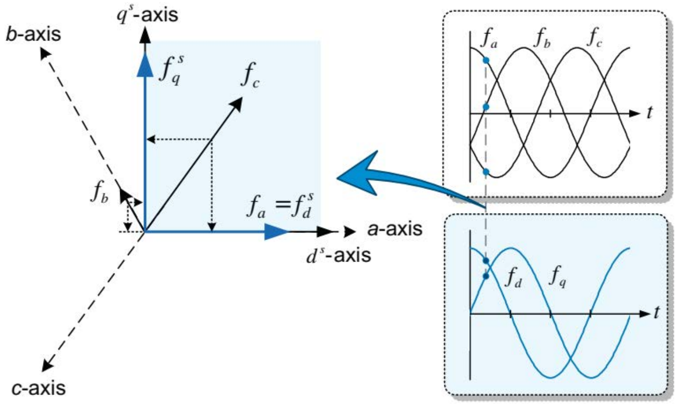

Fig. 4.16

The frame of reference can rotate at an angular velocity ω. So, the transformation of the three-phase stationary *abc* variables into *dqn* variables in the arbitrary reference frame rotating at a speed ω can be generally formulated as

$$f_{dqn}^{\omega} = T(\theta) f_{abc},$$

where $f_{dqn} = \left[f_d f_q f_n \right]^1$, $f_{abc} = \left[f_a f_b f_c \right]^T$ and $[\ ]^T$ denotes the transpose of a matrix. $\boldsymbol{f_x}$ can represent the variables of an AC motor such as voltage, current, and flux linkage.

The transformation matrix ***T*(θ)** is defined as

$$T(\theta) = \frac{2}{3} \begin{bmatrix} \cos\theta & \cos\left(\theta - \frac{2}{3}\pi\right) & \cos\left(\theta + \frac{2}{3}\pi\right) \\ -\sin\theta & -\sin\left(\theta - \frac{2}{3}\pi\right) & -\sin\left(\theta + \frac{2}{3}\pi\right) \\ \frac{1}{2} & \frac{1}{2} & \frac{1}{2} \end{bmatrix},$$

where the angular displacement $\theta = \int \omega(\tau) d\tau + \theta(0)$. The coefficient of 2/3 is normally used when applying the transformation to motor variables.

From this equation, it can be seen that the $\boldsymbol{f_n}$ variable is independent of the reference frame but is related arithmetically to the *abc* variables. Fig. 4.17 demonstrates the resolution of the three-phase *abc* variables f_a; f_b; f_c into the *d*- and *q*-axes in the stationary reference frame (d^s-q^s axes).

In the transformation matrix $T(\theta)$ the coefficient $\boldsymbol{k}$ is chosen as **2/3**. In this case the magnitude of the *dq* variables is exactly identical to that of the *abc* variables, so, this transformation is called **magnitude invariance transformation**.

On the other hand, when using the coefficient of sqrt(2/3), the power remains the same value in the two reference frames, i.e., $P_{dqn}=P_{abc}$. So, this transformation is called **power invariance transformation**. However, the magnitude of the *dq* variables is not equal to the magnitude of the *abc* variables.

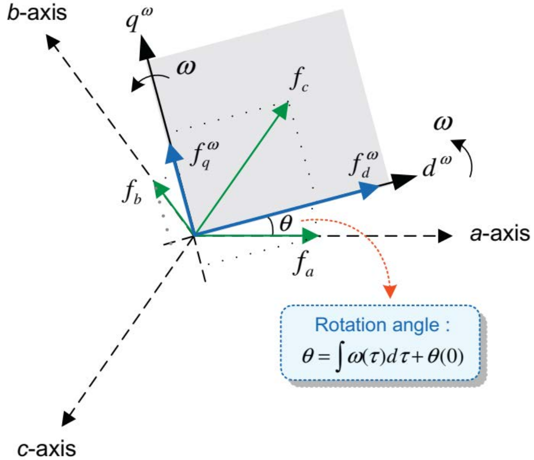

Fig. 4.17

4.3.3 Transformation of *abc* variables into *dqn* variables in the stationary reference frame. From setting θ = 0 the transformation of the three-phase *abc* variables into *dqn* variables in the stationary reference frame is given by

$$f_{dqn}^{s} = T(0) f_{abc} = \frac{2}{3}\begin{bmatrix} 1 & -\frac{1}{2} & -\frac{1}{2} \\ 0 & \frac{\sqrt{3}}{2} & -\frac{\sqrt{3}}{2} \\ \frac{1}{\sqrt{2}} & \frac{1}{\sqrt{2}} & \frac{1}{\sqrt{2}} \end{bmatrix}\begin{bmatrix} f_a \\ f_b \\ f_c \end{bmatrix}.$$

This is known as **Clark's transformation**.

Transformation of *abc* variables into *dqn* variables in the stationary reference frame

$$f_d^s = \frac{2f_a - f_b - f_c}{3},$$

$$f_q^s = \frac{1}{\sqrt{3}}\left(f_b - f_c\right),$$

$$f_n^s = \frac{2\left(f_a + f_b + f_c\right)}{3}.$$

In the stationary reference frame, the *dqn* variables are arithmetically related to the *abc* variables. In particular, if the sum of the *abc* variables in a balanced threephase system with no neutral connection is zero, i.e., $\boldsymbol{f_a + f_b + f_c = 0}$, then the *n*-axis variable is zero, i.e., $f_n^s = 0$. Thus, $f_d^s = f_a$, i.e., the *ds*-axis variable is always equal to the phase *a*-axis variable. In this case the *dq* variables are reduced as following

$$f_d^s = f_a\left(f_n^s = 0\right),$$

$$f_q^s = \frac{1}{\sqrt{3}}\left(f_b - f_c\right).$$

The **inverse transformation** of the *dqn* variables in the stationary reference frame into the *abc* variables is as following

$$f_a = f_d^s,$$

$$f_b = -\frac{1}{2} f_d^s + \frac{\sqrt{3}}{2} f_q^s,$$

$$f_c = -\frac{1}{2} f_d^s - \frac{\sqrt{3}}{2} f_q^s.$$

4.3.4 Transformation between reference frames. Consider a transformation between reference frames. For the analysis of AC motors, it is often required to transform the variables in one reference frame to variables in another reference frame as shown in fig. 4.18 ((A) Stationary into rotating frame and (B) rotating into stationary frame).

As a widely used transformation, the transformation of the stationary reference frame into the rotating reference frame can be formulated as

$$f_{dqn}^{e} = R(\theta)\, f_{dqn}^{s} = \begin{bmatrix} \cos\theta & \sin\theta & 0 \\ -\sin\theta & \cos\theta & 0 \\ 0 & 0 & 1 \end{bmatrix} \begin{bmatrix} f_d^s \\ f_q^s \\ f_n^s \end{bmatrix}.$$

This is known as **Park's transformation**.

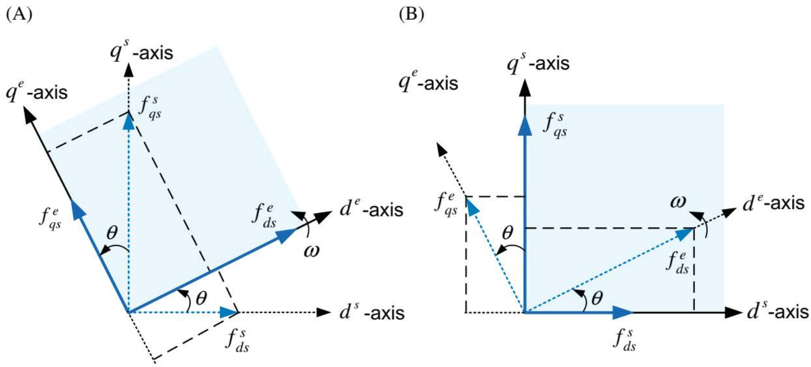

Fig. 4.18

Transformation of stationary reference frame into rotating reference frame

$$f_d^e = f_d^s \cos\theta + f_q^s \sin\theta,$$

$$f_q^e = -f_d^s \sin\theta + f_q^s \cos\theta.$$

Inverse transformation of stationary reference frame into rotating reference frame

$$f_d^s = f_d^e \cos\theta - f_q^e \sin\theta,$$

$$f_q^s = f_d^e \sin\theta + f_q^e \cos\theta.$$

The procedure for all the transformations just mentioned is summarized in fig. 4.19.

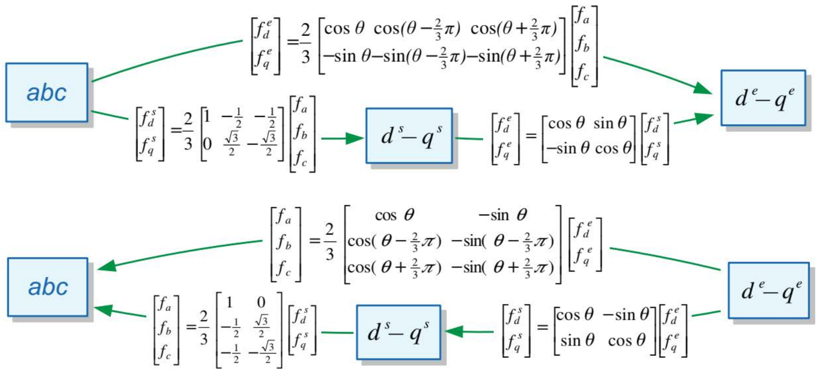

Fig. 4.19

The instantaneous power may be expressed in *abc* variables as

$$P = v_a i_a + v_b i_b + v_c i_c = V_{abc}^T I_{abc},$$

$$V_{abc}^T = \left[v_a v_b v_c\right]^T, \; I_{abc} = \left[i_a i_b i_c\right].$$

By transforming the above equation into the arbitrary reference frame rotating at any angular velocity ω, the instantaneous power is given by

$$P = V_{abc} I_{abc} = \left[T^{-1}(\theta) V_{dqn}^{\omega}\right] \left[T^{-1}(\theta) I_{dqn}^{\omega}\right] = -\left(V_{dqn}^{\omega}\right) \; I_{dqn}^{\omega} =$$

$$= \frac{3}{2}\left(v_d^{\omega} i_d^{\omega} + v_q^{\omega} i_q^{\omega} + v_n^{\omega} i_n^{\omega}\right).$$

4.4 Reference Frame Transformation by Complex Vector

The complex vector representation allows us to analyze the three-phase system as a whole instead of looking at each phase individually. A space vector is different from a phasor, which is a representation of the amplitude and phase for a sine wave in the steady-state condition.

Any three-phase quantity can be represented by a vector $\boldsymbol{f}_{abc}$ in the complex plane as shown in fig. 4.20.

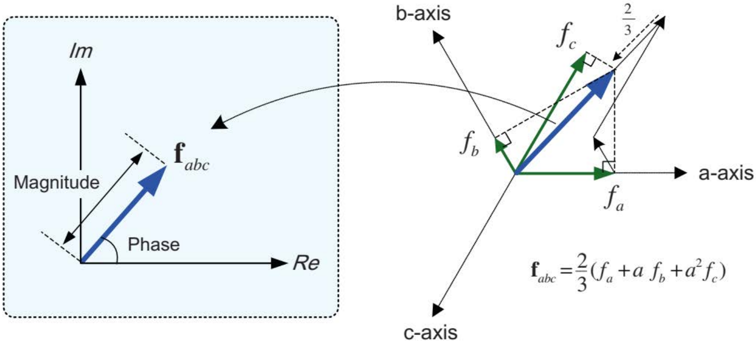

Fig. 4.20

This vector is called **the complex space vector**, or in short, **space vector**.

A complex space vector is defined as

$$f_{abc} \equiv \frac{2}{3}\left(f_a + af_b + a^2 f_c\right),$$

$$\left(a = e^{j(2\pi/3)}, a^2 = e^{j(4\pi/3)}\right).$$

This space vector rotates at the same angular velocity $\boldsymbol{\omega}_e$ as that of the three-phase quantities as shown in fig. 4.21.

The amplitude of a space vector is equal to the peak value of the phase quantity. The rotating magnetic field is identical to the space vector of magnetic fields produced by currents flowing in three-phase windings.

When comparing the complex plane with the *d-q* coordinate system, we can see that these two systems have similar orthogonal coordinates, that is, the real-axis and the imaginary-axis correspond to the *d*-axis and the *q*-axis in the stationary reference frame, respectively.

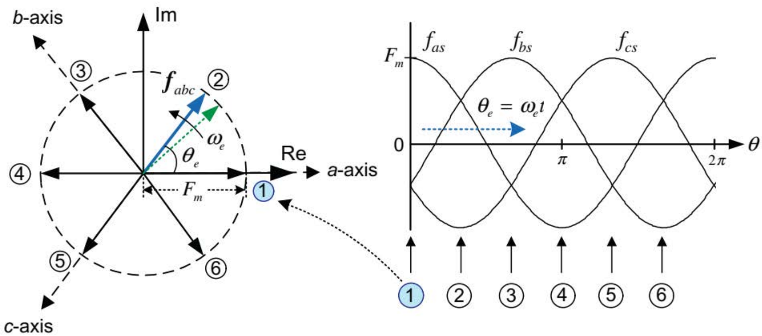

Fig. 4.21

Inversely, the quantities of a three-phase system from the space vector $\boldsymbol{f_{abc}}$ are given by

$$f_a = \text{Re}[f_{abc}] + f_n^{\omega} = \text{Re}\left[\frac{2}{3}\left(f_a + af_b + a^2 f_c\right)\right] + \frac{1}{3}\left(f_a + f_b + f_c\right) = f_a,$$

$$f_b = \text{Re}\left[a^2 f_{abc}\right] + f_n^{\omega},$$

$$f_c = \text{Re}[af_{abc}] + f_n^{\omega}.$$

where **Re** represents the real part of the complex vector.

The space vector $\boldsymbol{f_{abc}}$ equals to the vector $\boldsymbol{f_{dq}^{s}}$ in the stationary reference frame, which has the *d*- and *q*-axes components

$$f_{dq}^{s} = f_d^{s} + jf_q^{s}.$$

A vector $\boldsymbol{f_{dq}^{\omega}}$ in the arbitrary reference frame rotating at a speed **ω** in fig. 4.22 can be expressed as

$$f_{dq}^{\omega} = f_d^{\omega} + jf_q^{\omega}.$$

The *d*- and *q*-axes components of this vector are given by

$$f_d^{\omega} = \frac{2}{3}\left[f_a \cos\theta + f_b \cos\left(\theta - \frac{2}{3}\pi\right) + f_c \cos\left(\theta - \frac{4}{3}\pi\right)\right],$$

$$f_q^{\omega} = -\frac{2}{3}\left[f_a \sin\theta + f_b \sin\left(\theta - \frac{2}{3}\pi\right) + f_c \sin\left(\theta - \frac{4}{3}\pi\right)\right].$$

Since the *d*-*q* axis may rotate at any angular velocity, we need to take a look at the relationship between a space vector and a vector in the *d*-*q* axes rotating at an angular velocity.

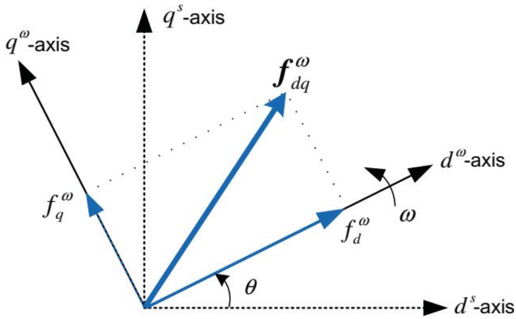

Fig. 4.22

We have just studied the transformation changing the reference frame of variables. Now, we are going to find out the model of AC motors expressed in the *d*-*q* reference frame. Then, it will be found that the time-varying inductances in the voltage equations of AC motors can be eliminated by employing the reference frame transformation. First, let us find out the *d*-*q* axes model for an induction motor.

Using Euler formula, becomes

$$f_{dq}^{\omega} = \frac{2}{3}\left[f_a\left(\cos\theta - j\sin\theta\right) + f_b\left(\cos\left(\theta - \frac{2}{3}\pi\right) - j\sin\left(\theta - \frac{2}{3}\pi\right)\right) + \right.$$

$$\left. + f_c\left(\cos\left(\theta - \frac{4}{3}\pi\right) - j\sin\left(\theta - \frac{4}{3}\pi\right)\right) = \right.$$

$$= \frac{2}{3}\left[f_a e^{-j\theta} + f_a e^{-j\left(\theta - \frac{2}{3}\delta\right)} + f_a e^{-j\left(\theta - \frac{4}{3}\pi\right)} \right] =$$

$$= \frac{2}{3}\left[f_a + a f_a + a^2 f_a \right] e^{-j\theta} = f_{abc} e^{-j\theta}.$$

We can see that there is only a phase difference of θ between *fabc* and f_{dq}^{ω}. This phase difference comes from the angular displacement between the complex plane and the *d*-*q* axes rotating at an angular velocity.

By letting **θ = 0**, we can identify that the space vector f_{abc} equals to the vector f_{dq}^{s} in the *d*-*q* axis of the stationary reference frame as

$$f_{dq}^{s} = f_{abc} e^{-j0} = f_{abc}.$$

A vector f_{dq}^{ω} in the rotating reference frame with the angular velocity $\omega = \omega_e$ can be expressed as

$$f_{dq}^{e} = f_{abc} e^{-j\theta_e} = f_{dq}^{s} e^{-j\theta_e} \quad \left(\theta_e = \int \omega_e(t)\, dt + \theta(0)\right).$$

The instantaneous power is expressed in terms of the complex vector as

$$P = \frac{3}{2}\mathrm{Re}\left[V_{abc} I_{abc}^{*} \right] = \frac{3}{2}\mathrm{Re}\left[V_{dq}^{\omega} I_{dq}^{\omega^{*}} \right],$$

where I_{abc}^{*}; I_{dq}^{*} are the complex conjugates of I_{abc}; I_{dq}, respectively.

4.5 *d-q* Axes Model of an Induction Motor

4.5.1 Voltage Equations on the *d*-*q* Axes. The voltage equations for the stator and rotor windings of an induction motor and the flux linkages are rewritten as

$$v_{abcs} = R_s i_{abcs} + \frac{d\lambda_{abcs}}{dt}, \qquad v_{abcr} = R_r i_{abcr} + \frac{d\lambda_{abcr}}{dt},$$

$$\begin{bmatrix} \lambda_{abcs} \\ \lambda_{abcr} \end{bmatrix} = \begin{bmatrix} L_s & L_{sr} \\ \left(L_{sr}\right)^T & L_r \end{bmatrix} \begin{bmatrix} i_{abcs} \\ i_{abcr} \end{bmatrix}.$$

The voltage equations expressed in currents and inductances as

$$\begin{bmatrix} \lambda_{abcs} \\ \lambda_{abcr} \end{bmatrix} = \begin{bmatrix} R_s + pL_s & L_{sr} \\ p\left(L_{sr}\right)^T & R_r + pL_r \end{bmatrix} \begin{bmatrix} i_{abcs} \\ i_{abcr} \end{bmatrix},$$

where ***p*** is the time derivative operator ***d/dt***.

The transformation of the stator voltage equations into the *d*-*q* axes rotating at an arbitrary speed ω is as follows

$$T(\theta) v_{abcs} = T(\theta) R_s i_{abcs} + T(\theta) \frac{d\lambda_{abcs}}{dt},$$

where $T(\theta) R_s T(\theta)^{-1} = R_s$.

$$v_{dqns}^{\omega} = R_s i_{dqns}^{\omega} + T(\theta) \frac{dT(\theta)^{-1}}{dt} \lambda_{dqns}^{\omega} + T(\theta) T(\theta)^{-1},$$

where $T(\theta) \dfrac{dT(\theta)^{-1}}{dt} = \begin{bmatrix} 0 & -\omega & 0 \\ \omega & 0 & 0 \\ 0 & 0 & 0 \end{bmatrix}$.

$$v_{dqns}^{\omega} = R_s i_{dqns}^{\omega} + \begin{bmatrix} 0 & -\omega & 0 \\ \omega & 0 & 0 \\ 0 & 0 & 0 \end{bmatrix} \lambda_{dqns}^{\omega} + \frac{d\lambda_{dqns}^{\omega}}{dt}.$$

This can be resolved into as

$$v_{ds}^{\omega} = R_s i_{ds}^{\omega} + \frac{d\lambda_{ds}^{\omega}}{dt} - \omega\lambda_{qs}^{\omega},$$

$$v_{qs}^{\omega} = R_s i_{qs}^{\omega} + \frac{d\lambda_{qs}^{\omega}}{dt} + \omega\lambda_{ds}^{\omega},$$

$$v_{ns}^{\omega} = R_s i_{ns}^{\omega} + \frac{d\lambda_{ns}^{\omega}}{dt}.$$

In addition, it should be noted that the flux linkages in these speed voltages are cross-coupled.

Next, we will transform the rotor voltage equations into *d*-*q* axes rotating at an arbitrary speed ω.

The angle used in the transformation should be $\theta - \theta_r = \beta$.

$$\theta\left(= \int \omega_e(t)\,dt\right), \qquad \theta_r\left(= \int \omega_{\mathrm{r}}(t)\,dt\right).$$

With the angle β, we can transform the rotor voltage equations into the *d*-*q* axes rotating at an arbitrary speed ω as

$$T(\beta)v_{abcr} = T(\beta)R_r i_{abc} + (\beta)\frac{d\lambda_{abcr}}{dt},$$

$$v_{dqnr}^{\omega} = T(\beta)R_r\left(T(\beta)^{-1} i_{dqnr}^{\omega}\right) + T(\beta)\frac{d\left[T(\beta)^{-1}\lambda_{dqnr}^{\omega}\right]}{dt},$$

$$T(\beta)R_s T(\beta)^{-1} = R_r,$$

$$v_{dqnr}^{\omega} = R_r i_{dqnr}^{\omega} + T(\beta)\frac{dT(\beta)^{-1}}{dt}\lambda_{dqnr}^{\omega} + T(\beta)T(\beta)^{-1}\frac{d\lambda_{dqnr}^{\omega}}{dt},$$

$$v_{dqnr}^{\omega} = R_r i_{dqnr}^{\omega} + \begin{bmatrix} 0 & -(\omega-\omega_r) & 0 \\ \omega-\omega_r & 0 & 0 \\ 0 & 0 & 0 \end{bmatrix}\lambda_{dqrs}^{\omega} + \frac{d\lambda_{dqnr}^{\omega}}{dt}.$$

This can be resolved into

$$v_{dr}^{\omega} = R_r i_{dr}^{\omega} + \frac{d\lambda_{dr}^{\omega}}{dt} - (\omega - \omega_r)\lambda_{qr}^{\omega},$$

$$v_{qr}^{\omega} = R_r i_{qr}^{\omega} + \frac{d\lambda_{qr}^{\omega}}{dt} + (\omega - \omega_r)\lambda_{dr}^{\omega},$$

$$v_{nr}^{\omega} = R_r i_{nr}^{\omega} + \frac{d\lambda_{nr}^{\omega}}{dt}.$$

From the standpoint of the rotor, which rotates at the speed ω_r, the *d*-*q* axes will rotate at the difference speed ω-ω_r.

For squirrel-cage rotor induction motors, since the rotor bars are short-circuited by the end rings, the rotor voltage is zero, and thus,

$$v_{dr}^{\omega} = 0, \qquad v_{qr}^{\omega} = 0, \qquad v_{nr}^{\omega} = 0.$$

4.5.2 Flux Linkage Equations in the *d*-*q* Axes.

$$T(\theta)\lambda_{abcs} = T(\theta)L_s i_{abcs} + T(\theta)L_{sr} i_{abcr},$$

$$\lambda_{dqns}^{\omega} = T(\theta)L_s\left(T^{-1}(\theta)i_{dqns}^{\omega}\right) + T(\theta)L_{sr}\left(T^{-1}(\beta)i_{dqnr}^{\omega}\right),$$

$$\lambda_{dqns}^{\omega} = \begin{bmatrix} L_{ls} + \frac{3}{2}L_{ms} & 0 & 0 \\ 0 & L_{ls} + \frac{3}{2}L_{ms} & 0 \\ 0 & 0 & L_{ls} \end{bmatrix} i_{dqns}^{\omega} + \begin{bmatrix} \frac{3}{2}L_{ms} & 0 & 0 \\ 0 & \frac{3}{2}L_{ms} & 0 \\ 0 & 0 & 0 \end{bmatrix} i_{dqn}^{\omega},$$

$$T(\theta) L_s T^{-1}(\theta) = \begin{bmatrix} L_{ls} + \frac{3}{2} L_{ms} & 0 & 0 \\ 0 & L_{ls} + \frac{3}{2} L_{ms} & 0 \\ 0 & 0 & L_{ls} \end{bmatrix},$$

$$T(\theta) L_{sr} T^{-1}(\beta) = \begin{bmatrix} \frac{3}{2} L_{ms} & 0 & 0 \\ 0 & \frac{3}{2} L_{ms} & 0 \\ 0 & 0 & 0 \end{bmatrix}.$$

The stator flux linkages in the *d*-*q* axes as

$$L_m = \frac{3}{2} L_{ms}, \qquad L_s = L_{ls} + L_m,$$

$$\lambda_{ds}^{\omega} = L_{ls} i_{ds}^{\omega} + L_m \left(i_{ds}^{\omega} + i_{dr}^{\omega} \right) = L_s i_{ds}^{\omega} + L_m i_{dr}^{\omega},$$

$$\lambda_{qs}^{\omega} = L_{ls} i_{qs}^{\omega} + L_m \left(i_{qs}^{\omega} + i_{qr}^{\omega} \right) = L_s i_{qs}^{\omega} + L_m i_{qr}^{\omega},$$

$$\lambda_{ns}^{\omega} = L_{ls} i_{ns}^{\omega}.$$

Next, we transform the rotor flux linkage.
The *d*-*q* axes rotating at an arbitrary speed ω as follows

$$T(\beta) \lambda_{abcr} = T(\beta) L_r i_{abcr} + T(\beta) L_{sr}^{T} i_{abcs},$$

$$\lambda_{dqnr}^{\omega} = T(\beta) L_r \left(T^{-1}(\beta) i_{dqnr}^{\omega} \right) + T(\beta) L_{sr}^{T} \left(T^{-1}(\theta) i_{dqns}^{\omega} \right),$$

$$\lambda_{dqnr}^{\omega} = \begin{bmatrix} L_{ls} + \frac{3}{2}L_{mr} & 0 & 0 \\ 0 & L_{ls} + \frac{3}{2}L_{mr} & 0 \\ 0 & 0 & L_{ls} \end{bmatrix} i_{dqnr}^{\omega} + \begin{bmatrix} \frac{3}{2}L_{ms} & 0 & 0 \\ 0 & \frac{3}{2}L_{ms} & 0 \\ 0 & 0 & 0 \end{bmatrix} i_{dqns}^{\omega}.$$

Assuming the turns ratio $N_s / N_r = 1$ and letting $L_m = \frac{3}{2}L_{mr} = \frac{3}{2}L_{ms}$, $L_r = L_{lr} + L_m$. We will have rotor flux linkages in the *d*-*q* axes as

$$\lambda_{dr}^{\omega} = L_{lr} i_{dr}^{\omega} + L_m \left(i_{dr}^{\omega} + i_{ds}^{\omega} \right) = L_r i_{dr}^{\omega} + L_m i_{ds}^{\omega},$$

$$\lambda_{qr}^{\omega} = L_{lr} i_{qr}^{\omega} + L_m \left(i_{qr}^{\omega} + i_{qs}^{\omega} \right) = L_r i_{qr}^{\omega} + L_m i_{qs}^{\omega},$$

$$\lambda_{nr}^{\omega} = L_{lr} i_{nr}^{\omega}.$$

From the flux linkage expressions of the stator and rotor in the *d*-*q* axes, it is found that the main purpose of the transformation has been achieved. In other words, by employing the reference frame transformation, the time-varying mutual-inductances due to the relative motion between the stator and rotor windings become constant in the *d*-*q* reference frame. This result can be valid regardless of the rotating speed of the reference frame. Furthermore, the flux linkages become magnetically decoupled between the *d*- and *q*-axes.

Fig. 4.23 shows the *d*-*q* axes equivalent circuits.

We can obtain voltage and flux linkage equations in the different reference frames by setting **ω=0** for the stationary reference frame, **ω=ω_e** for synchronously rotating reference frame, and **ω=ω_r** for rotor reference frame.

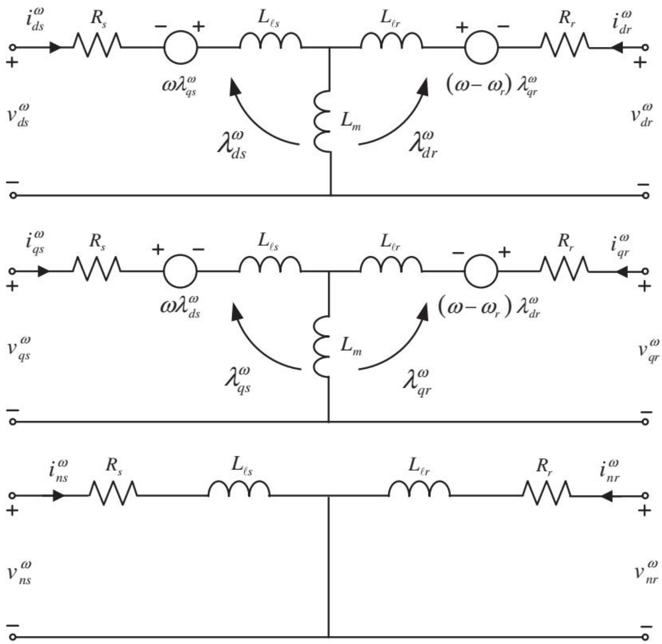

Fig. 4.23

Stationary reference frame (ω=0)

$$v_{ds}^{s} = R_s i_{ds}^{s} + p\lambda_{ds}^{s}, \qquad \lambda_{ds}^{s} = L_s i_{ds}^{s} + L_m i_{dr}^{s},$$

$$v_{qs}^{s} = R_s i_{qs}^{s} + p\lambda_{qs}^{s}, \qquad \lambda_{qs}^{s} = L_s i_{qs}^{s} + L_m i_{qr}^{s},$$

$$0 = R_r i_{dr}^{s} + p\lambda_{dr}^{s} + \omega_r \lambda_{qr}^{s}, \qquad \lambda_{dr}^{s} = L_r i_{dr}^{s} + L_m i_{ds}^{s},$$

$$0 = R_r i_{qr}^{s} + p\lambda_{qr}^{s} - \omega_r \lambda_{dr}^{s}, \qquad \lambda_{qr}^{s} = L_r i_{qr}^{s} + L_m i_{qs}^{s}.$$

Synchronously rotating reference frame (ω=ω_e)

$$v_{ds}^{e} = R_s i_{ds}^{e} + p\lambda_{ds}^{e} - \omega_e \lambda_{qs}^{e}, \qquad \lambda_{ds}^{e} = L_s i_{ds}^{e} + L_m i_{dr}^{e},$$

$$v_{qs}^{e} = R_s i_{qs}^{e} + p\lambda_{qs}^{e} + \omega_e \lambda_{ds}^{e}, \qquad \lambda_{qs}^{e} = L_s i_{qs}^{e} + L_m i_{qr}^{e},$$

$$0 = R_r i_{dr}^e + p\lambda_{dr}^e - (\omega_e - \omega_r)\lambda_{qr}^e, \qquad \lambda_{dr}^e = L_r i_{dr}^e + L_m i_{ds}^e,$$

$$0 = R_r i_{qr}^e + p\lambda_{qr}^e + (\omega_e - \omega_r)\lambda_{dr}^e, \qquad \lambda_{qr}^e = L_r i_{qr}^e + L_m i_{qs}^e.$$

Voltage equations of an induction motor in the *d*-*q* axes

$$\nu_{ds}^{\omega} = R_s i_{ds}^{\omega} + \frac{d\lambda_{ds}^{\omega}}{dt} - \omega\lambda_{qs}^{\omega},$$

$$v_{qs}^{\omega} = R_s i_{qs}^{\omega} + \frac{d\lambda_{qs}^{\omega}}{dt} + \omega\lambda_{ds}^{\omega},$$

$$v_{ns}^{\omega} = R_s i_{ns}^{\omega} + \frac{d\lambda_{ns}^{\omega}}{dt},$$

$$v_{dr}^{\omega} = R_r i_{dr}^{\omega} + \frac{d\lambda_{dr}^{\omega}}{dt} - (\omega - \omega_r)\lambda_{qr}^{\omega},$$

$$v_{qr}^{\omega} = R_r i_{qr}^{\omega} + \frac{d\lambda_{qr}^{\omega}}{dt} + (\omega - \omega_r)\lambda_{dr}^{\omega},$$

$$v_{nr}^{\omega} = R_r i_{nr}^{\omega} + \frac{d\lambda_{nr}^{\omega}}{dt}.$$

Flux linkages of an induction motor in the *d*-*q* axes

$$\lambda_{ds}^{\omega} = L_{ls} i_{ds}^{\omega} + L_m\left(i_{ds}^{\omega} + i_{dr}^{\omega}\right) = L_s i_{ds}^{\omega} + L_m i_{dr}^{\omega},$$

$$\lambda_{qs}^{\omega} = L_{ls} i_{qs}^{\omega} + L_m\left(i_{qs}^{\omega} + i_{qr}^{\omega}\right) = L_s i_{qs}^{\omega} + L_m i_{qr}^{\omega},$$

$$\lambda_{ns}^{\omega} = L_{ls} i_{ns}^{\omega},$$

$$\lambda_{dr}^{\omega} = L_{lr} i_{dr}^{\omega} + L_m\left(i_{dr}^{\omega} + i_{ds}^{\omega}\right) = L_r i_{dr}^{\omega} + L_m i_{ds}^{\omega},$$

$$\lambda_{qr}^{\omega} = L_{lr} i_{qr}^{\omega} + L_m\left(i_{qr}^{\omega} + i_{qs}^{\omega}\right) = L_r i_{qr}^{\omega} + L_m i_{qs}^{\omega},$$

$$\lambda_{nr}^{\omega} = L_{lr} i_{nr}^{\omega}.$$

4.5.3 Torque Equation in the *d-q* Axes. The torque of double-fed machines such as induction motors is given by

$$T_e = \left(\frac{P}{2}\right)\left(i_{abcs}\right)^T \frac{\delta L_{sr}}{\delta\theta_r} i_{abcr}.$$

The transformation of this torque into the *d-q* axes rotating at an arbitrary speed ω is as follows

$$T_e = \left(\frac{P}{2}\right)\left(i_{abcs}\right)^T \frac{\delta L_{sr}}{\delta\theta_r} i_{abcr} = \left(\frac{P}{2}\right)\left(T(\theta)^{-1} i_{dqns}^{\omega}\right)^T \frac{\delta L_{sr}}{\delta\theta_r}\left(T(\beta)^{-1} i_{dqnr}^{\omega}\right) =$$

$$= \left(\frac{P}{2}\right)\left(i_{dqns}^{\omega}\right)^T \left(\frac{3}{2} T(\theta)\frac{\delta L_{sr}}{\delta\theta_r} T(\beta)^{-1}\right) i_{dqnr}^{\omega} =$$

$$= \left(\frac{P}{2}\right)\left(i_{dqns}^{\omega}\right)^T \frac{3}{2}\begin{bmatrix} 0 & \frac{3}{2}L_{ms} & 0 \\ -\frac{3}{2}L_{ms} & 0 & 0 \\ 0 & 0 & 0 \end{bmatrix} i_{dqnr}^{\omega},$$

where $T^{-1}(\theta) = \frac{3}{2} T(\theta)^T$.

This torque can be resolved into

$$\therefore T_e = \frac{3}{2}\frac{P}{2} L_m\left(i_{qs}^{\omega} i_{dr}^{\omega} - i_{ds}^{\omega} i_{dr}^{\omega}\right),$$

where $L_m = \frac{3}{2} L_{ms}$.

The torque can be also expressed in terms of different motor variables but is independent of the speed of the reference frame as following

$$T_e = \frac{3}{2}\frac{P}{2}L_m \mathrm{Im}\left[i_{dqr}^* i_{dqs}\right] = \frac{3}{2}\frac{P}{2}L_m\left(i_{qs}i_{dr} - i_{ds}i_{qr}\right) =$$

$$= \frac{3}{2}\frac{P}{2}\frac{L_m}{L_r}\mathrm{Im}\left[\lambda_{dqr}^* i_{dqs}\right] = \frac{3}{2}\frac{P}{2}\frac{L_m}{L_r}\left(\lambda_{dr}i_{qs} - \lambda_{qr}i_{ds}\right) =$$

$$= \frac{3}{2}\frac{P}{2}\mathrm{Im}\left[\lambda_{dqm}^* i_{dqs}\right] = \frac{3}{2}\frac{P}{2}\left(\lambda_{dm}i_{qs} - \lambda_{qm}i_{ds}\right) =$$

$$= \frac{3}{2}\frac{P}{2}\mathrm{Im}\left[\lambda_{dqs}^* i_{dqs}\right] = \frac{3}{2}\frac{P}{2}\left(\lambda_{ds}i_{qs} - \lambda_{qs}i_{ds}\right) =$$

$$= \frac{3}{2}\frac{P}{2}\mathrm{Im}\left[i_{dqr}^* \lambda_{dqm}^*\right] = \frac{3}{2}\frac{P}{2}\left(i_{dr}\lambda_{qm} - i_{qr}\lambda_{dm}\right) =$$

$$= \frac{3}{2}\frac{P}{2}\mathrm{Im}\left[i_{dqr}^* \lambda_{dqs}^*\right] = \frac{3}{2}\frac{P}{2}\left(i_{dr}\lambda_{qr} - i_{qr}\lambda_{dr}\right) =$$

$$= \frac{3}{2}\frac{P}{2}\frac{L_m}{L_r}\mathrm{Im}\left[i_{dqr}^* \lambda_{dqs}\right] = \frac{3}{2}\frac{P}{2}\frac{L_m}{L_r}\left(i_{dr}\lambda_{qs} - i_{qr}\lambda_{ds}\right) =$$

$$= \frac{3}{2}\frac{P}{2}\frac{L_m}{L_\sigma L_r}\mathrm{Im}\left[\lambda_{dqr}^* \lambda_{dqs}\right] = \frac{3}{2}\frac{P}{2}\frac{L_m}{L_\sigma L_r}\left(\lambda_{dr}\lambda_{qs} - \lambda_{qr}\lambda_{ds}\right).$$

4.6 *d-q* Axes Model of a Permanent Magnet Synchronous Motor

Voltage and flux linkage equations of an IPMSM in the d^r-q^r axes

$$v_{ds}^r = R_s i_{ds}^r + \frac{d\lambda_{ds}^r}{dt} - \omega_r \lambda_{qs}^r,$$

$$v_{qs}^r = R_s i_{qs}^r + \frac{d\lambda_{qs}^r}{dt} + \omega_r \lambda_{ds}^r,$$

$$\lambda_{ds}^{r} = L_{ds} i_{ds}^{r} + \varphi_f,$$

$$\lambda_{qs}^{r} = L_{qs} i_{ds}^{r},$$

$$T_e = \frac{P}{2}\frac{3}{2}\left[\varphi_f i_{qs}^{r} + \left(L_{ds} - L_{qs}\right) i_{ds}^{r} i_{qs}^{r}\right].$$

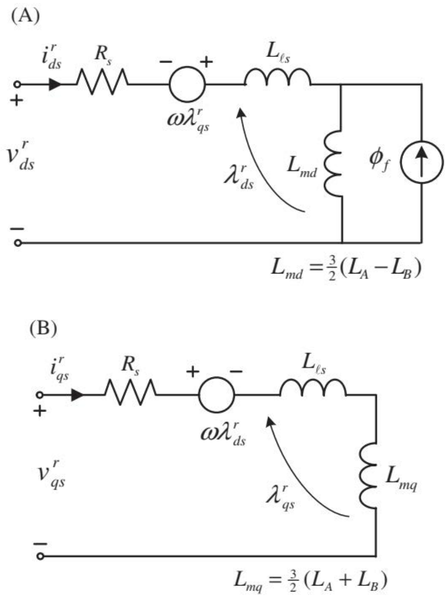

Fig. 4.24 d^r-q^r axes equivalent circuit
of an IPMSM. (A) d^r-axis and (B) q^r-axis

5 VECTOR CONTROL OF ALTERNATING CURRENT MOTORS

The output torque of a motor is the primary control object in motor drive systems. This is because the position or speed of loads can be controlled by controlling the torque of the driving motor. There are two methods of the torque control of alternating current (AC) motors: average torque control and instantaneous torque control.

There are two methods of the torque control of alternating current (AC) motors: **average torque control** and **instantaneous torque control**.

The **average torque control** is a cost-effective variable speed control solution for general-purpose applications, such as fans, blowers, and pump drives, which do not require an accurate speed or torque control. In these applications the main objective for control is the average speed of the motor/load, which is usually regulated by controlling the average torque of the motor.

A typical example of the **average torque control** technique (also called the **scalar control** method) is the constant V/f control in the induction motor drives. This method can control the motor torque only in the steady-state condition and thus cannot be used to control the dynamic behavior of the motor.

A **vector control method** based on the control of both the magnitude and the direction (phase) of the motor current can control its dynamics at the transient condition as well as the torque of a motor in the steady-state condition.

The **instantaneous torque control** is needed for high performance applications such as robots, elevators, CNC machine tools, and automation line drives. In these applications a precise speed/torque control and a fast dynamic response are required. To achieve these, it is necessary to control the instantaneous torque of the motor.

For AC motors, a complicated technique called the **vector control** method is required. The **field-oriented control** technique is a typical vector control method. The direct torque control is also another method for the instantaneous torque.

As shown in fig. 5.1, the instantaneous torque ***T*** of a motor is expressed as the cross-product of the magnetic flux vector **Φ** and current vector ***i***, and is denoted by

$$T = k\left(\Phi \times i\right),$$

$$T = k\,|\varphi|\;\;|i|\sin\theta.$$

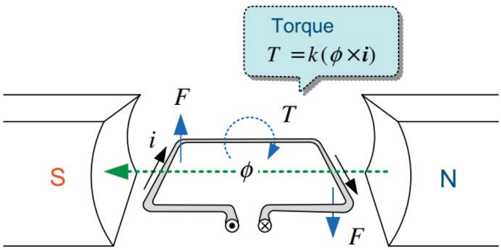

Fig. 5.1

In general, the direction of the current vector is controlled based on the flux vector **Φ**. Such method for the instantaneous torque control of AC motors is called **vector control** or **field-oriented control**.

5.1 Conditions for Instantaneous Torque Control of Motors

The vector control of AC motors imitates the torque control of a separately excited DC motor. Even though the output torque of induction motors is not easy to control, it can be controlled instantaneously like DC motors. In induction motors, unlike DC motors, the field flux-producing current and the torque-producing current (equivalent to armature current) are provided all together through the three-phase stator windings as shown in fig. 5.2.

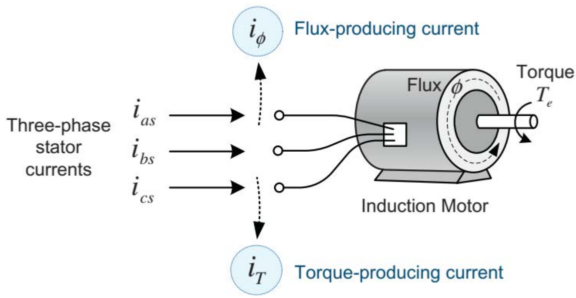

Fig. 5.2

The three requirements for controlling the instantaneous torque of a DC motor as mentioned earlier can also be applied to an induction motor as follows:

1. The space angle between the flux-producing current (or the field flux) and the torque-producing current has to be always be 90 degrees.
2. Both the flux-producing current (or the field flux) and the torque-producing current should be controlled independently.
3. The torque-producing current can be controlled instantaneously.

5.1.1 Instantaneous Torque Control of an Induction Motor. The field flux of an induction motor is rotating at the synchronous speed ω_e corresponding to the supply frequency. Thus we have to use the transformation into the synchronous reference frame rotating at the synchronous speed ω_e. The d-axis will then be located at the actual position of the flux vector. Through this process, the d-axis stator current i_{ds}^e in the synchronous reference frame becomes the true flux-producing current, and then can be used for controlling the magnitude of the flux. This d-axis stator current i_{ds}^e corresponds to the field current of a DC motor.

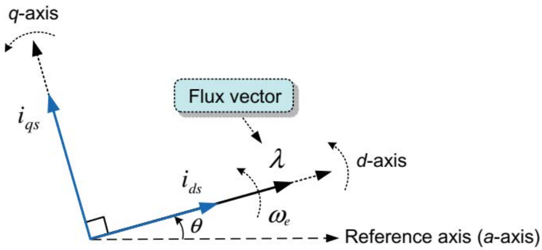

Fig. 5.3

Commonly, the d-axis stator current is assigned as the flux-producing current, whereas the q-axis stator current is assigned as the torque-producing current. By obtaining these orthogonal currents, the **requirement 1** can be fulfilled.

Here, the flux vector λ in the induction motor is the rotating magnetic field generated by the three-phase currents.

Since the field flux exists only on the d-axis, the torque equation for an induction motor becomes similar to that of a DC motor as

$$T_e = \frac{3}{2}\frac{P}{2}\frac{L_m}{L_r}\left(\lambda_{dr}^e i_{qs}^e - \lambda_{qr}^e i_{ds}^e\right) =$$

$$= k\,|\,\lambda\,|\,i_{qs}^{e}\left(\lambda_{dr}^{e} = |\,\lambda\,|, \lambda_{qr}^{e} = 0, k = \frac{3}{2}\frac{P}{2}\frac{L_m}{L_r}\right).$$

The torque can be directly controlled by the q-axis current i_{qs}^{e}, so the q-axis current is considered as the torque-producing current.

In this condition, if the magnitude of the flux vector is kept constant by controlling $\boldsymbol{i_{ds}^{e}}$

$$T_e = k' i_{qs}^{e} \left(k' = k\,|\,\lambda\,|\right).$$

The flux-producing current and the torque-producing current can be controlled independently. In this case the magnitude of the flux vector can be controlled independently by the d-axis stator current $\boldsymbol{i_{ds}^{e}}$, while the torque can be controlled independently by the q-axis stator current $\boldsymbol{i_{qs}^{e}}$. This indicates that the **requirement 2** can be fulfilled.

Finally, the torque-producing current can be controlled instantaneously by means of the current regulator and thus the **requirement 3** can also be fulfilled.

The actual implementation process of the vector control is demonstrated in fig. 5.4.

There is no cross-coupling between the d-axis stator current (thus, the flux vector) and the q-axis stator current because they are orthogonal to each other. In other words, i_{qs}^{e} is not influenced by i_{ds}^{e} and vice versa.

In summary, to control the instantaneous torque of an induction motor, first, the three-phase stator currents are separated into d- and q-axes stator currents by using the synchronous reference frame transformation in which the d-axis is assigned to the position of the flux vector. Then, the flux can be controlled by the d-axis stator current i_{ds}^{e} while the instantaneous torque can be controlled by the q-axis stator current i_{qs}^{e} independently.

Finally, the instantaneous torque control can be achieved by controlling these currents instantaneously. This instantaneous torque control method for an induction motor is called the vector control or field-oriented control.

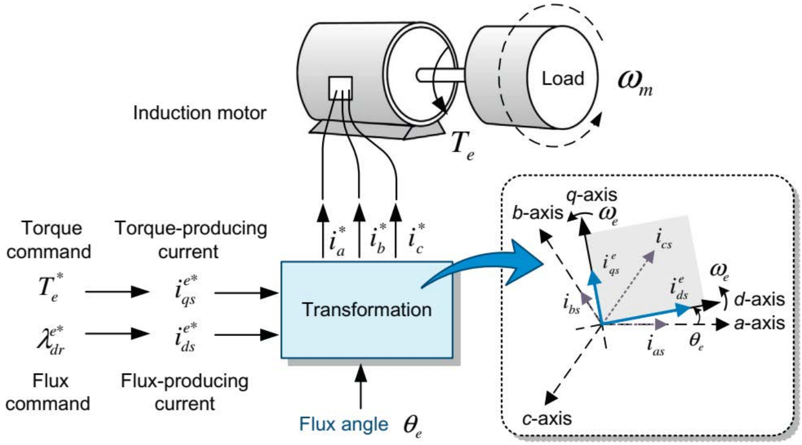

Fig. 5.4

In the vector control of an induction motor, the magnitude of the flux remains normally at a constant level of the rated value except for high-speed operations above the rated speed. Based on the rated flux command λ_{ds}^{e*}, the required flux-producing current command i_{ds}^{e*} is calculated. On the other hand, the torque-producing current command i_{qs}^{e*} is calculated based on the output torque command T_e^* required for driving a given load. These command currents i_{ds}^{e*} and i_{qs}^{e*} are given in the synchronous rotating reference frame. Thus we need to obtain the three-phase stator current commands through the inverse transformation into these *d-q* current commands. Here, it should be noted that this transformation requires the knowledge of the angular position of the flux vector, so called the flux angle.

5.2 Vector Control of an Induction Motor

It is necessary to use the synchronous *d*-*q* reference frame, which rotates at the same speed as that of the flux vector λ, i.e., the synchronous speed. Therefore, to accomplish the vector control, the flux angle θ is an inevitable information.

Important information for vector control: flux angle **θ**.

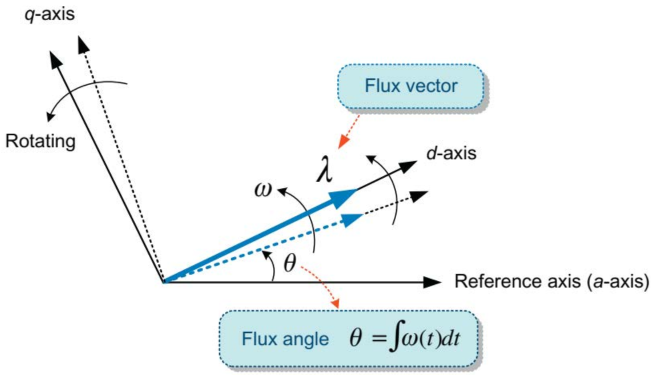

Fig. 5.5

The vector control of an induction motor can be classified into **direct vector control** and **indirect vector control** depending on how the information about the flux angle is obtained.

An induction motor has three fluxes available for reference: stator flux, rotor flux, and air-gap flux. The vector control of an induction motor can be classified according to the reference flux as

− Rotor flux-oriented (RFO) control;
− Stator flux-oriented (SFO) control;
− Air-gap flux-oriented (AFO) control.

5.2.1 Direct Vector Control Based on the Rotor Flux. In the direct vector control the flux angle is obtained directly from the flux itself, which can be either measured or estimated. On the other hand, in the indirect vector control, the flux is not used to obtain the flux angle. Instead, it uses the slip angular velocity, which is needed to separate the stator currents into the flux- and the torque-producing currents at the desired values. From this slip angular velocity and the rotor angular velocity, the flux angle can be obtained.

Among these, the RFO control is the most popular due to its simplicity. For the AFO control, there is a coupling between the slip angular velocity and the airgap flux, and for the SFO control, there is a coupling between the *q*-axis current and the stator flux. These couplings can make the associated vector control complex.

The rotor flux linkage generated by the three-phase rotor currents can be expressed as a complex vector $\boldsymbol{\lambda}_r$ as

$$\lambda_r = \frac{2}{3}\left(\lambda_{ar} + a\lambda_{br} + a^2\lambda_{cr}\right) = |\lambda_r| e^{j\omega_e t} = |\lambda_r| e^{j\theta_e} \times$$

$$\times\left(\theta_e = \int \omega_e(t)\,dt + \theta(0)\right).$$

The d-axis is always locked at the position of the rotor flux linkage vector. As a result, the rotor flux linkage in the synchronous *d*-*q* reference frame has entirely the *d*-axis component and no *q*-axis component

$$\lambda_r = \lambda_{dr}^e, \qquad \lambda_{qr}^e = 0.$$

The rotor flux linkage vector in the stationary reference frame as shown in fig. 5.6 has both the d-q axes components, $\boldsymbol{\lambda}_{dr}^s$, and $\boldsymbol{\lambda}_{qr}^s$, whose magnitudes are changed according to the position of the rotor flux linkage vector.

If these stationary *d*-*q* rotor flux linkages are known, then we can obtain the rotor flux angle from the following equation

$$\theta_e = \tan^{-1}\left(\frac{\lambda_{qr}^s}{\lambda_{dr}^s}\right).$$

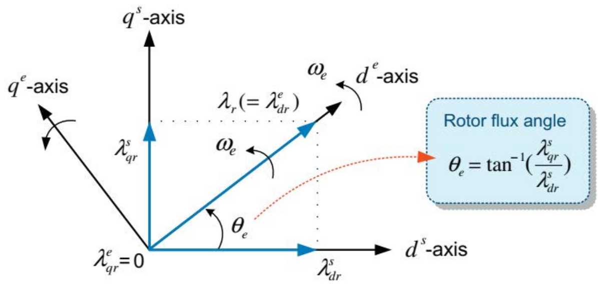

Fig. 5.6

5.2.1.1 Relation between the *d*-axis stator current and the rotor flux linkage. The *d*-axis rotor voltage equation in the synchronous reference frame is

$$0 = R_r i_{dr}^e + p\lambda_{dr}^e - (\omega_e - \omega_r)\lambda_{qr}^e.$$

The necessary and sufficient condition for the rotor flux-oriented vector control is

$$\lambda_{dr}^e = \lambda_r, \qquad \lambda_{qr}^e = 0.$$

The *d*-axis rotor current

$$i_{dr}^e = -\frac{p\lambda_{dr}^e}{R_r}.$$

The rotor flux linkage λ_{dr}^e can be found

$$\lambda_{dr}^e = L_r i_{dr}^e + L_m i_{ds}^e,$$

$$\lambda_{dr}^e = \frac{R_r L_m}{R_r + L_r p} i_{ds}^e = \frac{L_m}{1 + T_r p} i_{ds}^e, \qquad \left(T_r = \frac{L_r}{R_r}\right).$$

It can be seen that the rotor flux linkage λ_r is proportional to the *d*-axis stator current by the first-order lag with the rotor time constant T_r. Thus the rotor flux linkage to a sudden change in the d-axis current will change exponentially with the time constant of T_r as shown in Fig. 5.7. Although there is a time delay, the magnitude of the rotor flux linkage can be regulated by the d-axis stator current. Thus the d-axis stator current i_{ds}^e can be called the flux-producing current.

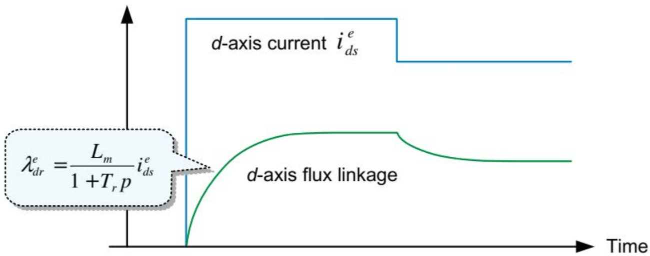

Fig. 5.7

With the d-axis current $\boldsymbol{i_{ds}^e}$ held constant, the magnitude of the rotor flux linkage $\boldsymbol{\lambda_{dr}^e}$ is directly related to $\boldsymbol{i_{ds}^e}$ as

$$|\lambda_r| = \lambda_{dr}^e = L_m i_{ds}^e .$$

Normally, the magnitude of the rotor flux linkage is kept constant for operations below the rated speed.

5.2.1.2 Relationship between the q-axis stator current and the output torque. The torque equation

$$T_e = \frac{3}{2}\frac{P}{2}\frac{L_m}{L_r}\left(\lambda_{dr}^e i_{qs}^e - \lambda_{qr}^e i_{ds}^e\right) = \frac{3}{2}\frac{P}{2}\frac{L_m}{L_r}\lambda_{dr}^e i_{qs}^e, \qquad \lambda_{qr}^e = 0.$$

With the rotor flux held constant, the torque equation reduces further to

$$T_e = K_T i_{qs}^e \left(K_T = \frac{3}{2}\frac{P}{2}\frac{L_m}{L_r}\lambda_{dr}^e \right).$$

The torque is directly related to the q-axis stator current $\boldsymbol{i_{qs}^e}$, so this current can be called the **torque-producing current**.

The torque can also be expressed in terms of the stator currents as

$$T_e = \frac{3}{2}\frac{P}{2}\frac{L_m^2}{L_r}\frac{1}{\left(1+\frac{L_r}{R_r}p\right)}i_{ds}^e i_{qs}^e, \qquad T_e = \frac{3}{2}\frac{P}{2}\frac{L_m^2}{L_r}i_{ds}^e i_{qs}^e.$$

An induction motor drive system that adapts the direct vector control based on the rotor flux is shown in fig. 5.8.

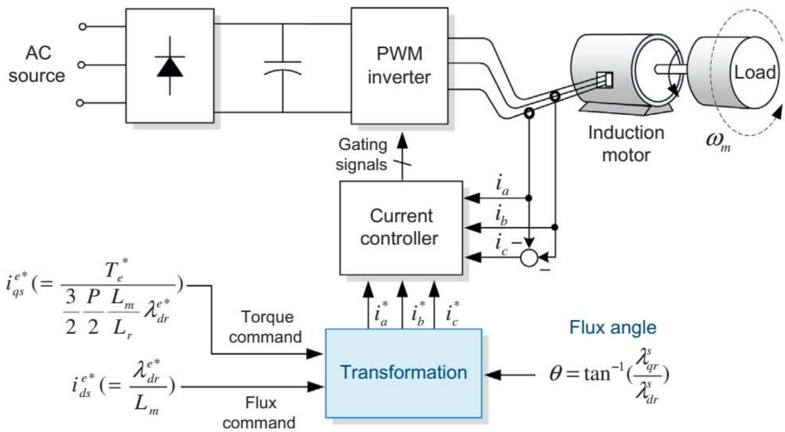

Fig. 5.8

In the direct vector control of an induction motor, the rotor flux linkage is kept constant and the torque is regulated by controlling $\boldsymbol{i_{qs}^e}$. Accordingly, the d-axis current command $\boldsymbol{i_{ds}^{e*}}$ will be given from the rotor flux command $\boldsymbol{\lambda_{dr}^{e*}}$

$$i_{ds}^{e*} = \frac{\lambda_{dr}^{e*}}{L_m}.$$

The q-axis current command $\boldsymbol{i_{qs}^{e*}}$ can be calculated from the output torque command T_e^* which may be given from a speed or torque controller, as

$$i_{qs}^{e*} = \frac{T_e^*}{K_T}, \qquad \left(K_T = \frac{3}{2}\frac{P}{2}\frac{L_m}{L_r}\lambda_{dr}^{e*} \right).$$

The rated value of the rotor flux linkage command $\boldsymbol{\lambda_{dr}^e}$ depends on the rated voltage and frequency of a given motor.

After applying the *d*-axis current command i_{ds}^e, a time to build up the rotor flux linkage to its final value is required. This build-up time depends on the rotor time constant Tr and will be normally about $5T_r$.

We need to regulate the stator currents of the induction motor to follow these current commands. It should be noted that these *d*-*q* current commands $\boldsymbol{i_{ds}^{e*}}$ and $\boldsymbol{i_{qs}^{e*}}$ are variables in the synchronous reference frame.

We need to know the threephase current commands $\boldsymbol{i_{as}^*}$; $\boldsymbol{i_{bs}^*}$; $\boldsymbol{i_{cs}^*}$ of the induction motor. To obtain these threephase current commands, we need to transform $\boldsymbol{i_{ds}^{e*}}$ and $\boldsymbol{i_{qs}^{e*}}$ into $\boldsymbol{i_{as}^*}$; $\boldsymbol{i_{bs}^*}$; $\boldsymbol{i_{cs}^*}$ by using the rotor flux angle $\boldsymbol{\theta_e}$. Alternatively, after transforming these synchronous current commands into stationary current commands as

$$i_{ds}^{s*} = i_{ds}^{e*}\cos\theta_e - i_{qs}^{e*}\sin\theta_e, \qquad i_{qs}^{s*} = i_{ds}^{e*}\sin\theta_e + i_{qs}^{e*}\cos\theta_e.$$

then, we can transform these stationary current commands into three-phase current commands as

$$i_{as}^* = i_{ds}^{s*}, \qquad i_{bs}^* = -\frac{1}{2}i_{ds}^{s*} + \frac{\sqrt{3}}{2}i_{qs}^{s*}, \qquad i_{cs}^* = -\frac{1}{2}i_{ds}^{s*} - \frac{\sqrt{3}}{2}i_{qs}^{s*}.$$

Finally, if the stator currents of an induction motor are regulated to instantaneously follow these three-phase current commands by using a current controller, then the instantaneous torque control of an induction motor can be achieved.

On the other hand, there is a more effective control method in regulating the stator currents. In this method of using a synchronous reference frame current regulator, the synchronous current commands, i_{ds}^{e*} and i_{qs}^{e*}, are used directly instead of the three-phase current commands as shown in fig. 5.9. In this case, the three-phase stator currents, i_{as}^{*}; i_{bs}^{*}; i_{cs}^{*}, of the induction motor are transformed into synchronous dq currents, i_{ds}^{e} and i_{qs}^{e}.

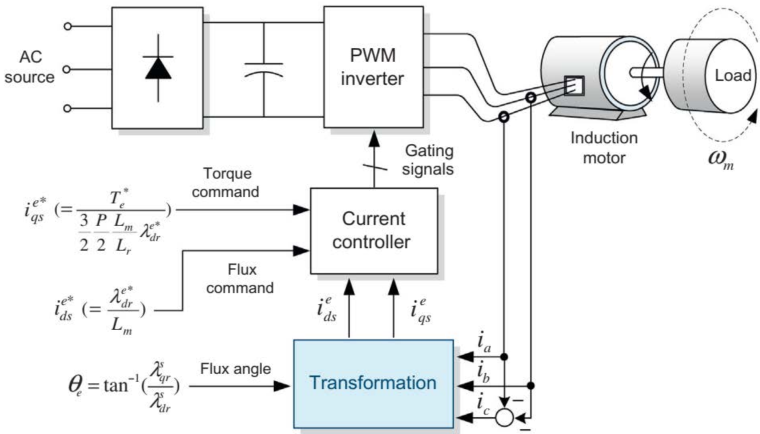

Fig. 5.9

In vector control we can see that both the magnitude and the phase of the stator current vector vary according to the output torque command.

The magnitude and the phase of the stator current vector vary according to the output torque command. As an example, fig. 5.10 describes how the stator current command vector alters when the torque command is changed. The stator current vector of the induction motor is assumed to be is initially.

If a larger torque needs to be produced, the q-axis current command will be increased from $\boldsymbol{i}_{qs}^{e*}$ to $\boldsymbol{i}_{qs1}^{e*}$, but the d-axis current command $\boldsymbol{i}_{ds}^{e*}$ will remain the same. This requires a new stator current command vector $\boldsymbol{i}_{s1}^{*}$, and thus both the magnitude and the phase of the stator current vector are changed. Likewise, if the flux command is changed, both the magnitude and the phase of the stator current vector will be also changed.

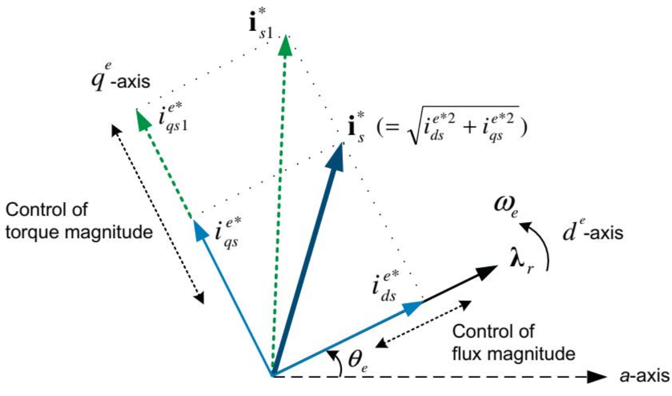

Fig. 5.10

The most difficult aspect of implementing the direct vector control is finding the instantaneous position of the rotor flux linkage, i.e., the rotor flux angle, accurately. It is not an overstatement to say that the performance of the instantaneous torque control depends on the accuracy of the rotor flux angle. A way to obtain the rotor flux angle is to calculate the rotor flux linkage from the air-gap flux detected by Hall effect sensors or sensing coils, which are installed in the applied motor. However, this method is costly and is not practical. A widely used method is to estimate the rotor flux linkage from voltages and currents of the motor.

5.2.2 Indirect Vector Control Based on the Rotor Flux. The indirect vector control does not use the rotor flux linkage directly for obtaining the rotor flux angle, so it may be implemented easily.

From the steady-state equivalent circuit of an induction motor in fig. 5.11, we can see that the slip *s* determines how the stator current can be divided into the flux- and torque (or rotor)-producing currents. Thus we can infer from this that the desired flux and torque can be obtained by controlling the slip. The flux- and the torque-producing currents in the stated-state equivalent circuit are not equal to those in the vector control. However, similar to this concept, the principle of the indirect vector control is to control the slip so that the stator current can be divided into the desired flux- and the torque-producing components. Now we will take a closer look at the principle of the indirect vector control.

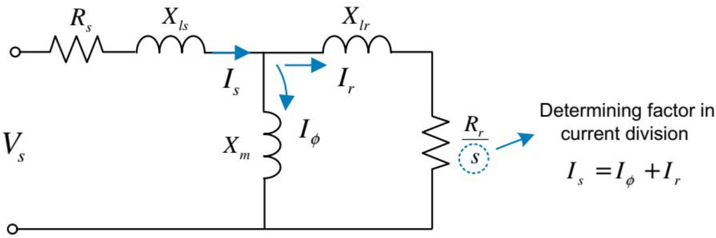

Fig. 5.11

In the vector control, the rotor voltage equation becomes

$$v_{qr}^e = R_r i_{qr}^e + p\lambda_{qr}^e + \left(\omega_e - \omega_r\right)\lambda_{dr}^e = R_r i_{qr}^e + \left(\omega_e - \omega_r\right)\lambda_{dr}^e = 0.$$

From this, the slip angular frequency $\boldsymbol{\omega}_{sl}$ required in the vector control can be derived as

$$\omega_e - \omega_r = \omega_{sl} = -\frac{R_r i_{qr}^e}{\lambda_{dr}^e}.$$

From the rotor flux linkage equation of

$$\lambda_{qr}^e = L_r i_{qr}^e + L_m i_{qs}^e = 0.$$

The rotor current can be obtained as $i_{qr}^e = -\dfrac{L_m}{L_r} i_{qs}^e$.

The slip angular frequency for the vector control

$$\omega_{sl} = \frac{L_m R_r}{L_r} \frac{i_{qs}^e}{\lambda_{dr}^e}, \qquad \omega_{sl} = \left(\frac{1}{T_r} + p\right)\frac{i_{qs}^e}{i_{ds}^e}, \qquad \left(T_r = \frac{L_r}{R_r}\right).$$

With the rotor flux linkage held constant, we can finally obtain the important slip requirement for the indirect vector control as

$$\omega_{sl} = \frac{1}{T_r} \frac{i_{qs}^e}{i_{ds}^e}.$$

After that, using the information of the rotor velocity ω_r, we can obtain the rotor flux angle as

$$\theta_e = \int \omega_e dt = \int \left(\omega_{sl} + \omega_r\right) dt.$$

Since the indirect vector control uses the rotor flux angle obtained from adding the slip angular velocity to the rotor velocity, this is often called the **feedforward field-oriented control**. The indirect vector control that does not require the information of the rotor flux linkage has an advantage of easy implementation and a better performance in low-speed operations.

A drawback of the indirect vector control is that the rotor speed is required to obtain the rotor flux angle. The rotor speed is normally found using an encoder, a type of a position sensor.

Fig. 5.12 shows the indirect vector control system of an induction motor, where the slip angular frequency ω_{sl}^* is calculated from *d*-*q* axes current commands for the required torque and flux production.

In addition, the indirect vector control is also problematic in which the rotor open circuit time constant T_r required in the calculation is sensitive to both the temperature and rotor flux level. The rotor resistance R_r can easily change with temperature, and the rotor inductance L_r can vary with the magnitude of the rotor flux. These variations result in an inaccurate slip angular frequency, and thus an accurate vector control cannot be achieved. Therefore, in the indirect vector control, the accuracy of the torque control depends on that of these parameters.

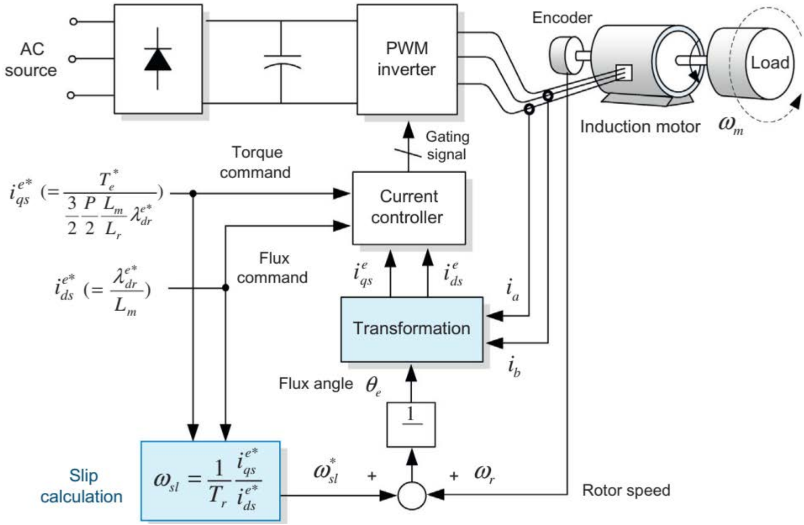

Fig. 5.12

5.3 Flux Estimation of an Induction Motor

In the direct method the rotor flux linkage is obtained from the air-gap flux acquired from the Hall effect sensors or the sensing coils installed inside the stator. However, since there are some difficulties in the practical usage of the direct method, the rotor flux linkages are commonly estimated from the mathematical motor model by using the motor voltage, current, and/or speed as follows.

There are two methods to obtain the stationary rotor flux linkages: one is **to measure the flux linkages** or the physical quantity proportional to the flux linkages, and the other one is

to estimate them indirectly from the mathematical motor model.

There are two typical open-loop observers for estimating the rotor flux linkage: one is based on the stator voltage equations, which is referred to as the **voltage model**, and the other one is based on the rotor voltage equations, which is known as the **current model**.

5.3.1 Voltage Model (Based on the Stator Voltage Equations). The stator flux linkages are obtained from the stator voltage equations and, in turn, the rotor flux linkages are estimated from these stator flux linkages. This method requires information on the stator voltages and currents.

The stator flux linkages can be found from the integral of stator voltages as

$$v_{ds}^s = R_s i_{ds}^s + \frac{d\lambda_{ds}^s}{dt},$$

$$v_{qs}^s = R_s i_{qs}^s + \frac{d\lambda_{qs}^s}{dt},$$

$$\lambda_{ds}^s = \int \left(v_{ds}^s - R_s i_{ds}^s \right) dt = \int e_{ds}^s dt,$$

$$\lambda_{qs}^s = \int \left(v_{qs}^s - R_s i_{qs}^s \right) dt = \int e_{qs}^s dt,$$

where $e_{ds}^s = v_{ds}^s - R_s i_{ds}^s$, $e_{qs}^s = v_{qs}^s - R_s i_{qs}^s$.

The d-axis rotor flux linkage in the stationary reference frame is given by

$$\lambda_{dr}^s = L_r i_{dr}^s + L_m i_{ds}^s.$$

The nonmeasurable rotor current i_{dr}^s can be obtained from the *d*-axis stator flux linkage and the stator current as

$$i_{dr}^s = \frac{\lambda_{ds}^s - L_s i_{ds}^s}{L_m} \leftarrow \lambda_{ds}^s = L_s i_{ds}^s + L_m i_{dr}^s.$$

The equation for the stationary *d*-axis rotor flux linkage as

$$\hat{\lambda}_{dr}^{s} = \frac{L_r}{L_m}\left(\lambda_{ds}^{s} - \sigma L_s i_{ds}^{s}\right),$$

where $\sigma = \left(1 - L_m^2 / L_s L_r\right)$.

The stationary *q*-axis rotor flux linkage as

$$\hat{\lambda}_{qr}^{s} = \frac{L_r}{L_m}\left(\lambda_{qs}^{s} - \sigma L_s i_{qs}^{s}\right).$$

Using the arctangent function of these estimated stationary *d*-*q* axes rotor flux linkages, the flux angle can be calculated as

$$\hat{\theta}_e = \tan^{-1}\left(\frac{\hat{\lambda}_{qr}^{s}}{\hat{\lambda}_{dr}^{s}}\right).$$

This method based on the voltage model is normally used in high-speed regions. The strength of this method is its simplicity and insensitivity to the parameter variations except for the stator resistance. However, since this method is fundamentally based on the estimation of the back-EMF esdqs its performance depends on the rotor speed. Thus this method works well in the medium- to high-speed range, in which the back-EMF becomes large enough. However, in the low-speed range with a low operation voltage, it may be easily influenced by the inaccuracy of the stator resistance, the sensor noise, and the inverter nonlinearity effect.

To estimate the rotor flux linkage accurately with this method, it should be noted that it is necessary to offer accurate stator voltages and currents. A voltage sensor may be used to obtain the stator voltages, but it is hard to measure the actual stator voltages precisely because the motor voltages are given by the inverter as a high-frequency pulse width modulator (PWM) waveform. Thus instead of measuring the actual stator voltages, the voltage commands or the voltages reconstructed by using the DC-link voltage and the commanded PWM duty are commonly used. However, the reconstructed value may differ from the actual output voltage due to inverter-nonlinearity such as the dead-time effect, turn-on/off delay time, and voltage drop across switching devices.

5.3.2 Current Model (Based on the Rotor Voltage Equations). The rotor flux linkages are obtained from the rotor voltage equations using the information on the stator currents and the rotor speed.

The rotor flux linkages can be directly obtained from the following rotor voltage equations as

$$v_{dr}^{\omega} = R_r i_{dr}^{\omega} + \frac{d\lambda_{dr}^{\omega}}{dt} - \left(\omega - \omega_r\right)\lambda_{qr}^{\omega} = 0,$$

$$v_{qr}^{\omega} = R_r i_{qr}^{\omega} + \frac{d\lambda_{qr}^{\omega}}{dt} + \left(\omega - \omega_r\right)\lambda_{qr}^{\omega} = 0.$$

The nonmeasurable rotor currents can be replaced by the rotor flux linkage and the stator current as

$$i_{dr}^{\omega} = \frac{\lambda_{dr}^{\omega} - L_m i_{ds}^{\omega}}{L_r} \leftarrow \lambda_{dr}^{\omega} = L_r i_{dr}^{\omega} + L_m i_{ds}^{\omega},$$

$$i_{qr}^{\omega} = \frac{\lambda_{qr}^{\omega} - L_m i_{qs}^{\omega}}{L_r} \leftarrow \lambda_{qr}^{\omega} = L_r i_{qr}^{\omega} + L_m i_{qs}^{\omega}.$$

The equations of the rotor flux linkage can be found as

$$\frac{d\lambda_{dr}^{\omega}}{dt} = -\frac{R_r}{L_r}\lambda_{dr}^{\omega} + R_r\frac{L_m}{L_r}i_{ds}^{\omega} + \left(\omega - \omega_r\right)\lambda_{qr}^{\omega},$$

$$\frac{d\lambda_{qr}^{\omega}}{dt} = -\frac{R_r}{L_r}\lambda_{qr}^{\omega} + R_r\frac{L_m}{L_r}i_{qs}^{\omega} - \left(\omega - \omega_r\right)\lambda_{dr}^{\omega}.$$

There is a difficulty in solving these equations due to the cross-coupling components between the axes. These undesirable cross-coupling components can be eliminated when the rotor flux linkages are estimated from the rotor reference frame $\boldsymbol{\omega}=\boldsymbol{\omega}_r$ using the measured rotor speed $\boldsymbol{\omega}_r$ as

$$\frac{d\lambda_{dr}^r}{dt} = -\frac{R_r}{L_r}\lambda_{dr}^r + \frac{R_r}{L_r}L_m i_{ds}^r,$$

$$\frac{d\lambda_{qr}^r}{dt} = -\frac{R_r}{L_r}\lambda_{qr}^r + \frac{R_r}{L_r}L_m i_{qs}^r.$$

The rotor flux linkages can be obtained from the integral of these two differential equations. The knowledge of the stator currents in the rotor reference frame is necessary to solve these equations.

These currents can be obtained by using the knowledge of the rotor speed ω_r as

$$i_{ds}^r = i_{ds}^s \cos\theta_r + i_{qs}^s \sin\theta_r,$$

$$i_{qs}^r = -i_{ds}^s \sin\theta_r + i_{qs}^s \cos\theta_r.$$

Finally, the required rotor flux linkage can be obtained by transforming back into the stationary reference frame as

$$\lambda_{dr}^s = \lambda_{dr}^r \cos\theta_r - \lambda_{qr}^r \sin\theta_r,$$

$$\lambda_{qr}^s = \lambda_{qr}^r \sin\theta_r + \lambda_{qr}^r \cos\theta_r.$$

Besides the knowledge of the rotor speed, this method requires the rotor resistance. Thus, the estimation performance is largely affected by the variation of the rotor resistance. Because of this, online identification and correction of the rotor resistance are essential for improving the estimation performance. In contrast to the voltage model that is advantageous for high-speed operations, this estimation method based on the current model is useful in low-speed regions because it may give an oscillatory response in high-speed regions.

5.3.3 Combined Flux Estimation Method. A method combining two models was introduced to produce a good performance over the whole speed range.

Fig. 5.13 shows the block diagram of this combined method that estimates the rotor flux linkages gradually by using the current model in the low-speed region and the voltage model in the high-speed region.

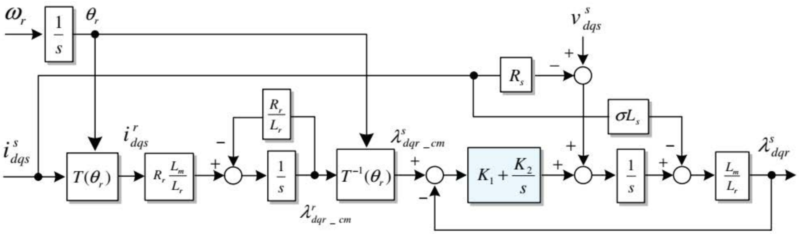

Fig. 5.13

Fig. 5.13 can be simplified to fig. 5.14. Here, $\lambda^s_{dqr\_cm}$ denotes the rotor flux linkage estimated by the current model, and $\lambda^s_{dqr\_vm}$ denotes the rotor flux linkage estimated by the voltage model.

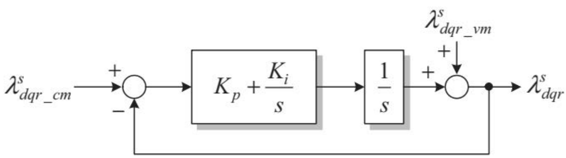

Fig. 5.14

The gains are given by

$$K_p = K_1 L_r / L_m, \qquad K_i = K_2 L_r / L_m.$$

In high-speed regions where the back-EMF is large enough, the flux estimation technique based on the voltage model using an integration of the back-EMF has an advantage of accuracy and robustness to parameters variation. However, in low-speed regions where it is hard to obtain accurate information on the backEMF, the flux estimation based on the current model using the rotor speed has an advantage over the one based on the voltage model. Therefore, it is desirable to estimate the rotor flux linkage by using the current model in low-speed regions and the voltage model in high-speed regions.

The output of simplified combined estimator can be expressed as

$$\lambda_{dqr}^{s} = \frac{s^2}{s^2 + K_p s + K_i}\lambda_{dqr\_vm}^{s} + \frac{K_p s + K_i}{s^2 + K_p s + K_i}\lambda_{dqr\_cm}^{s}.$$

This consists of the sum of the second-order, high-pass filtered rotor flux linkage $\boldsymbol{\lambda}_{dqr\_vm}^{s}$ based on the voltage model and the second-order, low-pass filtered rotor flux linkage $\boldsymbol{\lambda}_{dqr\_cm}^{s}$ based on the current model.

In this estimator the transition frequency ω_c between the two models is commonly selected at 10 Hz. The transition frequency $\boldsymbol{\omega}_c$ can be established through the gains of a proportional-integral (PI) controller.

By comparing the transfer function of a second-order, high-pass Butterworth filter with the first term of simplified combined estimator , we can see that there exists the following relationship between gains and parameters of the filter as

$$G(s) = \frac{s^2}{s^2 + 2\zeta\omega_n s + \omega_n^2} \leftrightarrow \frac{s^2}{s^2 + K_p s + K_i},$$

$$K_p = 2\zeta\omega_n, \qquad K_i = \omega_n^2.$$

In the Butterworth filter, if ζ=0,707, then ω_n becomes the bandwidth. To set the bandwidth ω_n equal to the transition frequency ω_c, the PI gains are given as

$$K_p = \sqrt{2}\omega_c, \qquad K_i = \omega_c^2.$$

Finally, K_1 and K_2 needed for the estimator in Fig. 5.13 are given as

$$K_1 = K_p \frac{L_m}{L_r} = \sqrt{2}\omega_c \frac{L_m}{L_r}, \qquad K_2 = K_i \frac{L_m}{L_r} = \omega_c^2 \frac{L_m}{L_r}.$$

This means that the final estimated flux linkage is automatically obtained from the current model in the low-frequency (low-speed) region and the voltage model in the high-frequency (high-speed) region.

Besides the estimators mentioned here, there are several different estimation methods that use the modern control theory such as observers using the state equations. The estimated rotor flux linkages can be also used for the sensorless vector control without using any position/speed sensors.

5.4 Flux Controller of Induction Motors

The estimated rotor flux linkage mentioned previously is primarily used to obtain the rotor flux angle. However, this estimated rotor flux linkage may also be used for flux control to improve the stability of the torque control or to achieve the field-weakening control for high-speed operations.

The magnitude of the rotor flux linkage can be controlled by the *d*-axis current. However, its instantaneous value is not proportional to the *d*-axis current when the d-axis current is changing. Thus when the magnitude of the rotor flux linkage has to be changed quickly for the field-weakening control, the rotor flux linkage needs to be controlled directly. Moreover, even when an induction motor is driven with a constant flux level, the flux control can enhance the stability of the drive system.

In the vector control based on the rotor flux, the magnitude of the rotor flux linkage can be controlled by the d-axis current i^e_{ds}, so the output of the PI flux controller has to be the *d*-axis current. The block diagram of the flux control system and a PI controller can be given as fig. 5.15.

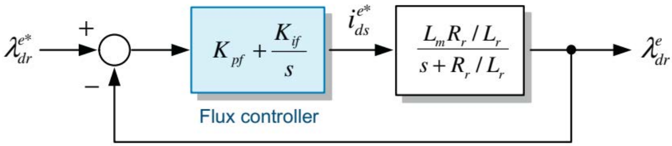

Fig. 5.15

The gains of a PI flux controller can be determined in a similar way as those of a current/speed controller for DC motor.

First, we assume that the dynamics of the *d*-axis current controller is fast enough compared to the flux change. The open-loop transfer function of the flux control system shown in fig. 5.15 is given as

$$G^o_f(s) = \left(K_{pf} + \frac{K_{if}}{s}\right) \cdot \frac{L_m \frac{R_r}{L_r}}{s + \frac{R_r}{L_r}} = \frac{K_{pf}\left(s + \frac{K_{if}}{K_{pf}}\right)}{s} \cdot \frac{L_m \frac{R_r}{L_r}}{s + \frac{R_r}{L_r}}.$$

The transfer function can be simplified as

$$G^o_f(s) = \frac{K_{pf} L_m \frac{R_r}{L_r}}{s}.$$

The proportional and the integral gains to obtain the required control bandwidth ω_f can be given as

$$K_{pf} = \frac{L_r}{R_r L_m}\omega_f,$$

$$K_{if} = \frac{R_r}{L_r}K_{pf} = \frac{\omega_f}{L_m}.$$

When the bandwidth of the current controller is several thousand radians per second, the bandwidth of the flux controller is designed generally within several ten to several hundred radians per second. This flux controller also needs an antiwindup control just like the speed/current controllers. The performance of the flux control can also be enhanced by the feedforward compensation using the flux command. The diagram of the vector control system including speed and flux controllers for an induction motor is shown in fig. 5.16.

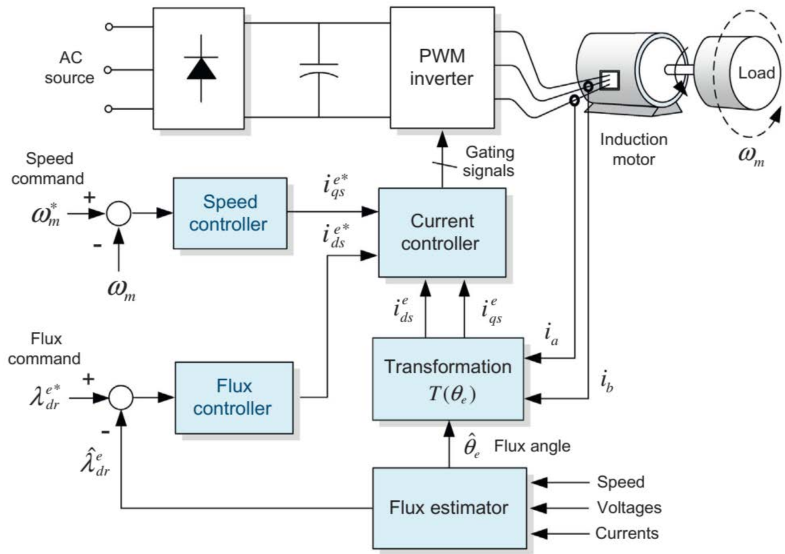

Fig. 5.16

5.5 Vector Control of Permanent Magnet Synchronous Motors

Due to their superior performance compared to DC motors or induction motors, PMSMs have become increasingly popular in various high-performance motor drive applications. The vector control for PMSMs is relatively simple compared to that of induction motors. As shown in fig. 5.17, this is because the rotor position itself is the position of the rotor flux, which is essential information for the vector control. Therefore, unlike for an induction motor, the complicated estimation algorithms are not required to obtain the rotor flux for the vector control of a PMSM.

PMSMs can be classified into SPM and IPM types. These two types differ in the output torque expression and thus are slightly different in the way of implementing the vector control. First, we will begin with the vector control method for an SPMSM.

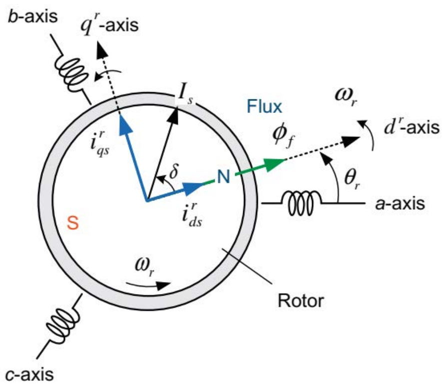

Fig. 5.17

The three requirements for the instantaneous torque control of a DC motor can be rewritten to apply to a PMSM as follows:

1. The space angle between the field flux and the torque-producing current is always 90 degrees.

2. Both the field flux and the torque-producing current can be controlled independently.

3. The torque-producing current has to be controlled instantaneously.

For a PMSM, the **requirement 2** for the instantaneous torque control can be inherently fulfilled. In PMSMs the field flux of the rotor is produced by permanent magnets, while the torque-producing current is given by the current of stator windings. Thus the field flux and the torque-producing current can be controlled independently. In addition, the torque-producing current (the stator current) can be controlled instantaneously by the synchronous reference frame current regulator and the PWM inverter and thus can satisfy the **requirement 3**.

Likewise, the requirements 2 and 3 are relatively easy to fulfill for a PMSM. For the vector control of a PMSM, it is important to fulfill the requirement 1, i.e., to maintain the space angle between the field flux and the torque-producing current at 90 degrees. To achieve this, it is necessary to first transform the three-phase *abc* stator currents into two *d*-*q* axes currents, just like in an induction motor. When transforming, the *d*-axis is aligned with the position of the rotor flux (i.e., the flux of the permanent magnet on the rotor) and then the *q*-axis current becomes the true torque-producing current, which is orthogonal to the rotor flux.

In a PMSM, the permanent magnet flux of the rotor is rotating at the same speed as the rotor speed ω_r as shown in fig. 5.17. We have to make the *d*-*q* axes rotate at the rotor speed ω_r. This implies that we need to use the transformation of the stator currents into the rotor reference frame (d^r-q^r axis). Such transformation requires the rotor position θ_r, i.e., the position of the permanent magnet. This can be obtained from the position sensors such as a resolver or an absolute encoder.

5.5.1 Vector Control of a Surface-mounted Permanent Magnet Synchronous Motor. In the vector control of an SPMSM, the stator currents are transformed into the rotor reference frame (d^r-q^r axis) where the *d*-axis is assigned as the rotor flux position $\boldsymbol{\theta}_r$ as shown in fig. 5.18.

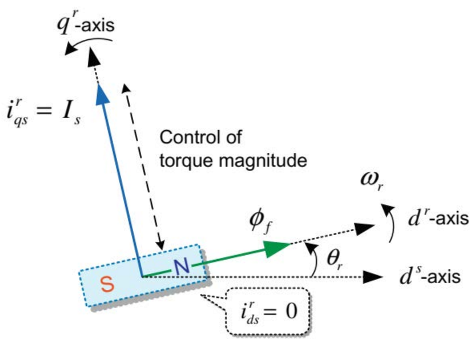

Fig. 5.18

The torque expression of an SPMSM

$$T_e = \frac{P}{2}\frac{3}{2}\varphi_f i^r_{qs}.$$

The necessary condition for the maximum torque per ampere (MTPA) in the vector control of an SPMSM is

$$i^r_{ds} = 0.$$

In such condition, if we can control the q-axis current $\boldsymbol{i^r_{qs}}$ instantaneously, then the torque of the SPMSM can be controlled instantaneously like in the DC motors.

In this system

$$i^{r*}_{ds} = 0, \qquad i^{r*}_{qs} = \frac{T^*_e}{\frac{P}{2}\frac{3}{2}\varphi_f}.$$

Therefore, it is desirable to assign all the stator currents to the *q*-axis current to make a full use of the allowed motor current. In other words, in the vector control of an SPMSM, all the stator current Is is used as the q-axis current i_{qs}^{r}, while the d-axis current is zero.

The diagram of the vector control system for an SPMSM is shown in fig. 5.19.

If the stator currents of the SPMSM can be regulated rapidly to follow these current commands by using a current regulator, then the instantaneous torque control can be achieved. As a current regulator, a synchronous reference frame current regulator is usually adopted due to its excellent current control performance. For the synchronous current regulators, we need to transform the three-phase stator currents, i_{as}; i_{bs}; i_{cs}, of the SPMSM into the synchronous dq stator currents i_{ds}^{r} and i_{qs}^{r} by using the rotor flux angle θ_r.

5.5.2 Vector Control of an Interior Permanent Magnet Synchronous Motor. In the vector control of an IPMSM the d-q axes currents required for the MTPA are different from those of an SPMSM. This is because, in contrast to that of SPMSMs, the torque of IPMSMs consists of two terms as

$$T_e = \frac{P}{2}\frac{3}{2}\left[\varphi_f i_{qs}^{r} + \left(L_{ds} - L_{qs}\right) i_{ds}^{r} i_{qs}^{r}\right].$$

In addition to the first term of Equation that represents the magnetic torque of an SPMSM, an IPMSM has a reluctance torque, the second term, which is produced by the difference between the inductance values of the two axes.

To produce the reluctance torque, both the d- and the q-axes components of the stator current are required. In most commonly used parallel topology IPMSMs, the q-axis inductance L_{qs} is typically larger than the d-axis inductance L_{ds}. Thus, the d-axis current must have a negative polarity for the reluctance torque to be added to the magnet torque, i.e., $i_{ds}^{r} < 0$. Similar to an induction motor, the stator current of an IPMSM needs to be divided into d- and q-axes components as shown in fig. 5.20. In this case, we need to know how the stator current is divided into the d- and q-axes stator currents properly to produce the MTPA. These optimal currents can be obtained as follows.

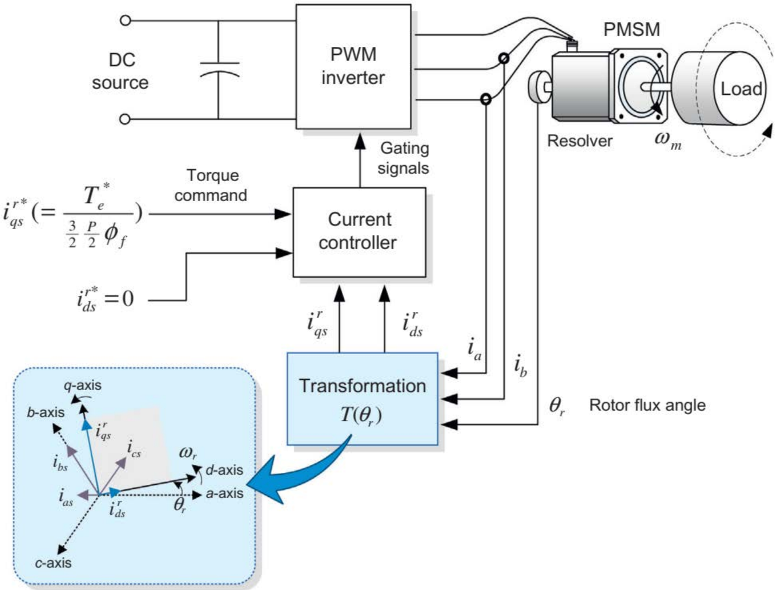

Fig. 5.19

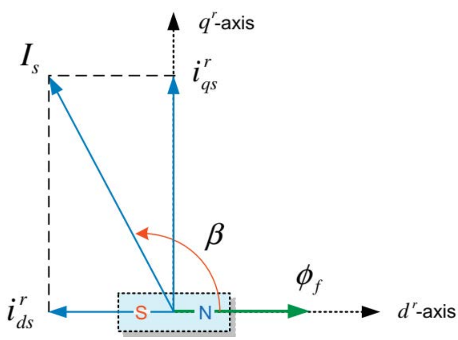

Fig. 5.20

There are many different combinations of *d*- and *q*-axes currents that produces the same torque. fig. 5.21 shows the curve consisting of these currents.

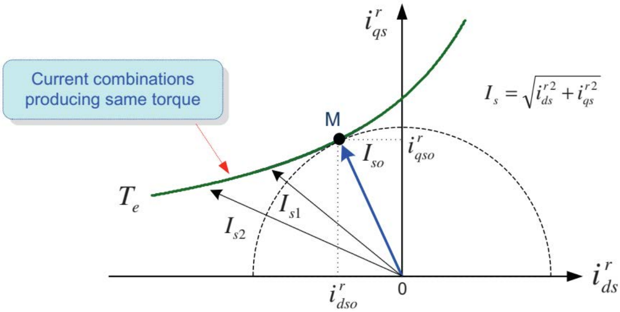

Fig. 5.21

Among these combinations, there is an optimal one that gives the smallest stator current. This optimal combination is the point *M*, at which the circle with a radius of I_{so} is tangent to the curve. Such operation method with the optimal combination of *d*- and *q*-axes currents that leads to the smallest stator current for producing the given torque command is called the MTPA control. The optimal combination of the *d*-and *q*-axes currents varies with the required torque.

The torque expression and *d*- and *q*-axes currents are normalized as

$$T_{en} = \frac{T_e}{T_b},$$

$$i_{dn} = \frac{i^r_{ds}}{i_b}, \qquad i_{qn} = \frac{i^r_{qs}}{i_b},$$

where $i_b \left(= \varphi_f / \left(L_{ds} - L_{qs} \right) \right)$, $T_b \left(= \frac{P}{2} \frac{3}{2} \varphi_f i_b \right)$.

The normalized torque can be rewritten as

$$T_{en} = \frac{T_e}{T_b} = \frac{\left[i_{qs}^r + \left(L_{ds} - L_{qs} \right) \dfrac{i_{ds}^r i_{qs}^r}{\varphi_f} \right]}{i_b} = \frac{i_{qs}^r}{i_b} - \frac{i_{qs}^r i_{ds}^r}{i_b^2} = i_{qn} \left(1 - i_{dn} \right).$$

The process of obtaining the optimal stator current for the MTPA control is as follows.

First, find the smallest d-axis current $\boldsymbol{i_{dno}}$ for producing the torque command $\boldsymbol{T_{en}}$. The stator current can be expressed as a function of $\boldsymbol{i_{dno}}$ as

$$I_{sno}^2 = i_{dno}^2 + i_{qno}^2 = i_{dno}^2 + \left(\frac{T_{en}}{1 - i_{dno}} \right).$$

Differentiating this Equation with respect to $\boldsymbol{i_{dno}}$ and making the result equal to zero gives

$$i_{dno}^4 - 3i_{dno}^3 + 3i_{dno}^2 + i_{dno} - T_{en}^2 = 0.$$

The optimal d-axis current $\boldsymbol{i_{dno}}$ can be obtained by solving Equation for the given torque command.

Likewise, we can find the smallest q-axis current $\boldsymbol{i_{qno}}$ for producing the torque command $\boldsymbol{T_{en}}$. After expressing the stator current as a function of $\boldsymbol{i_{qno}}$, differentiating this with respect to $\boldsymbol{i_{qno}}$ gives

$$i_{qno}^4 + T_{en} i_{qno} - T_{en}^2 = 0.$$

The optimal q-axis current i_{qno} can be obtained by solving this Equation for the given torque command.

Fig. 5.22 shows the optimal current commands for the MTPA operation. A look-up table for the optimal current commands is commonly used instead of online calculations.

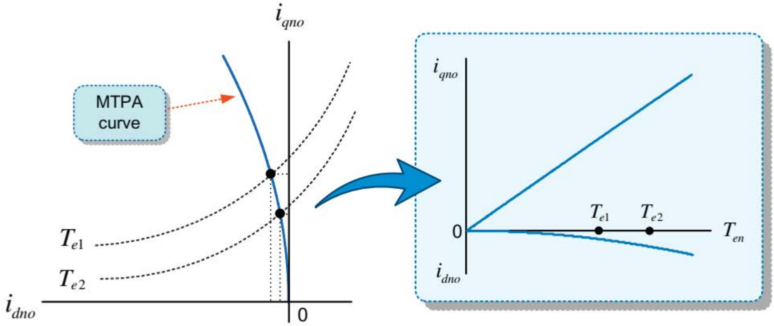

Fig. 5.22

In a speed controller the command to produce the output torque is often given as a stator current. For this stator current command $\boldsymbol{I_s^*}$, we can obtain the d-q axes stator current commands for the MTPA operation. The torque expression can be rewritten as a function of the stator current $\boldsymbol{I_s^*}$ as

$$T_e = \frac{P}{2}\frac{3}{2}\left[\varphi_f I_s^* \sin\beta + \frac{\left(L_{ds} - L_{qs}\right)}{2} I_s^{*2} \sin 2\beta\right],$$

where $\boldsymbol{\beta}$ denotes the angle between the d-axis and the stator current vector $\boldsymbol{I_s^*}$.

The $\boldsymbol{\beta_{max}}$ for producing the maximum torque can be obtained by solving

$$\frac{\delta T_e}{\delta\beta} = \frac{P}{2}\frac{3}{2}\left[\varphi_f I_s^* \cos\beta + \left(L_{ds} - L_{qs}\right) I_s^{*2} \cos 2\beta\right] = 0$$

$$\rightarrow \beta_{max} = \cos^{-1}\left(\frac{-\varphi_f + \sqrt{\varphi_f^2 + 8\left(L_{ds} - L_{qs}\right)^2 I_s^{*2}}}{4\left(L_{ds} - L_{qs}\right) I_s^*}\right).$$

To obtain the optimal currents for the MTPA operation by using the methods just mentioned, the exact knowledge of stator inductances and magnetic flux is necessary. The magnetic flux varies considerably with the operating temperature. In addition, each inductance value of *d*-*q* axes depends on the magnitude of the current of each axis. Furthermore, it is also known that each inductance of *d*-*q* axes may change with the current of the other axis due to cross-saturation effect between the *d*-*q* axes. Therefore the exact knowledge of the inductances and magnetic flux at various operating conditions is very important for a successful fulfillment of the MTPA control.

From $\boldsymbol{\beta}_{\mathbf{max}}$, the optimal *d*- and *q*-axes current commands are given as

$$i_{dso}^{r} = I_s^* \cos\beta_{\max} = \frac{-\varphi_f + \sqrt{\varphi_f^2 + 8\left(L_{ds} - L_{qs}\right)^2 I_s^{*2}}}{4\left(L_{ds} - L_{qs}\right)},$$

$$i_{qso}^{r} = I_s^* \sin\beta_{\max}.$$

The diagram of the vector control system for an IPMSM is shown in fig. 5.23. For the output torque command, the *d*-*q* axes stator current commands for the MTPA operation are given from the calculations or a look-up table as stated earlier. If the stator currents of the IPMSM can be regulated rapidly to follow these current commands by using a synchronous reference frame current regulator, then the instantaneous torque control of the IPMSM can be achieved.

When using this synchronous current regulator, we need to transform the threephase stator currents, i_{as}; i_{bs}; i_{cs}, of the IPMSM into synchronous *dq* currents i_{ds}^{r} and i_{qs}^{r} by using the rotor flux angle θ_r.

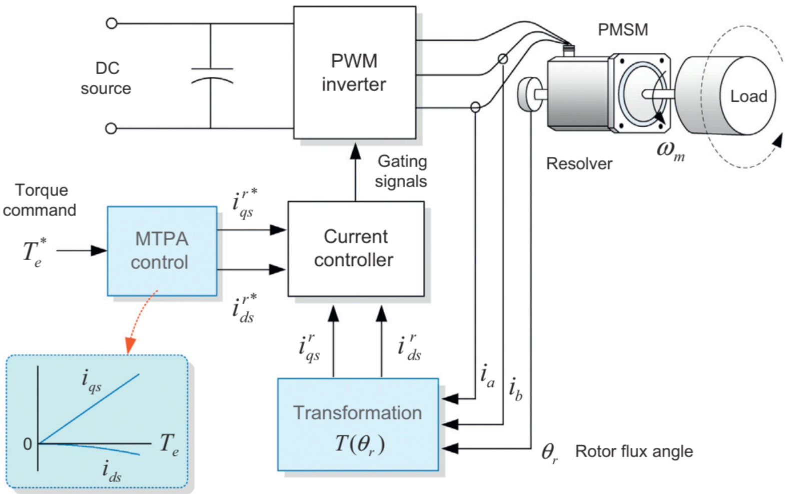

PMSM
DC
source
PWM
inverter
Load
Resolver
ω_m
Gating
signals
Torque
command
T_e^*
MTPA
control
i_{qs}^{r*}
i_{ds}^{r*}
Current
controller
i_{qs}^{r}
i_{ds}^{r}
i_a
i_b
i_{qs}
0
T_e
i_{ds}
Transformation
$T(\theta_r)$
θ_r
Rotor flux angle

Fig. 5.23

REFERENCES

1. Barnes Malcolm Practical Variable Speed Drives and Power Electronics // Malcolm Barnes. – Newnes, 2003. – 299 p.

2. Bose Bimal K. Power Electronics And Motor Drives: Advances and Trends // Bimal K. Bose. – Academic Press, 2006. – 935 p.

3. Chapman Stephen J. Electric Machinery Fundamentals // Stephen J. Chapman. – McGraw-Hill, 2012. – 680 p.

4. Crowder Richard Electric Drives and Electromechanical Systems: Applications and Control, Second Edition // Richard Crowder. – Butterworth-Heinemann, 2019. – 309 p.

5. El-Hawary Mohamed E. Principles of Electric Machines with Power Electronic Applications // Mohamed E. El-Hawary. – Wiley-IEEE Press, 2002. – 490 p.

6. Franchi Claiton Moro Electrical Machine Drives: Fundamental Basics and Practice // Claiton Moro Franchi. – CRC Press, 2019. – 403 p.

7. Franklin Gene F., Powell J. David, Emami-Naeini Abbas Feedback Control of Dynamic Systems, 7th Edition // Gene F. Franklin, J. David Powell, Abbas Emami-Naeini. – Pearson, 2014. – 860 p.

8. Gieras Jacek F. Electrical machines : fundamentals of electromechanical energy conversion // Jacek F. Gieras. – CRC Press, 2017. – 451 p.

9. Giri Fouad AC Electric Motors Control: Advanced Design Techniques and Applications // Fouad Giri. – Wiley, 2013. – 574 p.

10. Gürocak Hakan Industrial Motion Control: Motor Selection, Drives, Controller Tuning, Applications // Hakan Gürocak. – Wiley, 2015. – 320 p.

11. Herman Stephen Industrial Motor Control // Stephen Herman. – Delmar Cengage Learning, 2009. – 570 p.

12. Herman Stephen L. Electric Motor Control, 9th Edition // Stephen L. Herman. – Cengage Learning, 2009. – 473 p.

13. Herman Stephen L. Understanding Motor Controls // Stephen L. Herman. – Delmar Cengage Learning, 2016. – 643 p.

14. Hughes Austin, Drury William Electric Motors Drives, Fourth Edition // Austin Hughes, William Drury. – Newnes, 2013. – 436 p.

15. Keljik Jeffrey J. Electricity 4: AC/DC Motors, Controls, and Maintenance // Jeffrey J. Keljik. – Cengage Learning, 2012. – 416 p.

16. Krause Paul C., Wasynczuk Oleg, Sudhoff Scott D., Pekarek Steven Analysis of Electric Machinery and Drive Systems // Paul C. Krause, Oleg Wasynczuk, Scott D. Sudhoff, Steven Pekarek. – Wiley-Blackwell, 2013. – 680 p.

17. Krishnan Ramu Electric Motor Drives: Modeling, Analysis, and Control // Ramu Krishnan. – Prentice Hall, 2001. – 626 p.

18. Leonhard Werner Control of Electrical Drives, 3rd Edition // Werner Leonhard. – Springer Berlin Heidelberg, 2001. – 474 p.

19. Melkebeek Jan A. Electrical Machines and Drives: Fundamentals and Advanced Modelling // Jan A. Melkebeek. – Springer International Publishing, 2018. – 740 p.

20. Miller Rex, Miller Mark Industrial Electricity and Motor Controls, Second Edition // Rex Miller, Mark Miller. – McGraw-Hill Professional, 2013. – 512 p.

21. Mohan Ned Power Electronic and Drives // Ned Mohan. – MNPERE, 2003. – 251 p.

22. Muhammed Fazlur Rahman, Sanjeet K. Dwivedi Modeling, Simulation and Control of Electrical Drives // Muhammed Fazlur Rahman, Sanjeet K. Dwivedi. – The Institution of Engineering and Technology, 2019. – 715 p.

23. Petruzella Frank D. Electric Motors and Control Systems, Second Edition // Frank D. Petruzella. – McGraw-Hill, 2016. – 321 p.

24. Pyrhonen Juha, Jokinen Tapani, Hrabovcova Valeria Design of rotating electrical machines // Juha Pyrhonen, Tapani Jokinen, Valeria Hrabovcova. – Wiley, 2009. – 531 p.

25. Sahdev S. K. Electrical Machines // S. K. Sahdev. – Cambridge University Press, 2017. – 980 p.

26. Sang-Hoon Kim Electric Motor Control. DC, AC and BLDC Motors // Kim Sang-Hoon. – Elsevier Ltd., 2017. – 426 p.

27. Sen Paresh. C. Principles of Electric Machines and Power Electronics, Third Editions // Paresh. C. Sen. – Wiley, 2013. – 642 p.

28. Seung-Ki Sul Control of Electric Machine Drive Systems // Seung-Ki Sul. – Wiley-IEEE Press, 2011. – 415 p.

29. Tong Wei Mechanical Design of Electric Motors // Wei Tong. – CRC Press, 2014. – 737 p.

30. Umans Stephen D. Fitzgerald & Kingsley’s Electric Machinery, 7th edition // Stephen D. Umans. – McGraw-Hill Education, 2013. – 722 p.

31. Visioli Antonio Practical PID Control // Antonio Visioli. – Springer, 2006. – 322 p.

32. Wach Piotr Dynamics and Control of Electrical Drives // Piotr Wach. – Springer-Verlag Berlin Heidelberg, 2011. – 454 p.

33. Wilamowski Bogdan M., Irwin J. David // Bogdan M. Wilamowski, J. David Irwin. – CRC Press, 2017. – 1015 p.

34. Hand Augie Electric Motor Maintenance and Troubleshooting // Augie Hand. – McGraw-Hill Education TAB, 2011. – 432 p.

ДЛЯ НОТАТОК

ДЛЯ НОТАТОК

Навчальне видання

БІЛЮК Іван Сергійович
ГАВРИЛОВ Сергій Олексійович
САВЧЕНКО Олег Валерійович
ФОМЕНКО Андрій Миколайович
ШАРЕЙКО Дмитро Юрійович

СИСТЕМИ КЕРУВАННЯ ЕЛЕКТРОПРИВОДІВ

ELECTRIC DRIVES CONTROL SYSTEMS

Навчальний посібник

(*англійською мовою*)

Комп’ютерна правка й коректура *О. Є. Вакула*
Комп’ютерне верстання *В. В. Москаленко*

Формат 60×84/16. Ум. друк. арк. 10,0. Тираж 100 прим. Вид. № 23. Зам. № 1204-10.
Видавець і виготівник Національний університет кораблебудування
імені адмірала Макарова
просп. Героїв України, 9, м. Миколаїв, 54025
E-mail : publishing@nuos.edu.ua
Свідоцтво суб’єкта видавничої справи ДК № 6402 від 19.09.2018 р.